NUCLEAR MEDICINE AND MOLECULAR IMAGING

Annual Report

2009

University Medical Center Groningen

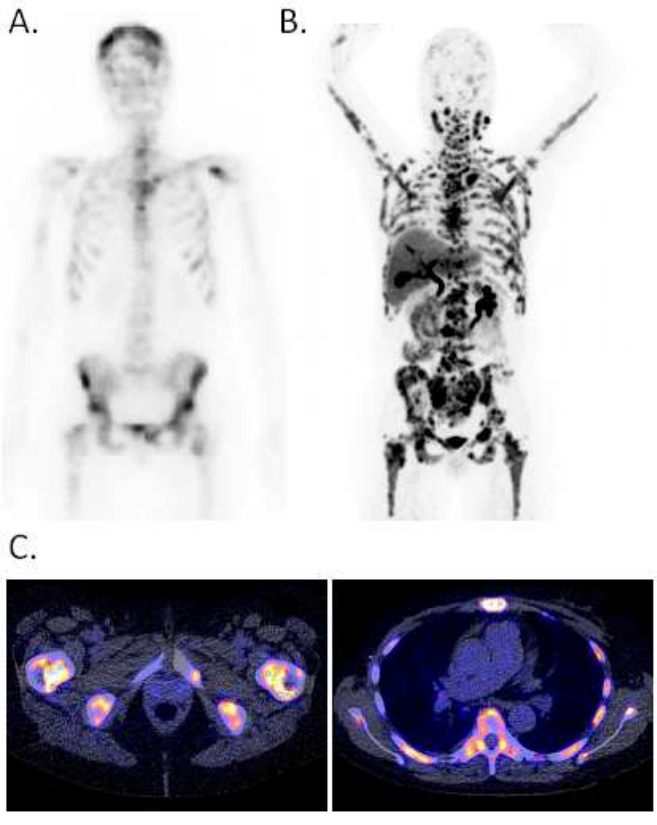

umcg

Cover illustration: Patient with estrogen-receptor positive breast cancer. (A) bone scan, (B) FES-PET, and (C) fusion of PET and CT. On FES-PET, extensive tracer uptake is seen in bone marrow, lymph nodes and the brain.

EDITORS: A.van Waarde
A.M.J.Paans

CONTENTS

CLINICAL APPLICATIONS

Table 1 presents an overview of the nuclear medicine studies which were performed in 2009. The total number of single-photon and positron emission studies was decreased in 2009 as compared to 2008 (from 16484 to 14986, i.e. by 9 %). The reason for this decrease is the extensive renovation of the Department which started in 2009 and will be continued in 2010. Several cameras and other imaging tools were replaced, and the radiochemistry lab, radiopharmacy facilities and patient waiting rooms were rebuilt and renovated in order to meet GLP/GMP conditions (see also chapter 4). For this reason, the production capacity and the capacity for patient scanning were reduced in the last months of 2009.

When data from 2009 are compared to those of the previous year, a few additional trends are evident. In the category "blood, infection, tumor", the number of hydroxytryptophan and FDOPA whole body PET scans was significantly increased compared to last year's values, even though the total amount of scans in this category declined by 9.3%. Also, the number of fluoroestradiol scans was increased (from 4 in 2008 to 23 in 2009). Sentinal node scintigraphy remained an important nuclear medicine examination in oncology.

The shift from SPECT towards PET in the category "central nervous system" which began in 2007 was continued in 2009. DAT scans disappeared completely, and the number of PET examinations of the brain showed a steady increase. The total number of nuclear medicine examinations of the CNS was increased from 409 in 2008 to 448 in 2009.

The number of examinations of the digestive tract remained about constant (469 in 2009 vs 462 in 2008). The decline of the number of examinations in endocrinology which began in 2008 was contined in 2009 (from 334 to 264).

Statistics for the production of PET tracers are summarized in Table 2, and statistics for the reliability of tracer production in Tables 3 and 4. The reliability of tracer production for human use (Table 3) was generally (much) greater than 90%. The reliability of the synthesis of 5-hydroxytryptophan was significantly increased as compared to 2008 (from 89% to 100%). ^{11}C-PK11195, ^{11}C-PIB and ^{11}C-meta-hydroxyephedrine (mHED) were the tracers with the lowest reliability (80, 90 and 90%, respectively). The low figure for ^{11}C-PK11195 is based on a very low number of synthetic runs (1 failure out of 5), therefore this may be considered as an incident.

The synthesis of PET tracers for animal studies was generally quite reliable (Table 4), with exception of the sigma ligand ^{11}C-SA4503. New precursor material for this tracer was acquired from Japan, and the reliability of the synthetic procedure will therefore be increased in 2010. Data on tracer production for the microPET are included in this chapter since some compounds (particularly ^{11}C-SA4503 and ^{18}F-IL2) may be employed for human studies in the near future.

Table 1. Nuclear medicine examinations in 2009

Type of study	Number of studies	Radiopharmaceutical	Average dose (MBq)	Age 0-15	Age 16-40	Age > 40	Males	Females
BLOOD, INFECTION, TUMOR								
Bevacizumab scan (high dose)	1	In-111 Bevacizumab (Avastin)	104	0	0	1	0	1
Bevacizumab scan (low dose)	2	In-111 Bevacizumab (Avastin)	59	0	0	2	0	2
Bevacizumab PET scan	20	Zr-89 Bevacizumab (Avastin)	38	0	0	20	19	1
Choline whole body scan	49	C-11 Choline	417	0	0	49	49	0
Hydroxytryptophan scan	50	C-11 5-Hydroxytryptophan	318	0	9	41	23	27
Methionine whole body scan	14	C-11 Methionine	434	0	1	13	6	8
Erythrocyte volume assessment	1	Cr-51 Na-chromate	1.1	0	0	1	0	1
FDOPA whole body scan	170	F-18 FDOPA	188	10	22	138	82	88
FDG whole body scan	1677	F-18 FDG	381	24	175	1478	992	685
Fluoroestradiol scan	23	F-18 FES	210	0	0	23	0	23
FLT whole body scan	15	F-18 FLT	356	0	3	12	10	5
Gallium scan	1	Ga-67 Gallium citrate	51	0	0	1	1	0
Leukocyte scan detail	72	Tc-99m Leukocytes	500	0	16	56	35	37
Leukocyte scan whole body	42	Tc-99m Leukocytes	505	0	9	33	26	16
Lymph node arms	6	Tc-99m Nanocolloid	20	0	0	6	2	4
Lymph node legs	56	Tc-99m Nanocolloid	20	0	16	40	20	36
MHED whole body scan	5	C-11 MHED	351	0	0	5	5	0
Plasma volume assessment	1	I-125 HSA serum albumin	0.26	0	0	1	0	1
Schilling test	7	Co-57 Cyanocobalamin	0.02	0	3	4	2	5
Sentinel node	18	Tc-99m Nanocolloid	64	0	2	16	6	12
Sentinel node mamma	196	Tc-99m Nanocolloid	60	0	9	187	2	194
Sentinel node other	38	Tc-99m Nanocolloid	62	0	5	33	20	18
Sentinel node vulva	24	Tc-99m Nanocolloid	102	0	3	21	1	23
Somatostatin receptor scintigraphy	77	In-111 Octreotide	184	0	9	68	43	34
Trastuzumab scan	4	Zr-89 Trastuzumab (Herceptin)	37	0	2	2	0	4
TRM-1 scan	10	In-111 TRM1	150	0	0	10	7	3
subtotal	**2579**							

Table 1 (continued)

Type of study	Number of studies	Radiopharmaceutical	Average dose (MBq)	Age 0-15	Age 16-40	Age > 40	Males	Females
CENTRAL NERVOUS SYSTEM								
MDL100907 scan	42	C-11 MDL100907	413	0	42	0	42	0
Methionine scan of the brain	70	C-11 Methionine	206	1	7	62	28	42
PiB scan	9	C-11 PiB	394	0	0	9	5	4
Raclopride scan	72	C-11 Raclopride	202	0	71	1	72	0
Cisternography - leakage	4	In-111 DTPA	21	0	1	3	2	2
FDG scan of the brain	158	F-18 FDG	205	3	10	145	92	66
FDOPA scan of the brain	92	F-18 FDOPA	191	0	4	88	53	39
Liquor drain function	1	In-111 DTPA	21	0	1	0	1	0
Subtotal	**448**							
DIGESTIVE TRACT								
Bile duct scintigraphy	13	Tc-99m Mebrofenine	42	4	2	7	8	5
Liver and spleen scintigraphy	4	Tc-99m Phytate	67	1	1	2	1	3
Spleen scan spherocytes	2	Tc-99m Denatured Erythrocytes	81	0	0	2	1	1
Gastric emptying	1	Tc-99m Phytate	11	0	0	1	0	1
Gastric emptying (solids)	132	Tc-99m CMC-gel	10	0	45	87	47	85
Meckel scan	5	Tc-99m Pertechnetate	124	4	0	1	3	2
Esophagus scintigraphy	312	Tc-99m Phytate	10	4	132	176	40	272
Subtotal	**469**							
ENDOCRINOLOGY								
Adrenal medulla scintigraphy	31	I-123 MIBG	126	19	2	10	15	16
Parathyroid scintigraphy	38	Tc-99m Sestamibi	474	0	5	33	12	26
Thyroid scintigraphy I-123	83	I-123 Na-iodide (capsule)	12	1	14	68	21	62
Thyroid scintigraphy I-131	4	I-131 Na-iodide (solution)	10	0	0	4	1	3
Thyroid scintigraphy I-123 i.v.	2	I-123 Na-iodide, i.v.	3	2	0	0	2	0
Thyroid cancer palpable	3	I-131 Na-iodide (solution)	179	0	0	3	2	1
Thyroid cancer scintigraphy (1 mCi)	31	I-131 Na-iodide (solution)	44	0	16	15	9	22
Thyroid cancer scintigraphy (2 mCi)	4	I-131 Na-iodide (solution)	73	0	0	4	0	4
Thyroid uptake	68	I-131 Na-iodide (diluted)	0.2	2	26	40	22	46
Subtotal	**264**							

Table 1 (continued)

Type of study	Number of studies	Radiopharmaceutical	Average dose (MBq)	Age 0-15	Age 16-40	Age > 40	Males	Females
HEART, VESSELS								
Myocardial metabolism (FDG)	44	F-18 FDG	192	0	1	43	37	7
Heart L-R sbunt	1	Tc-99m HDP	693	0	0	1	1	0
Heart R-L shunt	3	Tc-99m albumin aggregates	80	1	0	2	1	2
MUGA first pass	405	Tc-99m Pertechnetate	455	44	21	340	245	96
MUGA rest	781	Tc-99m Pertechnetate	495	6	77	698	456	307
Myocardial innervation	12	I-123 MIBG	179	0	0	12	7	5
Myocardial scintigraphy (at rest)	791	Tc-99m Tetrofosmin	595	1	36	754	432	359
Myocardial scan (with adenosine)	570	Tc-99m Tetrofosmin	595	0	17	553	299	271
Myocardial scintigraphy (exercise)	219	Tc-99m Tetrofosmin	593	1	16	202	129	90
Subtotal	**2826**							
LUNGS								
Lung perfusion scintigraphy	280	Tc-99m albumin aggregates	96	31	50	199	121	159
Lung ventilation scintigraphy	190	Kr-81m						
Subtotal	**470**							
SKELETON								
Skeletal scintigraphy total body	752	Tc-99m HDP	682	38	90	624	336	415
Skeletal scintigraphy total body + flow	69	Tc-99m HDP	688	2	18	49	21	48
Skeletal scintigraphy detail	374	Tc-99m HDP	679	18	130	226	172	202
Skeletal scintigraphy detail + flow	159	Tc-99m HDP	673	14	54	91	80	79
Yttrium citrate colloid scan	3	Y-90 Yttriumcitrate colloid	186	0	3	0	2	1
Bone densitometry measurements	5036	----						
Subtotal	**6393**							
THERAPY								
Polycytemia vera	6	P-32 Na-Orthophosphate	181	0	0	6	2	4
Neuroendocrine tumors	3	I-131 MIBG	5573	0	1	2	0	3
Hyperthyroidism (treatment 1)	78	I-131 Na-Iodide (solution)	489	1	28	49	18	60
Hyperthyroidism (treatment 2)	10	I-131 Na-Iodide (capsule)	1242	0	3	7	2	8
Thyroid carcinoma	59	I-131 Na-Iodide (capsule)	5038	0	18	41	17	42
Samarium therapy	1	Sm-153 EDTMP (Quadramet)	4312	0	0	1	1	0
Samarium therapy	4	Sm-153 EDTMP (Quadramet)	1816	0	0	4	1	2
Samarium therapy	1	Sm-153 EDTMP (Quadramet)	2573	0	0	1	0	1
Samarium therapy	4	Sm-153 EDTMP (Quadramet)	2909	0	0	4	3	1
Yttrium-90 Zevalin therapy	1	Y-90 Ibritumomab (Zevalin)	870	0	0	1	0	1
Subtotal	**167**							

Table 1 (continued)

Type of study	Number of studies	Radiopharmaceutical	Average dose (MBq)	Age 0-15	Age 16-40	Age > 40	Males	Females
UROGENITAL SYSTEM								
Renal scintigraphy	93	Tc-99m DMSA (succimer)	43	70	13	10	45	48
Priming hippuran clearance children	2	I-131 Hippuran	0.28	2	0	0	1	1
Renography	24	Tc-99m NephroMAG	72	3	8	13	8	16
Renography / captopril	3	Tc-99m NephroMAG	80	0	2	1	2	1
Renography / lasix	203	Tc-99m NephroMAG	58	84	39	80	122	81
Renography of renal transplant	19	Tc-99m NephroMAG	79	0	6	13	11	8
Iothalamate	2	I-125 Na-iothalamate	0.21	2	0	0	1	1
I131-hippuran clearance children	2	I-131 Hippuran	0.45	2	0	0	1	1
Priming iothalamate clearance children	2	I-125 Na-iothalamate	0.15	2	0	0	1	1
Clearance studies ERPF / GFR	915	I-131 Hippuran or I-125 Iothalamate						
Determination of GFR with EDTA	1	Cr-51 EDTA	4	0	1	0	1	0
Subtotal	**1266**							
MISCELLANEOUS								
Measurement of perfusion leak Tc	5	Tc-99m Pertechnetate	8	0	0	5	2	3
Measurement of perfusion leak 1	5	I-131 HSA (diluted)	5	0	0	5	2	3
Measurement of perfusion leak 2	6	I-131 HSA (diluted)	2	0	0	6	2	3
Amyloid scintigraphy (SAP scan)	53	I-123 SAP	167	0	7	46	27	26
Lymph scintigraphy	32	Tc-99m Pertechnetate	61	0	8	24	11	21
Tc-99m Tin colloid	2	Tc-99m Phytate	21	0	2	0	1	1
Lacrimal scintigraphy	1	Tc-99m Pertechnetate	4	0	0	1	0	1
Subtotal	**104**							
TOTAL NO. EXAMINATIONS	**14986**							

Table 2. Statistics Radiochemistry (2009 and previous years)

Preparation of radiopharmaceuticals for PET

Tracer	**2009**	**2008**	**2007**	**2006**	**2005**	**2004**	**2003**	**2002**	**2001**	**2000**
$H_2{}^{15}O$	**362**	20	30	126	538	393	507	245	491	557
^{18}F-FDG	**264**	256	262	225	272	251	239	219	222	200
$^{13}NH_3$	**144**	120	144	73	50	210	160	200	222	461
^{18}F-DOPA	**138**	144	128	134	99	104	66	50	59	42
^{11}C-Raclopride	**76**	75	43	3	32	18	30	61	49	25
^{11}C-HTP	**55**	38	37	60	7	-	-	-	-	-
^{11}C-Methionine	**52**	56	48	38	29	22	16	6	-	-
^{11}C-MDL100907	**33**	-	-	-	-	-	-	-	-	-
^{11}C-Choline	**32**	38	21	28	30	26	22	13	22	57
^{18}F-FES	**17**	3	-	-	-	-	-	-	-	-
^{18}F-FLT	**12**	17	19	8	12	31	46	56	11	-
^{11}C-mHED	**10**	24	10	-	-	-	-	-	-	-
^{11}C-PIB	**10**	6	-	-	-	-	-	-	-	-
^{11}C-PK11195	**5**	23	38	-	-	-	-	-	-	-
^{18}F-NaF	**3**	3	2	3	16	19	-	-	-	-
^{11}C-Verapamil	-	44	4	30	40	-	2	24	14	15
^{11}C-SA4503	-	-	1	21	3	-	-	-	-	-
^{15}O-CO	-	-	-	-	4	-	-	-	-	1
^{18}F-FMISO	-	-	-	-	2	2	2	2	2	-
^{18}F-FHBG	-	-	-	4	1	-	-	-	-	-
^{11}C-CGP-12388	-	-	-	-	-	4	3	13	9	12
^{11}C-Carvedilol	-	-	-	-	-	1	2	-	-	-
^{11}C-Tyrosine	-	-	-	-	-	-	-	11	42	35
^{18}F-MPPF	-	-	-	-	-	-	-	9	9	8
^{11}C-Acetate	-	-	-	-	-	-	-	-	2	8
^{11}C-VC002	-	-	-	-	-	-	-	-	-	-
^{18}F-Fluorcarazolol	-	-	-	-	-	-	-	-	-	-
^{11}C-Thymidine	-	-	-	-	-	-	-	-	-	-
^{18}F-FESP	-	-	-	-	-	-	-	-	-	-
^{11}C-CGP-12177	-	-	-	-	-	-	-	-	-	-
^{11}C-Bicarbonate		-	-	-	-	-	-	11	34	12

Table 3. Reliability of radiopharmaceutical production for human PET studies

Tracer	Number of syntheses in 2009	Number of failures	Reliability (%)
$H_2{}^{15}O$	362	**7**	98
^{18}F-FDG	264	**15**	94
$^{13}NH_3$	144		100
^{18}F-DOPA	138	**1**	99
^{11}C-Raclopride	76	**5**	93
^{11}C-HTP	55		100
^{11}C-Methionine	52	**4**	92
^{11}C-MDL100907	33	**1**	97
^{11}C-Choline	32	**2**	94
^{18}F-FES	17		100
^{18}F-FLT	12		100
^{11}C-mHED	10	**1**	90
^{11}C-PIB	10	**1**	90
^{11}C-PK11195	5	**1**	80
^{18}F-NaF	3		100

Table 4. Reliability or radiopharmaceutical production for microPET studies

Tracer	Number of syntheses	Number of failures	Reliability (%)
$H_2{}^{15}O$	12		100
^{18}F-FDG	83		100
$^{13}NH_3$	30		100
^{11}C-HTP	18		100
^{11}C-Choline	14	**1**	93
^{11}C-mHED	4		100
^{11}C-PK11195	19	**1**	95
^{11}C-MC18/267	4		100
^{11}C-SA4503	16	**3**	81
^{11}C-DAA1106	1		100
^{18}F-IL2	27	**1**	96
^{18}F-FEanGA	26		100
^{89}Zr-mAb	48		100

CLINICAL RESEARCH

2.1 Cardiology

2.1.1 PET-based revascularisation

In cooperation with Dept. Cardiology

Revascularisation strategies based on positron emission tomography (PET) proven viability have been widely accepted. However not all patients treated this way benefit from revascularisation. Atherosclerosis is a disease not limited to epicardial arteries, but also affects the microvasculature. We have previously shown that myocardial perfusion reserve (MPR) influences survival in ischemic heart disease (IHD) patients not amenable for intervention. In the present study we evaluated whether MPR has prognostic value in patients after a PET driven intervention. We hypothesized that MPR is an important prognostic factor also in revascularised patients.

Between 1995 and 2003, 119 consecutive patients with chronic IHD underwent a PET driven revascularization based on dipyridamole stress and rest ^{13}N-ammonia PET to determine MPR, as well as an FDG PET for viability (mismatching defects), infarction (matching defects) and LVEF assessment. Patients were followed for cardiac mortality.

One-hundred nineteen patients underwent a PET-driven revascularization (67 PCI, 52 CABG). The mean age of the patients was 67 ± 11 yrs (97 men). MPR was 1.54 ± 0.43. Patients were divided into tertiles based on the MPR (inter-tertile boundaries: 1.33 and 1.68). In the lowest and middle MPR tertiles, significantly more cardiac deaths were observed than in the highest tertile. The age- and sex-corrected hazard ratio for the middle tertile was 7.9 (95% CI: 0.97 – 64.9) and for the lowest tertile 24.5 (95% CI: 3.2 – 186.2) (p=0.001). Also LV ejection fraction (LVEF) was of prognostic significance: HR for the middle tertile 1.7 (95%CI 0.5-6.4) and for the lower tertile 4.8 (1.4-16.0; p=0.015). After adding LVEF to the model, MPR remained significant with HR's of 6.5 (0.8-54.4) and 18.5 (2.3 -145.5)(p=0.004), whereas LVEF did not reach significance in this model. No difference in percentage mismatch between the three groups was observed (13.7 ± 10.8% in the lowest, 13.6 ± 11.7% in the middle and 11.1 ± 9.6% in the highest MPR tertile)

Thus, patients with IHD revascularized based on PET viability assessment who have a low MPR are at risk of cardiac death. In addition to viability, the MPR results of the PET scan should be taken into account.

2.1.2 Abdominal aortic calcification detected with routine vertebral fracture assessment: a strong predictor of cardiovascular events

In cooperation with Depts. Surgery (Division of Vascular Surgery), Clinical Pharmacology, Epidemiology and Cardiology

Aorta calcification is correlated with the degree of atherosclerosis in other arteries. Some studies showed that abdominal aorta calcification (AAC) detected by conventional x-ray systems can be a risk factor for cardiovascular outcomes. Vertebral fracture assessment (VFA) images performed by dual-energy x-ray absorptiometry (DXA), routinely used for osteoporosis screening, has been shown in previous studies to be able to detect aorta calcification with a minimal radiation dose of 0.01 mSv. We hypothesized that AAC detected by VFA images can predict incidences of cardiovascular events.

VFA images of 2500 subjects were evaluated by two physicians to score AAC according to an eight-point scoring scale. AAC-positive subjects (n=164) were divided into two groups according to mean AAC score. An age- and sex-matched random set of subjects (n=331) without AAC served as control group. Baseline cardiovascular risk factors, cardiovascular events (TIA, CVA, and myocardial infarction), and cardiovascular deaths were checked by the digital hospital information system. An enriched Cox regression model was applied for AAC classes versus cardiovascular outcomes using age and gender as covariates.

AAC-positive subjects were divided into two groups: low-AAC (score 1-3; n=105, age average: 68 ± 9 yr, 61% female), and high-AAC group (score>3; n=59, age average: 71 ± 11yr, 66% female). In the control group (score=0) age average was 66 ±8 yr, 66% female. Follow-up period for cardiovascular events was between 0.1 to 5 years (median: 2.7 year). Proportion of total (mortal or non-mortal) cardiovascular events within each group was: 1.2%, 6.7%, and 11.9% for control, low-AAC and high-AAC groups, respectively. Multivariate analysis using age and gender as covariates, showed significant higher cardiovascular events in both low-AAC (HR: 5.00; CI 95%: 1.4-17.2; p= 0.011) and high-AAC (HR: 7.00; CI 95%: 1.7-28.4; p= 0.007) groups, compared to the control group.

Thus, AAC routinely measured with VFA proved to be a strong predictor for cardiovascular events.

2.1.3 Left ventricular volume assessment by planar radionuclide ventriculography evaluated by MRI.

In cooperation with Dept. Cardiology

Assessment of left ventricular (LV) ejection fraction (LVEF) and LV volume are essential for the prediction of prognosis in cardiac disease. LVEF and LV volumes can be assessed with several imaging modalities. However, these are relatively expensive and time consuming. In contrast, planar radionuclide ventriculography (PRV) is a low-cost, fast and reliable technique for LVEF assessment. Yet, PRV for LV volume assessment is less common.

We aimed to validate a new count-based method (CBM) in comparison with the traditional geometrical method (GM) for the calculation of LV volumes with PRV, using magnetic resonance imaging (MRI) as reference.

Thirty cardiac patients underwent routine PRV with a standard dose of 500 MBq of ^{99m}Tc-pertechnetate and additional cardiac MRI. LV volumes of PRV data were calculated by two different methods. The traditional GM is based on the assumption that the shape of the LV can be approximated by an ellipsoid, whereas in CBM the volume is extracted from the projected count rates themselves.

The average LV ejection fraction measured with PRV was 49 ± 14 % (range 22 % to 70 %). The average end-diastolic volumes (EDV) measured with PRV were 151 ± 40 ml for GM, 177 ± 37 ml for CBM. The difference (mean ± sd) of EDV between PRV and MRI was -38 ± 23 ml for GM and -12 ± 27 ml for CBM. The correlation coefficients for EDV between both PRV methods and MRI were 0.89 ($p < 0.001$) for GM and 0.84 ($p < 0.001$) for CBM. The average end-systolic volume (ESV) measured with PRV were 81 ± 40 ml for GM, and 94 ± 42 ml for CBM. The difference (mean ± sd) of ESV between PRV and MRI was -23 ± 19 ml for GM and -9 ± 22 ml for CBM. The correlation coefficients for ESV between both PRV methods and MRI were 0.95 ($p < 0.001$) for GM and 0.91 ($p < 0.001$) for CBM. Bland-Altman plots for EDV and ESV are shown in Figures 1a and 1b.

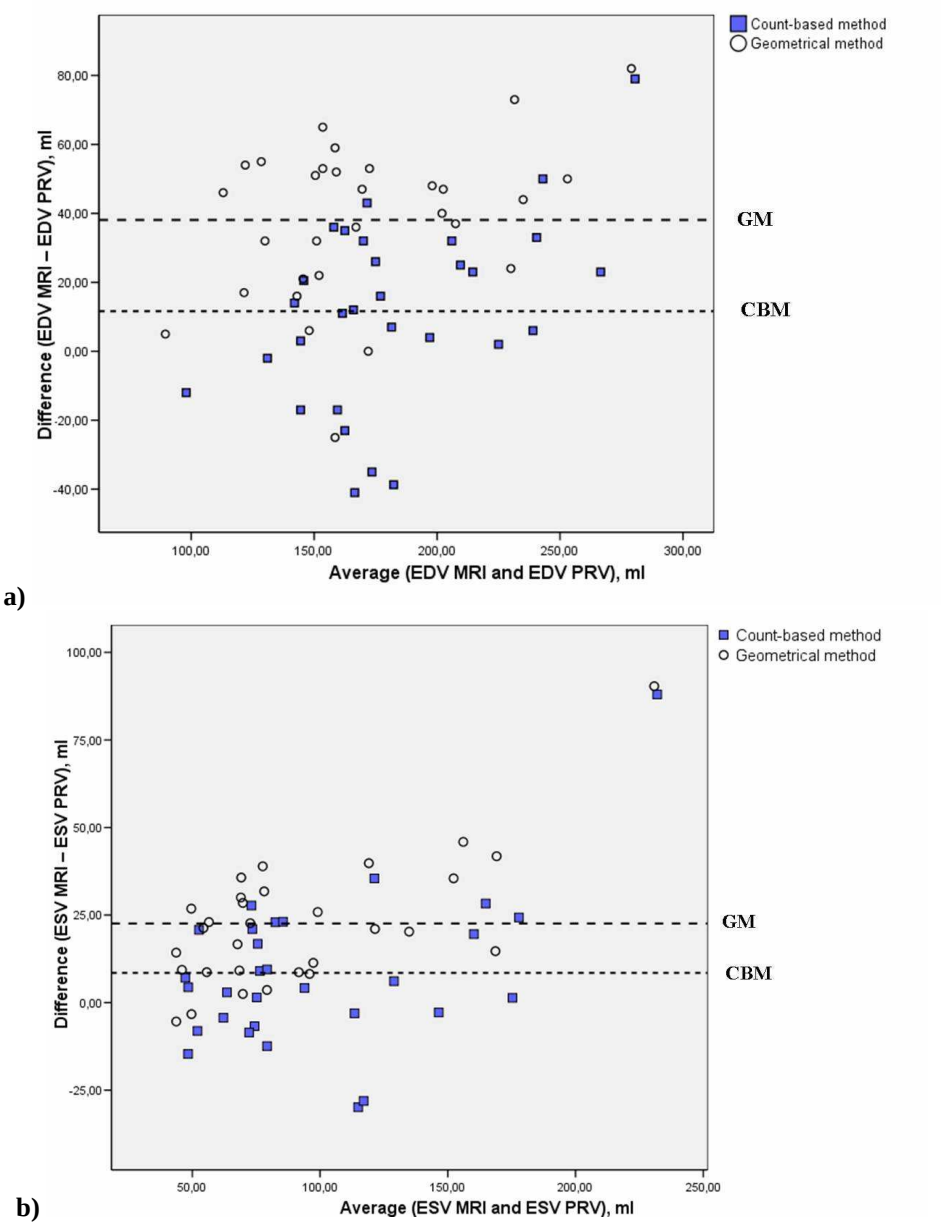

Figure 1. Bland-Altman plot for: a) EDV and b) ESV.

In conclusion, EDV and ESV calculated with PRV and CBM agree better with MRI than EDV and ESV estimated with GM. However, both PRV-based methods underestimate ESV and EDV slightly.

2.2 Neuroscience

2.2.1 Increased P-glycoprotein function in schizophrenia: A PET study with [^{11}C]-verapamil as a probe for P-glycoprotein function in the blood-brain barrier

In cooperation with Dept. Psychiatry, UMCG and GGZ Drenthe, Assen

In normal circumstances, the Blood-Brain Barrier (BBB) protects the brain against harmful substances from the environment. P-glycoprotein (P-gp), a major efflux pump in the BBB, limits the entry of drugs, peptides and other substances into the central nervous system. The permeability of the brain can be increased by modulation of the transport function of P-gp. Such modulation may be the result of different stimuli such as inflammatory mediators, known to play a role in schizophrenia. Moreover, P-gp function may be compromised in schizophrenia due to a functional polymorphism of the MDR-1 gene coding for P-gp. We hypothesized that P-glycoprotein function would be altered in dorsolateral prefrontal cortex, amygdala, thalamic nuclei, temporal areas as well basal ganglia since these areas are known to play a role in schizophrenia. We further hypothesised that a change in P-gp expression would be associated with polymorphisms of the MDR1 gene. In vivo assessment of P-gp function at the BBB was performed with PET and the tracer [^{11}C]-verapamil.

Ten patients with paranoid schizophrenia and ten matched controls underwent a [^{11}C]-verapamil PET scan. For all patients a PANSS (Positive And Negative Symptom Scale) was done at the time of the PET study and blood was drawn for MDR1 genotyping (polymorphisms T129C, G2677T/A and C3435T). Drugs with a known modulating effect on P-gp were excluded. The data were analyzed in three ways. First the data for the whole brain were compared between patients and controls (Logan's graphical model). Then a-priori defined brain regions were tested with SPM2 and appropriate small volume correction. Finally, a hypothesis generating test was performed on all voxels using SPM2 and FDR correction. In all cases the Volume of Distribution (VT) was used as a measure of P-gp function. Analysis of covariance was used to test for any influence of clinical parameters (number of psychotic episodes, antipsychotic medication in Haldol equivalents, score on PANSS scale) on measured P-gp function.

We found a significant decrease in VT in the temporal cortex (PFDR = 0.032), basal ganglia (PFDR = 0.019), amygdala (PFDR = 0.028), but not in thalamus (PFDR = 0.108), and prefrontal cortex (PFDR = 0.076). A trend towards a decrease of P-gp function in the entire brain was noticed after Logan analysis (p = 0.052). The same trend was seen in SPM (p= 0.09), mainly in temporal and frontal cortex (Figure 1). None of the cofactors had a significant effect on

VT. No differences were found in the influx parameter K1. No differences were seen between different MDR1 genotypes.

In conclusion, this study shows regionally decreased [^{11}C]-verapamil uptake in temporal cortex, amygdalae and basal ganglia in patients with schizophrenia, which corresponds to a regional increase in P-gp function in schizophrenia. An increase in P-gp function may be related to an inflammatory process, since proinflammatory cytokines appear to increase P-gp-activity in models of chronic neuroinflammation. An increased activity of P-gp may however also be induced by the use of antipsychotics in the patient group. Increased P-gp function may explain why treatment resistance may develop after sustained use of medication. Future studies that focus on the role of P-gp in schizophrenia without the confounding influence of medication, as well as studies that focus on the effect of antipsychotics on P-gp function are warranted.

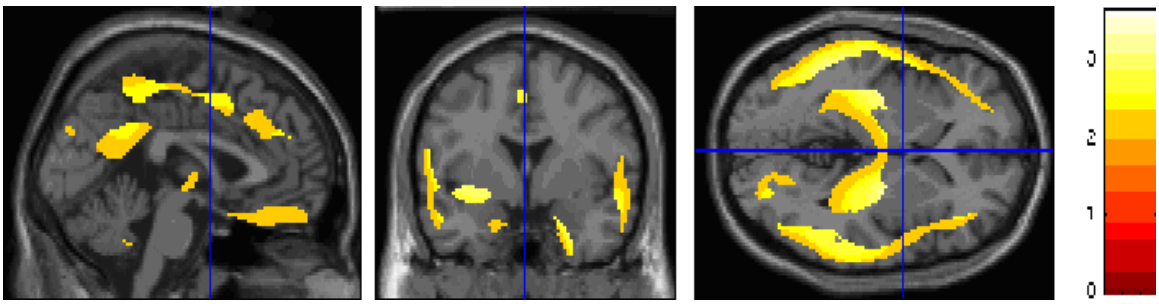

Figure 2: T-map showing a trend towards a decreased Distribution Volume of [^{11}C]-verapamil in 10 patients with schizophrenia, compared to 10 healthy controls in sagital, coronal and axial sections. The clusters of voxels at PFDR = 0.09 (in SPM2) on a MRI-overlay are shown.

2.2.2 Typical cerebral metabolic patterns in neurodegenerative brain diseases

In cooperation with Dept. Neurology

The differential diagnosis of neurodegenerative brain diseases on clinical grounds is difficult, especially at an early disease stage. Several studies have found specific regional differences of brain metabolism applying [18F]-fluorodeoxyglucose positron emission tomography (FDG-PET), suggesting that this method can assist in early differential diagnosis of neurodegenerative brain diseases.

We have studied patients who had an FDG-PET scan on clinical grounds at an early disease stage and included those with a retrospectively confirmed diagnosis according to strictly defined clinical research criteria. 96 patients could be included of which 20 patients with Parkinson's disease (PD), 21

multiple system atrophy (MSA), 17 progressive supranuclear palsy (PSP), 10 corticobasal degeneration (CBD), 6 dementia with Lewy bodies (DLB), 15 Alzheimer's disease (AD) and 7 frontotemporal dementia (FTD). FDG PET images of each patient group were analysed and compared to18 healthy controls using Statistical Parametric Mapping (SPM5).

Disease-specific patterns of relatively decreased metabolic activity were found in PD (contralateral parieto-occipital and frontal regions), MSA (bilateral putamen and cerebellar hemispheres), PSP (prefrontal cortex and nucleus caudatus, thalamus and mesencephalon), CBD (contralateral cortical regions), DLB (occipital and parieto-temporal regions), AD (parieto-temporal regions), and FTD (fronto-temporal regions).

The integrated method addressing a spectrum of various neurodegenerative brain diseases provided means to discriminate patient groups also at early disease stages. Clinical follow up enabled appropriate patient inclusion. This implies that an early diagnosis in individual patients can be made by comparing each subject's metabolic findings with a complete database of specific disease related patterns.

2.3 Oncology

2.3.1 16α-[^{18}F]-fluoro-17β-estradiol positron emission tomography (FES-PET) to detect ER positive tumor lesions in breast cancer patients with a diagnostic dilemma

Supported by grant RUG 2009-4529 of the Dutch Cancer Society

In metastasized, estrogen receptor (ER) positive breast cancer patients, it can sometimes be problematic to elucidate the nature of a new lesion or complaint with standard techniques. A biopsy is often required, but many lesions are difficult to access. Positron emission tomography (PET) with the tracer 16α-[^{18}F]-fluoro-17β-estradiol (FES) is used with success to predict therapy response. This noninvasive technique also provides information about the nature of these lesions by quantification of ER expression in these lesions. We analyzed the FES-PET results of 24 metastasized breast cancer patients who presented with a diagnostic dilemma.

Whole body FES-PET was performed, using a PET camera with 5 mm or a PET-CT with 2 mm spatial resolution, 60 minutes after intravenous administration of 185 MBq ^{18}F-FES. A lesion was defined positive when the SUV max was higher than 2.0. Patients received also the standard imaging modalities based on their complaints and/or lesions. The clinical indications to perform a FES-PET were: 1) to find a substrate for localized pain (2 patients); 2) to verify whether lesions found by standard techniques were of malignant origin (14 patients); and 3) to prove retained expression of ER after hormonal treatment before initiating a subsequent treatment line (8 patients).

No infusion-related adverse events were noticed. In the 2 patients with localized pain, bone scan and MRI in the patient with lower back pain and CT in the patient with abdominal pain showed no abnormalities. In contrast, FES-PET did detect an ER positive lesion in the left sacroiliac joint and in the gut, respectively. Radiotherapy and systemic anti-tumor treatment was initiated and complaints were resolved. In 14 patients, FES PET was performed to verify whether lesions detected on a bone scan (5 patients) or CT/MRI (9 patients) were malignant. In 7 of these patients, the lesions showed FES uptake, demonstrating the presence of metastases. The remaining 7 patients were negative, which reduces the likelihood of a malignant origin of these lesions. In all 8 patients that showed resistance to hormonal treatment, retained ER expression was found and consequently an additional line of hormonal treatment was initiated. In all three indication categories, FES-PET provided information which helped therapy decision-making.

Our preliminary experiences with FES-PET indicate that this technique has potential to support and guide clinical decision-making in case of clinical dilemmas in metastasized ER-positive breast cancer patients.

2.3.2 Effect of radiotherapy and chemotherapy on bone marrow activity: a ^{18}F-FLT PET study

In cooperation with Depts. Surgery, Radiotherapy, Hematology, UMCG, Dept. Radiation Oncology, Maastro Clinic, Maastricht, and Section of Hematology/ Oncology, Dept. Internal Medicine, University of Oklahoma Health Sciences Center, Oklahoma City, USA

Radiotherapy and chemotherapy are important treatment modalities for a variety of malignant tumour types. During therapy for malignant disease, the scope for further therapy is often limited by the capability of the bone marrow to withstand radiochemotherapy. Hematologic toxicity is commonly evaluated through peripheral blood counting, and occasionally, sampling of bone marrow via a biopsy. Neither method provides a comprehensive assessment, bone marrow biopsy is invasive, and both are subject to sampling variability. 3'-fluoro-3'-deoxy-L-thymidine (^{18}F-FLT) PET is a non-invasive technique related to the rate of DNA synthesis and visualizes the cycling activity of hematopoietic cells in the bone marrow compartment. In order to prove clinical consistency of marrow function and imaging, we investigated populations of patients typically seen in clinical practice, post radiation and post chemotherapy. In this feasibility study, populations were evaluated 1) to prove the ability of ^{18}F-FLT PET to visualize and quantify the activity of the bone marrow compartment, and 2) to evaluate the effect of radiotherapy and chemotherapy on bone marrow activity and to correlate this with clinical findings.

Bone marrow activity in the cervical region of 10 patients with laryngeal carcinoma that received a mean total dose of 68 Gy (range 30-41 fractions) was evaluated with ^{18}F-FLT PET before and 6 months after radiotherapy. Whole Body FLT images were assessed in 9 patients with non-seminomatous testicular germ cell tumors before and 4 months after the last chemotherapy consisting of 4 courses of bleomycin, cisplatin, and etoposide. Maximal standardized uptake value (SUVmax) was used to quantify FLT uptake in bone marrow at standard bone marrow regions.

A significant decrease in ^{18}F-FLT uptake was observed in all of the studied laryngeal carcinoma patients in the cervical region after RT of the adjacent bone marrow compartment. Tumor stage and additional field of view of RT was inversely related to the FLT uptake in bone marrow. The mean FLT SUVmax before RT was 3.0 ± 1.34 and after RT 1.94 ± 0.60 ($p = 0.013$). The

mean FLT SUVmax of the spine (Th5-Th12) regions outside the field of view of RT were stable and reproducible and not significantly different (5.56 ± 1.56 versus 5.16 ± 1.35, p = 0.16). Chemotherapy did not result in a significant difference of whole body SUVmax value, with a mean SUVmax of 4.99 ± 1.15 pre-chemo, and a mean SUVmax of 5.28 ± 1.0 post-chemo (p = 0.21). Laboratory analysis of hematologic parameters confirmed repopulation of bone marrow.

In conclusion, radiotherapy but not chemotherapy decreased FLT uptake in bone marrow. We conclude that FLT-PET is a potential non-invasive tool that can be used to quantify cellular division in the hematopoetic organ.

2.3.3 HER2-PET imaging with 89Zr-trastuzumab in metastatic breast cancer patients

In cooperation with Dept. Medical Oncology, UMCG and VU Medical Center, Amsterdam

Non-invasive diagnostic tools can optimize and evaluate HER2 directed therapy in HER2 positive breast cancer patients. HER2 imaging with ^{111}In-trastuzumab SPECT showed promising results (Perik *et al.*, J Clin Oncol 2006). To further optimize HER2 imaging, we developed ^{89}Zr-trastuzumab for high resolution, quantitative and sensitive PET imaging. A feasibility study was performed to determine optimal conditions (tracer dose and scans) for visualization HER2 positive lesions. This study was already initiated in 2008 and described in our Annaul Report of that year. In 2009, additional patients were included.

Trastuzumab was labeled with 89Zr according to Verel *et al.* (J Nucl Med 2003). HER2 positive metastatic breast cancer patients received 37 MBq ^{89}Zr-trastuzumab at 3 protein doses of trastuzumab: 1) 10 mg, or 2) 50 mg trastuzumab, or 3) 10 mg trastuzumab when on trastuzumab treatment. Patients underwent 2 or 3 PET-scans during 1-7 days post tracer injection. Images were analyzed visually and the relative tissue or tumor uptake was calculated as the ratio tissue/tumor to whole body uptake.

Fourteen patients were included. Optimal time point to assess ^{89}Zr-trastuzumab tumor uptake was 4-5 days post injection. The tracer dose of 10 mg was sufficient for patients on trastuzumab treatment, while best imaging results in trastuzumab naive patients were obtained with the 50 mg dose as 10 mg resulted in rapid tracer clearance. In trastuzumab naive patients, ^{89}Zrtrastuzumab clearance was not only dose-dependent but also clearly influenced by tumor burden, indicating a need for individualization of therapy. ^{89}Zr-trastuzumab PET-imaging detected not only known tumor lesions in the

liver, lung, bone and brain but also unknown brain and bone lesions were detected. The mean relative tumor uptake(± SD) in liver, bone and brain lesions was respectively 13.0±5.2, 4.2±1.5 and 3.5±4.2, while mean relative tissue uptake in normal liver, spleen, kidneys and brain was respectively 6.1±2.3, 2.7±0.8, 3.8±1.0 and 0.19±0.11.

In conclusion, HER2-PET imaging with ^{89}Zr-trastuzumab shows excellent tumor tracer uptake and can be used to detect HER2 positive breast cancer metastases and to quantify ^{89}Zr-trastuzumab uptake, non-invasively. Patients on trastuzumab can be imaged with 37 MBq ^{89}Zr-trastuzumab at a protein dose of 10 mg trastuzumab while trastuzumab naive patients require 50 mg.

2.4 Miscellaneous subjects

2.4.1 ^{18}F-FLT is an excellent tool to visualize the bone marrow compartment in patients with aplastic anemia

In cooperation with Depts Hematology and Pathology

Aplastic anaemia (AA) is a rare haematological disorder characterized by peripheral pancytopenia in association with a decreased bone marrow cellularity. Identification of patchy haematopoietic areas in the bone marrow compartment can be of value for making a proper diagnosis of AA. 3-^{18}F-fluoro-3-deoxy-L-thymidine (^{18}F-FLT) PET is directly related to the rate of DNA synthesis in cells. In this study we investigated the feasibility of visualization and quantification of the activity of the bone marrow compartment with ^{18}F-FLT PET in patients with AA.

We studied the haematopoietic stem cell compartment in 10 patients (8 male and 2 female) with AA. Six patients were studied at presentation (n=4) or relapse (n=2) and 4 patients were studied after having achieved a partial of complete normalization of peripheral blood cells following therapy with prednisolone, anti-thymocyte globulin and cyclosporine. Bone marrow histology and lab findings of these patients were correlated with the results of ^{18}F-FLT PET using visual analysis and the standardized uptake value (SUV). Data was compared to normal controls.

In patients with presenting or relapsing AA a significantly abnormal ^{18}F-FLT scan was observed. A significantly reduced uptake of the pelvis was observed in patients where no hotspot was present, while the vertebral column showed patchy areas that varied between 2-7 spots. The patchy areas showed increased uptake compared to normal controls. In patients (7-10) which were studied after therapy, the uptake of ^{18}F-FLT was not normalized. In most (75%) patients patchy areas of increased uptake were identified that were also localized in areas that normally do no demonstrate ^{18}F-FLT uptake, including the upper arms and upper and lower legs. In 6 patients with severe AA at presentation or relapse, the findings of the bone marrow biopsy corresponded to the peripheral blood cell counts; severe peripheral pancytopenia in conjunction with aplasia. In 2 patients with a partial or complete normalization of peripheral blood cell counts following treatment, the bone marrow biopsy demonstrated a hypocellularity to normocellularity of the different haematopoietic lineages.

In conclusion, the results of the present study demonstrate that ^{18}F-FLT is an excellent tool to visualize the haematopoietic compartment and identifies patchy areas of increased haematopoietic activity that can frequently be

recognized in patients with AA. Whether the uptake of ^{18}F-FLT by the bone marrow compartment is predictive for therapy response is unknown at the moment but requires further study in a larger group of patients.

2.4.2 ^{99m}Tc-labelled rituximab for imaging CD20 positive B-lymphocytes in inflammatory autoimmune disease patients

In cooperation with Unit of Rheumatology Allergy and Immunology, and Nuclear Medicine Unit, Second Faculty of Medicine and Surgery, "Sapienza" University of Rome, Italy

Rituximab is an IgG1κ isotype chimeric anti-CD20 monoclonal antibody that binds to CD20 antigen, expressed on the surface of B cells. These cells have been found in pathological infiltrates in tissues affected by autoimmune diseases and are implicated in disease progression. Therefore, attempts have been made to treat some autoimmune disease with Rituximab (Sjogren's, Rheumatoid Arthritis, Psoriasis, SLE, etc.)

The rationale of the present study was to radiolabel rituximab with ^{99m}Tc to image CD20 positive B-lymphocytes in affected tissues of patients with chronic autoimmune diseases and candidate to be treated with unlabelled rituximab, in order to provide a rationale for this type of therapy.

Rituximab (200μg) was labelled with 20mCi of $^{99m}TcO_4^-$ via 2-ME reduction of disulphide bonds. Several titrations were performed to obtain best labelling efficiency (LE). *In vitro* quality controls included SDS-PAGE and autoradiography of labelled antibody, Cysteine challenge, Immunoreactive fraction assay, binding assay on RAJI cell line (CD20+). *In-vivo* studies included a tumour targeting experiment in athymic nude mice xenografted subcutaneously with RAJI cells in thigh. Mice were injected in the tail vein with approx. 300 μCi (about 3μg) of radiolabelled anti-CD20 mAb. High resolution portable gamma camera (5x5cm field of view; 2mm spatial resolution) images were acquired at 1h, 3h, 6h and 20h after injection and target to background radioactivity ratios were calculated. After 20h all the mice groups were sacrificed and single organ counting assay was performed.

For a human pilot study, ^{99m}Tc-rituximab (10 mCi) was injected in 12 patients with inflammatory diseases (Sjogren's, Arthritis, Dermatitis, Miositis, Vasculitis, SLE, Psoriasis). Whole body and anterior-posterior images of regions of interest were acquired at 6h and 20h p.i.

Rituximab was always prepared with a high labelling efficiency (LE>95%) and specific activity (SA = 95-100 mCi/mg). SDS-PAGE and autoradiography analysis demonstrated its structural integrity, moreover, Cysteine challenge and

immunorective fraction assay also confirms its *in-vitro* stability and binding property. The results of tumor targeting experiment showed an increase of uptake of radiolabelled mAb to CD20+ tumor cells during the time period.

Scintigraphy with ^{99m}Tc-rituximab in patients showed rapid and persistent spleen uptake. Kidneys appeared to be the prominent source for excretion of the radioactivity. Inflamed joints and salivary glands were clearly detectable at 6h p.i. in patients with Arthritis and Sjogren's syndrome. In contrast, the patients with negligible CD20 positive B-lymphocytes counts, showed no uptake of this radiopharmaceutical in any inflamed tissue.
In conclusion, rituximab can be efficiently labelled with ^{99m}Tc with high LE using a direct method with 2-ME. It can be used for imaging CD20 positive B-lymphocyte infiltration, in particular in patients with inflammatory and autoimmune disease thus providing a rationale for anti-CD20 therapy.

BASIC RESEARCH

3.1 Animal studies

3.1.1. MicroPET for assessment of developmental neurotoxicity: A model study in rats with MeHg

In cooperation with TNO Quality of Life, Zeist, Radboud University Medical Center, Nijmegen, and SILS-CNS, University of Amsterdam

A developmental neurotoxicity study was carried out in rats with the model neurotoxin methylmercury (MeHg). The study was designed to gather information on the relationship between conventional indicators of developmental (neuro)toxicity and new innovative technologies such as (i) microPET, (ii) number of cerebellar granular cells assessed by stereological means (Q-neuropathology), (iii) electrophysiology of brain slices (field potentials in the stratum pyramidale of the CA1 region of the hippocampus), and (iv) examination of gene expression in the cerebellum.

Female F0 Wistar rats were treated with MeHg (0.1, 0.4, 0.7, 1.0, 1.5, or 2.0 mg/kg body weight, i.p., during day 13-15 of pregnancy) or corn oil. The F1 offspring was tested for several conventional endpoints (developmental landmarks, behaviour, neuropathology) and was also examined using the innovative techniques.

Cerebral [^{18}F]FDG uptake (representing brain activity) was repetitively and non-invasively monitored by microPET in F1 offspring from postnatal day 18 to 61 (PN18 - PN61). To this purpose, pups were intraperitoneally injected with 20 MBq [^{18}F]FDG and subsequently placed in a black box in a dark room with monotonous background noise (open field test). After 50 min, the pups were anesthetised with isoflurane gas and placed in the µPET scanner. A 20 min emission scan, followed by a 5 min transmission scan were made. PET data were reconstructed, co-registered to an age-dependent FDG template and a ROI analysis was performed.

No effects of prenatal exposure to MeHg were observed with the conventional guideline endpoints (behaviour, neuropathology). A significant effect of MeHg (at 1.5 mg/kg) was observed on the developmental landmark “vaginal opening” (retardation from PN40 to PN43).

The innovative technologies (Q-neuropathology, synaptic excitation in the hippocampus, gene expression in the cerebellum, and microPET) all detected effects of prenatal exposure to MeHg which could not be detected by

conventional means. The results point to a delay in neural development and in the onset of brain activity (see Figure 3).

The innovative technologies can lead to greater understanding of the processes and mechanisms underlying developmental neurotoxicity. These technologies are more sensitive, use fewer animals, and thus, save animals, time and costs.

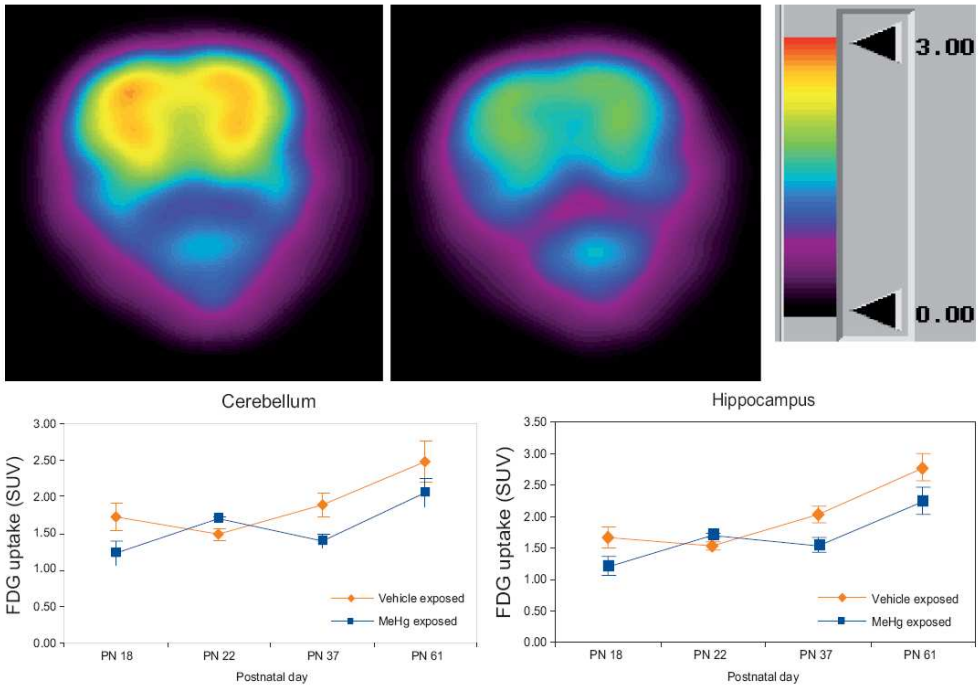

Figure 3. Effect of MeHg (1.5 mg/kg body weight) on brain metabolism in F1 offspring. Notice increased activity on PN22 and reduced activity on PN18, PN37 and PN61. The dip in glucose metabolism is retarded by 4 days in the prenatally exposed offspring.

3.1.2 Prenatal and early childhood alcohol exposure causes abnormal brain development

In cooperation with TNO Quality of Life, Zeist

During pregnancy and early childhood, the developing brain is highly vulnerable to toxic compounds. Alcohol is frequently used by pregnant women and may affect the developing brain. Several studies have shown that high alchohol intake by pregnant woman can cause disturbed behavior and abnormal brain morphology in the offspring. However, expert opinions are still divided on the effects of low to moderate alcohol consumption during pregnancy. In this study, we used FDG PET to investigate the feasibility of monitoring the

effect of prenatal and postnatal alcohol exposure on the development of brain function.

From 2 weeks before gestation to postnatal day 25, pregnant Wistar rats were exposed to alcohol via drinking water that contained 0% (control), 4% or 9% alcohol. After lactation, the offspring was given drinking water with the same alcohol concentration as their mothers until postnatal day 62. On postnatal day 18, 21, 35 and 62, FDG PET scans of the brains of the female offspring were made (n=5 per group). After intraperitoneal injection of about 25 MBq FDG, the animals were place in a black wooden box (1x1 m) in a dark room without external stimuli for 45 minutes. After the animals were anesthetized with isoflurane, a 15 minute emission scan was acquired, followed by an emission scan. At day 62, the animals were terminated and the body and brain weights were determined.

At day 62, the body weight (-21%, $p<0.000005$) and brain weight (-7%, $p<0.001$) of the animals in the 9% alcohol group was significantly lower than controls, whereas there were no significant differences between the 4% group and controls. In control animals, FDG brain uptake showed a significant decrease between day 18 and 21 (-23%, $p=0.002$), followed by significant increase between day 21 and 35 (+109%, $p=0.003$), whereas FDG uptake did not significantly change anymore between day 36 and 62 (-13%, $p=0.4$). This pattern in FDG brain uptake during the early development of control animals was in accordance with the data we had obtained in previous studies (see 3.1.1). In contrast to control animals, animals in both alcohol treatment groups did not show any significant differences in FDG brain uptake between consecutive scan days. In all alcohol treated animals, a gradual - but not statistically significant - increase (0-27%) in FDG brain uptake between two consecutive scan days was found, with the exception of a non-significant decrease in tracer uptake between day 18 and 21 in the 9% alcohol (-14%). At day 21, FDG brain uptake in the 4% alcohol group was significantly higher than in controls (+29%, $p<0.05$), whereas on the other days FDG brain uptake was 8-9% lower than in controls, but these reductions in brain uptake were not statistically significant. FDG brain uptake in the 9% alcohol group was always lower than that in both the 4% group and controls. The difference between the 9% alcohol group and controls was statistically significant on days 35 and 62 (-47% and -25%, $p<0.05$), whereas the difference between the 9% and the 4% alcohol group was only significant on day 35 (-33%, $p<0.05$).

Prenatal and postnatal exposure to alcohol causes a dose-dependent effect on brain metabolism in offspring.

3.1.3 Behavioral and functional consequences of herpes virus infection in rats

In cooperation with Dept.Psychiatry

Schizophrenia is a chronic, severe and disabling brain disease that is characterized by abnormal mental functioning and disturbed behavior. Many functional abnormalities have been found in the schizophrenic brain, including disturbances in dopaminergic and glutamatergic neurotransmission, on which the antipsychotic treatment of schizophrenia is (partly) based. Although schizophrenic patients can be treated, a cure has not yet been found. Perhaps one of the most important reasons for the lack of a cure for schizophrenia is that the etiology of the disease is still unknown. However, both gene mutations and various environmental factors have been suggested to play a role in the etiology of schizophrenia. Among the environmental factors that have been proposed to play an important role in the development of schizophrenia are infectious agents, including herpes viruses.

Herpes viruses are a family of DNA viruses, of which primary infection usually occurs during childhood without the appearance of clinical symptoms. Herpes viruses may underlie the development of schizophrenia in genetically predisposed individuals. Evidence for the role of herpes viruses in schizophrenia derives from studies where an association was found between sero-positivity for antibodies against herpes viruses and reduced prefrontal grey matter, increased cortical atrophy and lower cognitive functioning.

In order to gain more insight into the role of herpes viruses in schizophrenia, the behavioral and functional consequences of a herpes virus infection of the brain was studied in rats. Rats were intranasally inoculated with the herpes simplex virus type-1 (HSV-1), resulting in brain infection. To assess the behavioral consequences of HSV-1 infection of the brain, the open field behavior of the rats was studied. The functional consequences, focusing on glutamatergic and dopaminergic neurotransmission, were studied with the glutamatergic NMDA antagonist ketamine and with positron emission tomography (PET) using the dopamine D_2 receptor ligand [^{11}C]-raclopride, respectively. The neuroinflammation as a result of HSV-1 infection in the brain was studied using [^{11}C]-PK11195 PET. In addition, the effect of treatment with the antipsychotics clozapine and risperidone on the behavioral and functional consequences of HSV-1 infection of the brain was studied.

A total of 8 groups were used in this study: control and HSV-1 infected rats that received saline, ketamine, clozapine or risperidone daily for 5 consecutive days. The study design is shown in figure 4. Rats were intranasally inoculated with $1x10^7$ PFU of HSV-1, after which the first dose of saline, ketamine, clozapine or risperidone was given. Open field behavior was studied on day -1

pre-inoculation and on day 2 and 4 post-inoculation. The [^{11}C]-raclopride and [^{11}C]-PK11195 PET scans were performed on day 5 post-inoculation.

The first symptoms resulting from HSV-1 inoculation (ruffled fur, and irritated nose and eyes) were seen on day 2 post-inoculation in rats that received saline, where after the severity of the symptoms increased. On day 5 post-inoculation the most seen symptoms included behavioral signs, like stress and lethargy, and a hunched posture. Ketamine did not affect the first appearance and severity of the symptoms, but both clozapine and risperidone delayed the onset of symptoms. The symptoms in these rats were first seen on day 4 post-inoculation. At day 5 post-inoculation, when the rats did not receive clozapine and risperidone, the symptoms were not different from the rats that received saline.

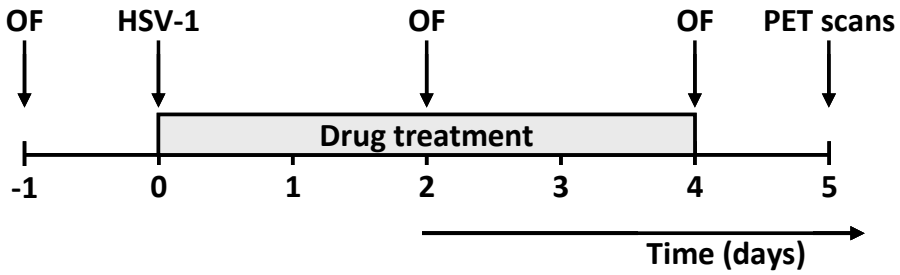

Figure 4. Study design. Rats were inoculated with HSV-1 or PBS (control) at day 0. Open field (OF) experiments were carried out on day -1 pre-inoculation and on day 2 and day 4 post-inoculation. [^{11}C]-PK11195 and [^{11}C]-raclopride PET scans were performed on day 5 post-inoculation. Drug treatment (saline, ketamine, clozapine and risperidone) started on day 0 and finished on day 4 post-inoculation.

The open field experiment showed an increase in the explorative behavior in HSV-1 infected rats, when compared to control rats. On day 4 post-inoculation the frequency of exploration (21.9±13.2 vs. 10.1±11, $p=0.008$) and the frequency of rearing (17.6±11.5 vs. 7.9±8.1, $p=0.006$) was statistically significantly higher in HSV-1 infected rats. Ketamine significantly decreased the frequency of rearing in HSV-1 infected rats only (1.5±2.0 vs. 17.6±11.5, $p<0.001$), on day 4 post-inoculation. In addition, the increased frequency of rearing in HSV-1 infected rats was decreased by clozapine (4.5±2.1 vs.17.6±11.5, $p=0.008$) and risperidone (9.0±8.5 vs. 17.6±11.5, $p=0.033$). Clozapine and risperidone did not affect open field behavior in control rats.

[^{11}C]-PK11195 PET (Figure 5) showed neuroinflammation in HSV-1 infected rats, throughout the whole brain ($p<0.05$, when compared to control rats). Most severe neuroinflammation was found in the bulbus olfactorius, frontal cortex and the brainstem. Ketamine did not affect neuroinflammation. However, in the rats that received clozapine and risperidone, [^{11}C]-PK11195 PET did not

show neuroinflammation, when compared to control rats that received clozapine and risperidone.

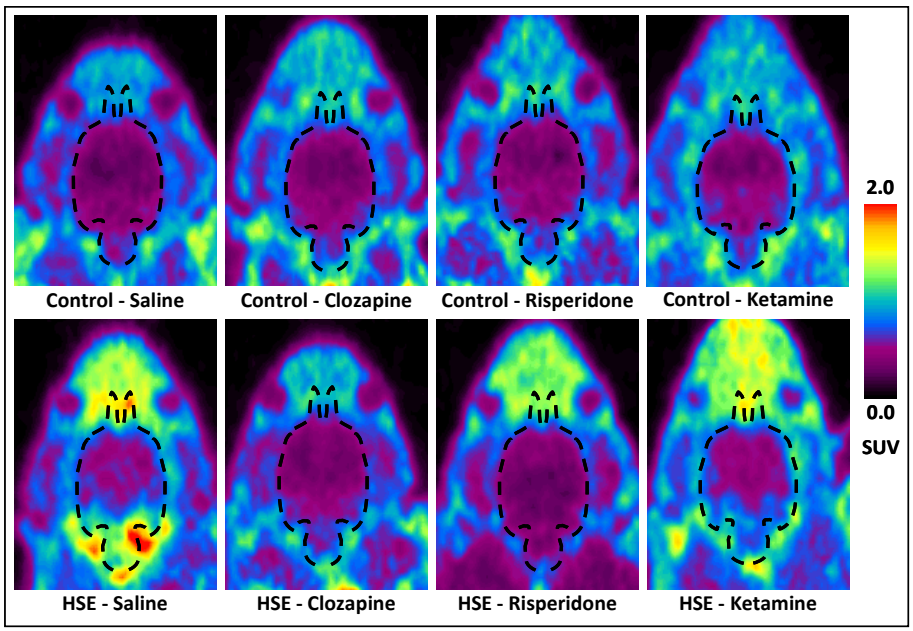

Figure 5. [^{11}C]-PK11195 small animal PET images of control rats (control) and rats inoculated with HSV-1 (HSE), which receive saline, clozapine, risperidone or ketamine, on day 5 post-inoculation. The images display a coronal play of the rats head at the level of the brainstem, in which the brain is delineated by a dashed line. The images represent brain uptake between 15 and 60 minutes after injection.

The [^{11}C]-raclopride binding potential, as a measure of dopamine D_2 receptor availability, was not affected by HSV-1 infection. In addition, clozapine and risperidone did not affect the [^{11}C]-raclopride binding potential. However, ketamine did cause a statistically significant increase in the [^{11}C]-raclopride binding potential in the frontal cortex (0.84±0.21 vs. 0.51±0.16, p0.046), in HSV-1 infected rats only when compared to control rats.

In conclusion, HSV-1 infection of the brain resulted in the appearance of disease symptoms, an increase in exploratory behavior and neuroinflammation, which were all decreased by the antipsychotics clozapine and risperidone. While ketamine did not affect HSV-1 induced neuroinflammation, the increased exploratory behavior was decreased by ketamine and an increase was found in the [^{11}C]-raclopride binding potential in the frontal cortex. Since both ketamine induced changes were seen in HSV-1 infected rats only, this suggests that HSV-1 influences glutamatergic and dopaminergic neurotransmission.

The antipsychotics induced decrease in HSV-1 induced neuroinflammation may imply a novel mechanism of action of antipsychotics in schizophrenic patients. In addition, HSV-1 may be responsible for the observed disturbances in glutamatergic and dopaminergic neurotransmission in schizophrenic patients. Additional research on the role of HSV-1 and the accompanied neuroinflammation as a potential target for the treatment of schizophrenic is warranted.

3.1.4 The role of vascular damage in the development of radiation-induced loss of pulmonary function

In cooperation with Dept.Radiotherapy

The risk of radiation pneumonitis limits the treatment dose and efficacy for many thoracic tumors. Therefore treatment optimization requires more insight into the risk factors for the development of radiation pneumonitis and mechanisms involved in radiation-induced pulmonary dysfunction. Previously we found that, depending on dose and irradiated volume, early damage in the lung manifests in two distinct forms: parenchymal and vascular inflammation (Novakova-Jiresova A et al. Int J Radiat Oncol Biol Phys 2007; 67(5): 1510-8).

Since vascular damage occurs at lower doses we hypothesize that radiation-induced vascular damage is the primary determinant of early pulmonary function loss. Radiation-induced endothelial cell loss may initiate vascular damage leading to pulmonary vascular remodeling. Moreover, endothelial dysfunction is known as a hallmark of pulmonary hypertension. Therefore, in this study the relation between radiation-induced vascular damage, pulmonary hypertension and pulmonary function loss was investigated at three time points after radiation.

Different combinations of vascular and parenchymal damage were induced by high-precision proton irradiation to 75, 50 and 33% of rat lungs with 17, 22 and 28 Gy respectively. To assess pulmonary function loss, breathing rate was measured before and every two weeks after irradiation. Cardiac function was assessed with FDG-PET 8, 16 and 26 weeks after irradiation. Subsequently the rats were sacrificed and lung tissue was sampled for pulmonary vascular remodeling analysis. Right ventricle hypertrophy (RVH) was assessed directly by measuring the ratio of right ventricle to left ventricular plus septal weight.

Features of pulmonary vascular remodeling such as endothelial cell loss, hypertrophy and proliferation of smooth muscle cells in irradiated lung tissue were comparable to those common in pulmonary hypertension models. Surprisingly these features were also present outside of the radiation field.

RVH as a known consequence of pulmonary hypertension was detected both by PET scans as an increase in FDG uptake of the right ventricles and also directly by the right ventricle/(left ventricle+septum) weight ratio. This effect increased with increasing irradiated lung volume (Fig. 6). Moreover, increasing the irradiated volume led to a more pronounced reduction of pulmonary function. Interestingly, a remarkable correlation (r=0.988) between lung function and RVH was found early after irradiation. This strong correlation indicates that early pulmonary function loss depends strongly on radiation-induced vascular damage. Therapeutic interventions targeting early radiation-induced vascular damage by e.g. repairing endothelial cell injury may be a promising strategy for further optimization of thoracic radiotherapy.

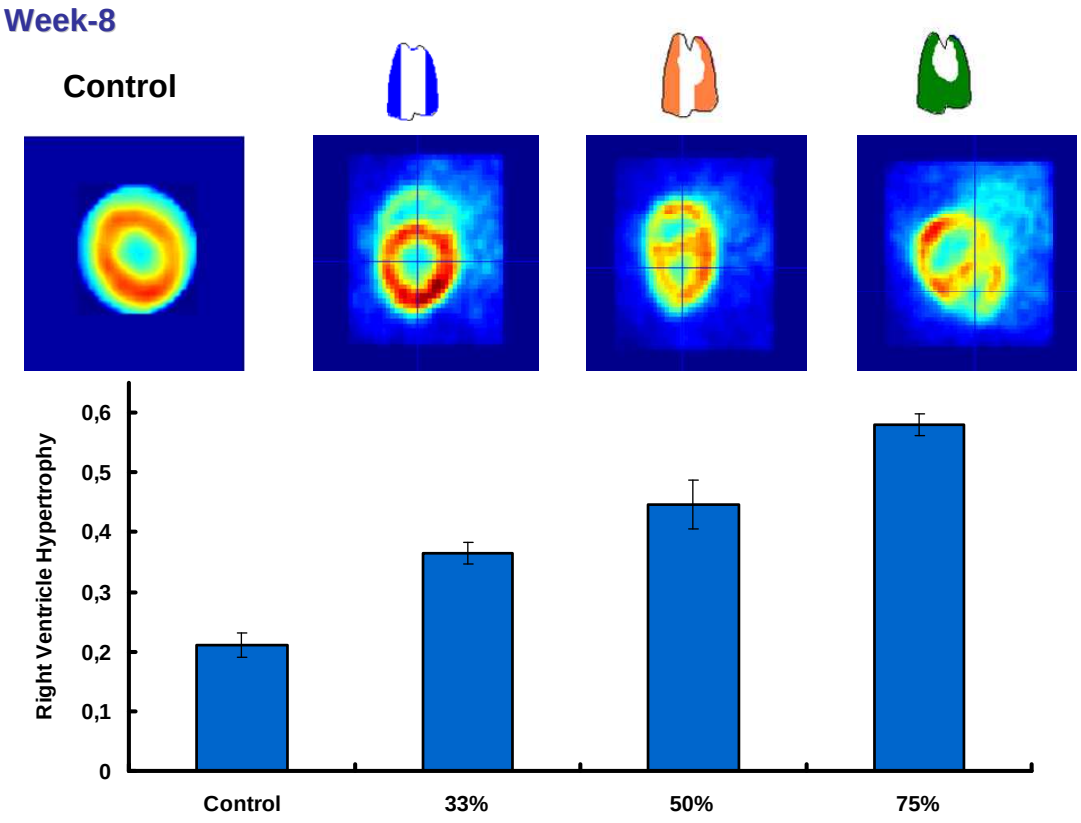

Figure 6. Right ventricular hypertrophy detected in FDG-PET scans and by directly measuring the ratio of right ventricle to left ventricular plus septal weight, 8 weeks after irradiating different fractions of the lung volume.

3.1.5 ^{13}N-ammonia enables quantification of left ventricular volume and left ventricular ejection fraction in rats using ECG-gated micro-PET

In cooperation with Depts.Cardiology and Epidemiology, Groningen, and Dept. Nuclear Medicine, University Hospital Münster, Münster, Germany

In vivo assessment of therapy effects on cardiac function is important in pre-clinical studies. Measuring left ventricular volumes (End Diastolic Volume, EDV, End Systolic Volume, ESV) and ejection fraction (LVEF) with gated positron emission tomography (PET) is a valuable tool to monitor cardiac function. In nuclear imaging, ^{13}N-ammonia is used for quantification of myocardial perfusion. However, data on the use of this tracer for LV-function assessment in rats is lacking. The aim of this pilot study was to evaluate ^{13}N-ammonia as a PET tracer for quantification of LV volumes and LVEF in rats using ECG gated micro-PET. A direct comparison was made with the reference compound ^{18}F-FDG.

^{13}N-ammonia and ^{18}F-FDG were sequentially injected into healthy Wistar rats (n = 5, i.v.) and Wistar rats with myocardial infarction (MI) (n = 4, i.v.). ^{13}N-ammonia and ^{18}F-FDG scans were made using a dedicated small-animal PET scanner (microPET Focus 220). The micro-PET data were reconstructed into 8 ECG-gated bins. A validated automated 3-dimensional segmentation algorithm was used to identify the endocardial contours to calculate LV volumes (Stegger L. et al., *J Nucl Med.* 50:132-138,2009). A Bland-Altman assessment for agreement was used to compare results obtained with the two tracers. The range of agreement was defined as mean bias ± 1.96 SD. LV volumes and LVEF for both tracers and groups are presented as mean ± SD.

In the control animals, mean values for EDV were 0.44 ± 0.08 ml and 0.47 ± 0.12 ml, whereas mean values for ESV were 0.09 ± 0.06 ml and 0.10 ± 0.04 ml, for ^{13}N-ammonia and ^{18}F-FDG respectively. Mean LVEF values of ^{13}N-ammonia were 81.9 ± 8.4 %, compared to 79.7 ± 6.9 % for ^{18}F-FDG. In the infarcted animals, mean values for EDV were 0.88 ± 0.20 ml and 0.84 ± 0.25 ml, whereas mean values for ESV were 0.47 ± 0.12 ml and 0.41 ± 0.13 ml, for ^{13}N-ammonia and ^{18}F-FDG respectively. Mean values of LVEF using ^{13}N-ammonia were 45.9 ± 5.5 %, whereas ^{18}F-FDG rendered values of 51.2 ± 9.4 %. In the complete group the Bland-Altman analysis indicated that the 95 % limits of agreement between ^{13}N-ammonia and ^{18}F-FDG for measuring LV volumes ranged from -0.28 and 0.25 mL with a mean difference of -0.01 ± 0.14 mL. For LVEF of ^{13}N-ammonia and ^{18}F-FDG these limits ranged from -14.0 to 19.0 % with a mean difference of 2.6 ± 8.5 %.

In conclusion: This pilot study indicated that LVEF and LV volumes in rats can be determined using ^{13}N-ammonia, and that the estimated values are in good agreement with values provided by ^{18}F-FDG.

3.1.6 Opposite effects of chronic stress and antidepressant treatment on P-glycoprotein-mediated drug efflux at the blood-brain barrier

In cooperation with Depts. Psychiatry and Molecular Neurobiology

The blood-brain barrier (BBB) protects the brain from potentially harmful substances. A major efflux pump at the BBB is P-glycoprotein (P-gp), which acts as a gate keeper. P-gp is a key determinant of drug entry to the brain. P-gp function is modulated by a wide variety of stimuli, such as proinflammatory cytokines. Depressive disorders have been linked to neuroinflammatory events. In a recent PET study, an increased function of P-gp at the BBB was found in medicated patients with major depressive disorder (MDD) (de Klerk et al., *Int.J.Neuropsychopharmacol*. 1-10, 2009). The interpretation of this finding was complicated because of the use of antidepressants.

The present study was aimed at disentangling the influence of stress and of the use of an antidepressant on the function of P-gp. Our hypothesis was that chronic stress inhibits P-gp whereas antidepressant treatment increases P-gp-mediated drug efflux. [^{11}C]-verapamil positron emission tomography (PET) was used for assessment of P-gp function in vivo.

In a first experiment, 16 male Wistar rats underwent a 3–week footshock procedure as a model of human depression. In a second experiment, 8 rats were chronically treated with the antidepressant venlafaxine (25 mg/kg/d) via an implanted osmotic mini-pump. In both experiments, control animals were left undisturbed in their home cages. At the end of the 3-week treatment, microPET imaging with [^{11}C]-verapamil was performed in the chronic stress and antidepressant treatment groups, plus the two control groups. The distribution volume (V_T) of [^{11}C]-verapamil within the entire brain was used as a measure of P-gp function.

In the chronically stressed rats, the distribution volume (V_T) of [^{11}C]-verapamil was significantly increased, whereas treatment with venlafaxine had the opposite effect and caused a significant reduction in V_T. The changes in V_T could not be attributed to a difference in the influx rate constant of [^{11}C]verapamil.

Our data indicate that P-gp function at the BBB is inhibited by chronic stress and increased by chronic administration of venlafaxine. Apparently, chronic stress in rats impairs blood-brain barrier function because of a decreased function of P-glycoprotein. This may imply an increased vulnerability of the brain to toxic substances and an increased chance of central nervous system dysfunction. This finding supports the hypothesis that reduced BBB-function contributes to the pathophysiology of stress-related disorders such as depression. Furthermore, our results suggest that an additional therapeutic

benefit of antidepressants may be normalization of P-gp activity and BBB-function. Further studies using structurally different antidepressants are required to confirm these findings.

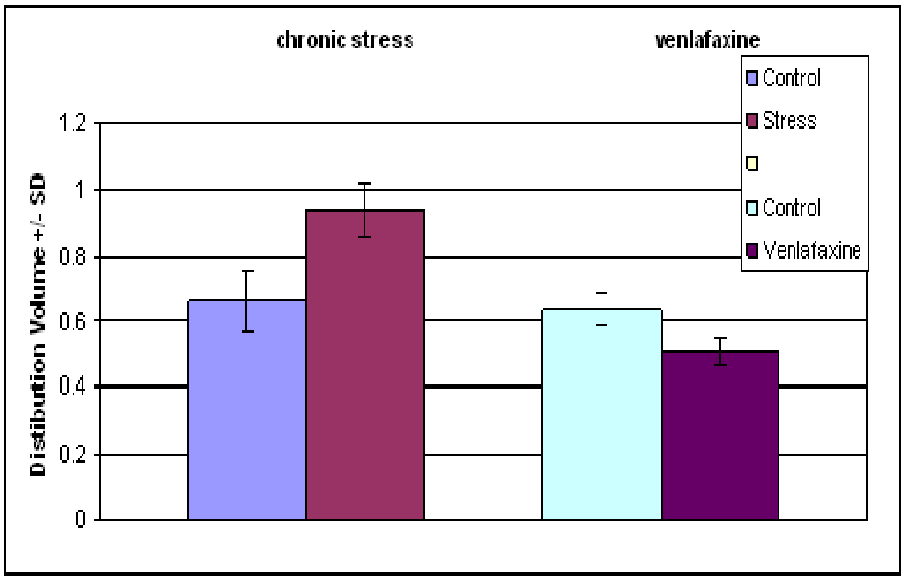

Figure 7. Changes of the distribution volume of ^{11}C-verapamil in rat brain after chronic stress and treatment of animals with venlafaxine.

3.1.7 Indoleamine 2,3 Dioxygenase: a Link Between Neuroinflammation and Depression in Alzheimer's Disease?

In cooperation with Depts.Molecular Neurobiology, Biological Psychiatry, Neuroscience and Laboratory Center (Groningen) and Dept. Anatomy and Neurosciences, VU University Medical Center, Amsterdam

Alzheimer's disease (AD) is an irreversible neurodegenerative disorder which is often accompanied by symptoms of depression, anxiety, irritability and mood instability. Sometimes patients have undergone long time treatments against these psychiatric symptoms before a clinical diagnosis of AD was made. Thus, anxiety/depression is not just a side effect of AD but is rather an integral part of the typical symptoms and may also be of predictive value for disease development.

Neuroinflammation plays an important role in AD as well as in depression. A central role for indoleamine 2,3-dioxygenase (IDO), an enzyme which is activated by pro-inflammatory cytokines, has been suggested. IDO metabolizes tryptophan, the precursor of serotonin, via the kynurenine pathway. The resulting depletion of serotonin levels in the brain may account for symptoms of depression, whereas neurotoxic end products of the kynurenine pathway

could account for neurodegeneration. This makes IDO a very likely common factor in inflammation, depression and neurodegeneration. The purpose of this study was to determine whether neuroinflammation causes increased IDO levels in the brain leading to depressive-like behaviour and increased anxiety.

In male C57Bl/6J mice (9wk old) neuroinflammation was induced by a single intracerebroventricular injection of lipopolysaccharide (LPS). Cerebral inflammation was monitored 1, 2, 3 and 4 days after the injection with small animal PET scanning using the inflammatory marker [11C]-PK11195.

LPS induced neuroinflammation culminated 3 days after injection. The animals were tested on the 3rd and 4th day after injection in several behavioural tasks. These behavioural studies showed that LPS injected animals had higher anxiety levels, were less explorative and they also showed more depressive-like behaviour compared to vehicle injected animals. These findings were paralleled by a significant increase of IDO in the brain stem, a trend towards decreased levels of tryptophan and increased levels of kynurenine in the serum.

In summary, our findings show that neuroinflammation leads to increased IDO expression in the brain stem which may be responsible for depressive-like symptoms and increased anxiety.

3.1.8 Validation of [^{11}C]-5-HTP for measurement of serotonin synthesis in the rat brain, using microPET

In cooperation with Dept. Pathology and Laboratory Medicine

The neurotransmitter serotonin (5-HT) is synthesized in serotonergic neurons. Serotonin synthesis occurs in two enzymatic steps: 1) metabolism of the amino acid tryptophan to 5-HTP by tryptophan hydroxylase (TPH) and 2) conversion of 5-HTP to 5-HT by aromatic amino acid decarboxylase (AADC). So far, no well-established tracer for measuring serotonin synthesis exists.

We have examined if changes in serotonin synthesis in the rat brain can be measured by the tracer [^{11}C]-5-HTP and microPET. [^{11}C]-5-HTP is chemically identical to endogenous 5-HTP and thus a substrate for AADC.

Radioactive metabolites in rodent plasma were measured and biodistribution studies were performed to assess uptake of the tracer in different organs. Since serotonin is formed in peripheral organs, peripheral AADC activity was inhibited with carbidopa to increase tracer delivery to the brain, and the dose-dependency of the carbidopa effect was examined. Both enzymes involved in 5-HT synthesis were inhibited (TPH with p-chlorophenylalanine [PCPA] and AADC with NSD 1015). Rats were depleted of the precursor tryptophan by

providing them with a synthetic diet with low tryptophan content. The microPET data was analyzed with a two-tissue compartment model with irreversible tracer trapping or with graphical analysis (Patlak plot).

Carbidopa increased the brain uptake of [^{11}C]-5-HTP most efficiently at a dose of 10 mg/kg. Therefore, all groups were treated with 10 mg/kg carbidopa. After 60 min there was still 70-80 % of parent tracer present in plasma of control and tryptophan depleted animals, indicating no need for metabolite correction. High uptake of the tracer in kidney and urine indicated renal clearing. There was a remarkably high uptake in the pancreas.

Surprisingly, neither treatment with NSD 1015 nor dietary tryptophan depletion affected [^{11}C]-5-HTP trapping in rat brain. However, inhibition of TPH resulted in a decrease.

A possible explanation of our data is that after AADC inhibition, [^{11}C]-5-HTP rather than [^{11}C]-5-HT accumulated in brain and contributed to the radioactive signal. Tryptophan depletion may not have had any effect because of the minor decrease (~ 30%) in plasma levels of unbound tryptophan. Since [^{11}C]-5-HTP could detect changes in the activity of the rate-limiting enzyme TPH, HTP-microPET may provide an indication of serotonin synthesis rates. However, the effect of PCPA on [^{11}C]-5-HTP trapping is small whereas PCPA should have major effects on serotonin synthesis. This raises the question if [^{11}C]-5-HTP is sensitive enough to measure serotonin synthesis in rat brain.

3.1.9 Effect of ageing on sigma-1 receptor density in the healthy brain: a microPET study with ^{11}C-SA4503

In cooperation with Depts. Neurosciences and Molecular Neurobiology

Sigma-1 receptors are distinct from any other known neurotransmitter or hormone binding site and have a wide distribution within the CNS and in peripheral organs. Unlike the density of dopamine, serotonin, acetylcholine and glutamate receptors which reduces during aging, sigma-1 receptor density has been reported to be preserved or even increased in primate brain during healthy aging, although it is reduced in the brain of Alzheimer patients compared to age-matched healthy controls. Sigma-1 agonists are potentially useful in the treatment of neurodegenerative disease, stroke, and depression.

PET studies of sigma-1 receptors have been performed in primate brain but not in the aging brain of rodents. Quantification of sigma-1 receptors in rodent brain could be of interest for the study of animal models of human disease and the mechanisms of action of sigma-1 agonists. The aim of this study was to

measure sigma-1 receptor density in young and aged rats using the agonist tracer ^{11}C-SA4503 and microPET.

Sigma-1 receptors in young (6 weeks) and aged (24 months) Wistar Hannover rats were visualized using ^{11}C-SA4503. A canula placed in a femoral artery was used for blood sampling. The time-dependent uptake of ^{11}C-SA4503 in rat brain was measured with a Siemens/Concorde microPET Focus 220 camera, and various tracer-kinetic models were fitted to this data, using plasma radioactivity as input function. Radioactive metabolites in plasma were quantified using reversed-phase HPLC.

Preliminary data analysis indicates that sigma-1 receptors (quantified as the distribution volume of ^{11}C-SA4503 from a Logan plot) are preserved rather than increased in Wistar Hannover rats during healthy ageing. Metabolite correction of the plasma input function has a large impact on the calculated distribution volume; therefore this correction seems essential for group comparisons.

3.1.10 Preparation and preliminary biological evaluation of novel bombesin receptor ligands

In cooperation with Dept.Urology and Dept.Surgery, Martini Hospital, Groningen

Six new tracers for bombesin receptors have been prepared: ^{18}F-FB-BNC5, ^{18}F-FB-BNC6, ^{123}I-Cubane-BN(7-14), ^{123}I-Cubane-BNC5, ^{123}I-Cubane-BNC6, ^{99m}Tc-HYNIC-BN(7-14)dimmer. Binding of three of these ligands (^{18}F-FB-BNC5, ^{18}F-FB-BNC6, ^{123}I-Cubane-BN(7-14)) to the target receptor has been confirmed by cell experiments. The Log P value of the tracers was determined (Table 5).

Table 5. Lipophilicity (measured log P) of bombesin receptor ligands

	^{99m}Tc-HYNIC-BN(7-14)	^{18}F-FB-BNC5	^{18}F-FB-BNC6	^{123}I-cubane-BN(7-14)
LogP	-1.60	-0.51	0.84	1.20
SD	0.06	0.01	0.03	0.02

The in vitro stability of ^{18}F-FB-BNC5, ^{18}F-FB-BNC6 and ^{123}I-Cubane-BN(7-14) in saline and serum was investigated. The tracers are quite stable in saline solution. The in vitro stability of ^{18}F-FB-BNC5 is excellent, RCP was higher than 95% after 3 h incubation with serum. However, ^{18}F-FB-BNC6 is quite unstable in the serum. Most of the tracer was degraded within 1 h of incubation with serum. The stability of ^{123}I-Cubane-BN(7-14) was also relatively poor.

RCP of ^{123}I-Cubane-BN(7-14) was 81%, 52% and 9% after 1, 2, 4 h incubation with serum.

The in vitro binding affinity of several bombesin analogues were compared. (Table 6)

Table 6. Affinity of bombesin analogues to the target receptor

	BN(1-14)	BN(7-14)	*H-BN(7-14)	BNC5	BNC6	BN7
IC_{50}(nM)	3.48	3.27	12.81	26.03	248.2	462.5

*H-BN(7-14)=HYNIC-Aca-BN(7-14)

The IC_{50} values of bombesin C5 and C6 are in the acceptable range.

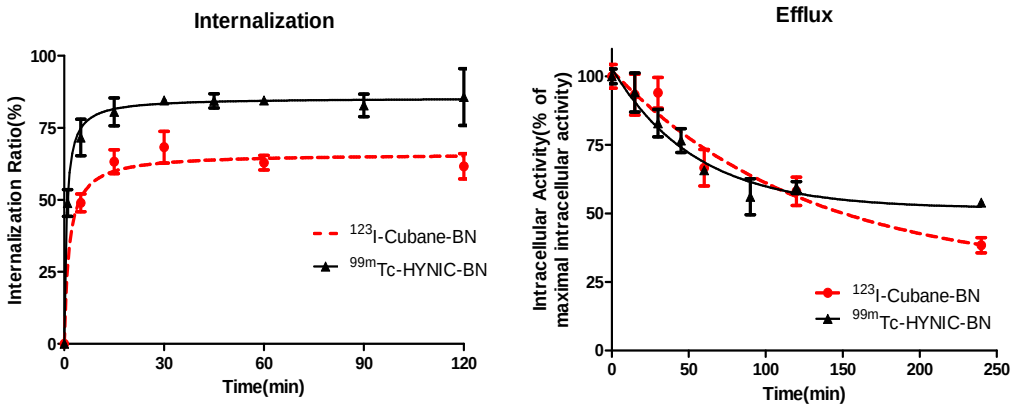

Figure 8. Internalization and efflux kinetics of ^{123}I-Cubane-BN(7-14) and ^{99m}Tc-HYNIC-BN(7-14)

The internalization and efflux kinetics of ^{123}I-Cubane-BN(7-14) were investigated (Fig.8). The internalization ratio of ^{123}I-Cubane-BN(7-14) is relatively low but as fast as ^{99m}Tc-HYNIC-BN(7-14). The efflux of ^{123}I-Cubane-BN(7-14) is slower, but less ^{123}I-Cubane-BN(7-14) is retained in PC-3 cells as compared to ^{99m}Tc-HYNIC-BN(7-14).

Biodistribution studies were performed in twelve subcutaneous human prostate cancer-bearing athymic mice 30, 60 and 240 minutes after injection of ^{99m}Tc-HYNIC-BN(7-14). Tumour uptake at these intervals was 2.2±0.6, 1.5±0.4 and 0.67±0.26, respectively. There was also high uptake in the GRPR-rich pancreas, as expected, and radioactivity was excreted via the renal-urinary system. Injection of an excess of cold HYNIC-BN(7-14) in four mice prior to

injection of ^{99m}Tc-HYNIC-BN(7-14) significantly reduced uptake of the radiotracer in the tumour.

MicroSPECT scans of seven mice were performed after injection of ^{99m}Tc-HYNIC-BN(7-14). Excellent tracer uptake was noted in tumour, pancreas and kidneys. Further data analysis is in progress. A human pilot study with this tracer in 20 patients with prostate cancer is expected to start in 2010.

3.1.11 Poly(trimethylene carbonate) as barrier membrane in rat mandibular defects. An evaluation by micro-CT.

In cooperation with Dept. Oral and Maxillofacial Surgery

The objectives of this study were to determine whether a new degradable synthetic barrier membrane composed of Poly(trimethylene carbonate) (PTMC) can be useful in implant dentistry and to compare it with collagen.

In 123 male Sprague-Dawley rats, a standardised 5.0 mm circular defect was created through the right angle of the mandible. New bone formation was evaluated by post-mortem micro-CT (µCT) imaging. Three groups (control, PTMC, collagen) were evaluated at 3 time intervals (2, 4 and 12 weeks). In the membrane groups the defects were covered; in the control group the defects were left uncovered. Data were analysed using a multiple regression model.

New bone formation could be detected by post-mortem microradiography in 122 samples and by µCT imaging in 122 samples. Bone formation was progressive in 12 weeks, when the mandibular defect was covered with a membrane. Overall, significantly more bone formation was observed underneath the collagen and PTMC membranes than the control group ($p<0.05$). There were no differences in bone formation between the groups treated with collagen and PTMC membranes (69% vs 70%, $p=0.98$).

In contrast to uncovered mandibular defects, substantial bone healing was observed in defects covered with a PTMC membrane. Moreover, bone formation in PTMC covered defects was the same as in the defects covered with collagen.

3.1.12 Evaluation of [^{18}F]-FEAnGA as a PET tracer for β-Glucuronidase Activity

In cooperation with Dept. Therapeutic Gene Modulation, University Center of Pharmacy

Extracellular β-glucuronidase (β-GUS) in tumors has been investigated as a target-enzyme for prodrug therapy, as it can convert nontoxic prodrugs into cytostatic drugs, thus decreasing cytostatic side effects while therapeutic efficacy is maintained. To optimize β-GUS-based prodrug therapies, noninvasive positron emission tomography (PET) imaging could be a useful tool by providing information regarding the localization and activity of β-GUS**.** Recently, we developed a promising PET tracer, 1-O-(4-(2-fluoroethyl-carbamoyloxymethyl)-2-nitrophenyl)-O-β-D-glucopyronuronate ([^{18}F]-FEAnGA) that proved to be selectively cleaved by β-GUS.

C6 glioma cells incubated with the tracer and *Escherichia coli* β-GUS or bovine liver β-GUS showed a 4 and 1.5-fold higher uptake of radioactivity respectively, as compared to control C6 cells without β-GUS. Incubation of CT26 murine colon adenocarcinoma cells or the genetically engineered CT26mβGUS cells, which express membrane-anchored GUS on the outer cell membrane, resulted in a 3 fold higher uptake of the tracer into GUS expressing cells as compared to control cells (Fig.9). The efflux analysis of [^{18}F]-FEA indicate that 50% of the cell-associated radioactivity is bound loosely to the extracellular domain. Nevertheless, it was observed that in the absence of radioactivity in the medium, 50% of the radioactivity still remains trapped in the cells.

In vivo microPET studies in mice bearing both CT26 and CT26mβGUS tumors showed that [^{18}F]-FEAnGA exhibited a 2 times higher retention of radioactivity in the tumor expressing β-GUS (SUV 0.25 ± 0.08) than in the control tumor (SUV 0.17±0.07). Wistar rats bearing C6 glioma tumors showed an increased accumulation of radioactivity in the viable part of the tumor with increasing necrotic fraction of the tumor (R^2=0.89; P=0.0004). [^{18}F]-FEA did not show any difference in tracer uptake between tumors (Fig.10). Metabolite analysis of [^{18}F]-FEAnGA in mice revealed that the conversion of [^{18}F]-FEAnGA into [^{18}F]-FEA was 2 times higher in CT26mβGUS tumors than in CT26 tumors. The radioactivity accumulation in CT26/CT26mβGUS tumors correlated well with the conversion of [^{18}F]-FEAnGA into [^{18}F]-FEA (R^2=0.68; P=0.02). In addition, we were able to correlate the accumulation of radioactivity in the viable part of the C6 tumors with the extent of necrosis (R^2=0.89, P=0.0004)

In conclusion, [^{18}F]-FEAnGA is a suitable PET tracer for evaluation of β-GUS activity, since it is specifically cleaved by β-GUS and the released [^{18}F]-FEA remains attached to targeted cells. Furthermore, necrotic C6 tumors where extracellular β-GUS levels are elevated mainly because of secretion by infiltrating neutrophils and macrophages (and to some extent because of secretion of β-GUS by necrotic cells) have shown to be an appropriate model for studying the glucuronide prodrug approach.

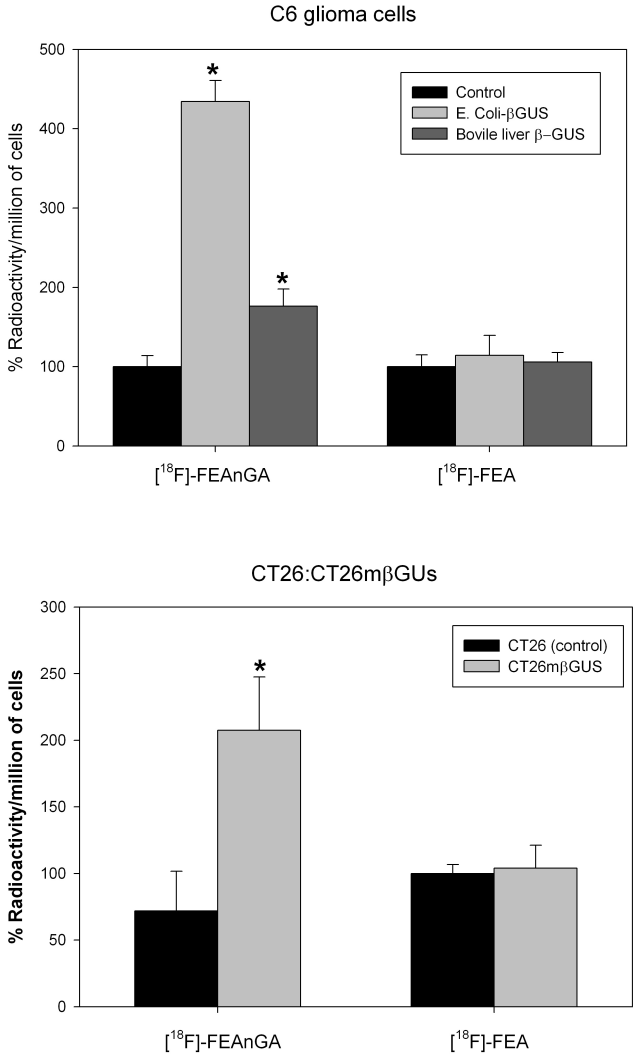

Figure 9. Cell-associated radioactivity of [^{18}F]-FEAnGA and [^{18}F]-FEA in control C6 cells and in C6 cells in the presence of E.Coli β-GUS and bovine liver β-GUS (A) and in control (CT26)

and CT26mβGUS cells (B). Data are expressed as % Radioactivity/million cells and are mean values of triplicate samples ± SD.* P<0.05, paired bidirectional Student *t* test.

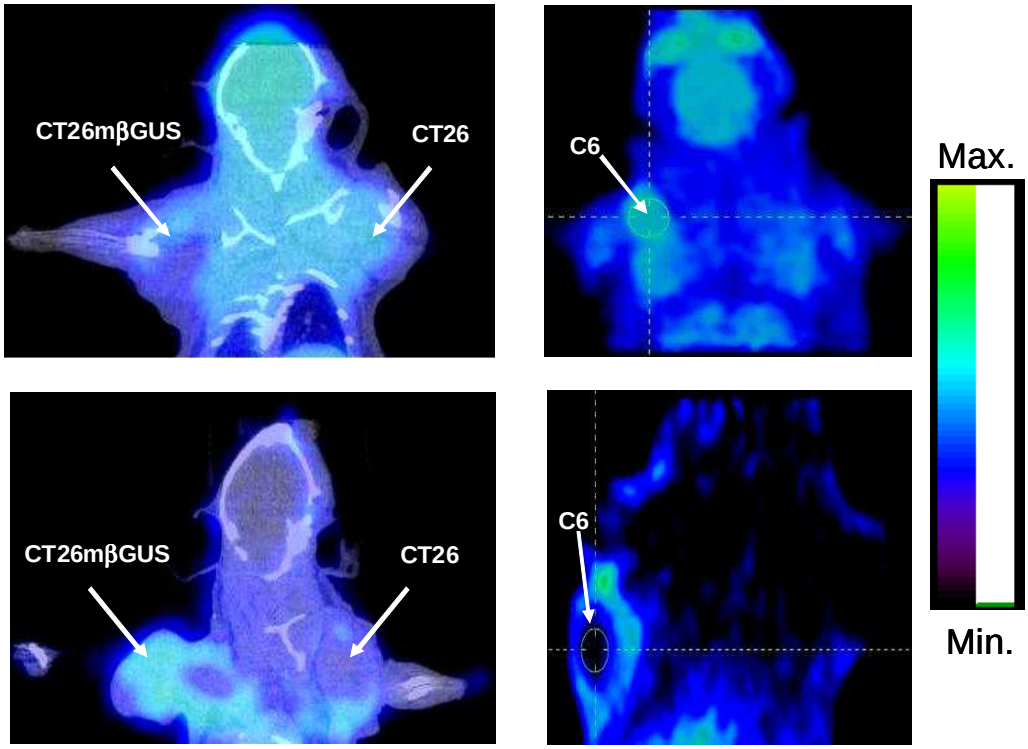

Figure 10- Left: a microPET/CT fusion image of mice bearing a CT26mßGUS tumor and a CT26 tumor. Right: a microPET image of rats bearing a C6 tumor injected with either [^{18}F]-FEAnGA (lower row) or [^{18}F]-FEA (upper row).

3.1.13 ^{89}Zr-ranibizumab VEGF microPET imaging during sunitinib treatment

In cooperation with Dept.Medical Oncology

Anti-angiogenic compounds targeting the VEGF receptor, like sunitinib, have shown activity in various tumor types. Currently no biomarkers are available to select patients for treatment or to function as early response predictor. Previously, we showed that radiolabeled ranibizumab, an anti-VEGF Fab tracer with high affinity for all VEGF-A isoforms, allows non-invasive, frequent, quantitative and rapid insight in VEGF levels in the tumor and its microenvironment. Therefore, radiolabeled ranibizumab was used to monitor sunitinib treatment to obtain insight in locoregional changes of tracer uptake during therapy.

Direct cytotoxicity of sunitinib was evaluated in vitro in a VEGF producing human A2780 ovarian tumor cell line. Nude mice were inoculated with A2780 cells. When the tumor was established, mice were treated 1) once daily with sunitinib (60 mg/kg ip) or vehicle (ip) for 7 days followed by a stop week, thus reflecting the patient regimen, or 2) sunitinib/vehicle was continued for an additional 7 days. ^{89}Zr-ranibizumab (or control ^{89}Zr-Fab-IgG for aspecific uptake) was injected at baseline, following 7 or 14 days of treatment. MicroPET images were made 0, 6 and 24 h after injection of the tracer.

In vitro no cytotoxicity occurred at sunitinib levels (0-5000 nM) comparable to plasma levels in patients. On day 7 tumor growth was inhibited by sunitinib treatment (+ 33% vs +121% for vehicle). At baseline, tumor uptake of ^{89}Zr-ranibizumab was homogeneous. Vehicle did not affect ^{89}Zr-ranibizumab uptake, while after 7 days of sunitinib treatment, ^{89}Zr-ranibizumab uptake was inhomogeneous (overall Δ -20.5 ± 9.7% uptake/cc, p=0.018) with low uptake in the center of the tumor as compared to the rim (-56.8 ± 8.2% vs rim, p=0.0018). When treatment was stopped, ^{89}Zr-ranibizumab tumor uptake increased to a higher level than post treatment and baseline (overall Δ + 59.4 ± 32.4% vs Δ + 25.7 ± 20.9% uptake/cc, p=0.034). This coincided with 79.1% tumor growth within 3 days after stopping sunitinib. Changes in ^{89}Zr-ranibizumab uptake at 7 days and off treatment were higher compared to ^{89}Zr-Fab-IgG (3.3 fold, p=0.040; 2.8 fold, p=0.031). Furthermore, there was a good correlation between plasma levels of human VEGF and ^{89}Zr-ranibizumab tumor uptake (r^2=0.99, p=0.036) at the scanning days. Immunohistochemical staining of VEGF was intense at the tumor rim and lower in the center after 7 days of treatment.

In conclusion, ^{89}Zr-ranibizumab revealed an inhomogeneous change in tumor uptake with a rebound phenomenon after stopping sunitinib treatment, resulting in 59% increased tracer uptake which corresponded with rapid tumor growth and an increase of plasma levels of human VEGF. Radiolabeled ranibizumab is a good candidate for guidance of patient-tailored anti-angiogenic therapy.

3.1.14 ^{89}Zr-trastuzumab immunoPET visualizes HER2 downregulation induced by the HSP90 inhibitor NVP-AUY922 in a human tumor xenograft

In cooperation with Dept. Medical Oncology and Novartis Institutes for Biomedical Research, Basel, Switzerland

The 90 kDa Heat Shock Protein (HSP90) is a molecular chaperone protein which is involved in maturation and stability of many oncogenic client proteins. It serves as a target for anticancer drugs, since its inhibition affects

multiple cancer-associated signaling pathways. NVP-AUY922 is a potent HSP90 inhibitor and is currently in clinical development. The Human Epidermal growth factor Receptor 2 (HER2) is overexpressed in ~25% of the breast cancers and is associated with aggressive tumor behavior. HER2 is also a client protein of HSP90, and therefore a potential biomarker for early evaluation of the molecular response to HSP90 targeted therapies in HER2 overexpressing tumors. For this purpose, we have used the HER2 antibody trastuzumab labeled with the positron emitting isotope ^{89}Zr to assess the alterations in HER2 expression after HSP90 targeted therapies with the non-invasive, high resolution, quantitative and sensitive immunoPET technique.

Experiments were performed with NVP-AUY922 and the HER2 overexpressing human ovarian tumor SKOV-3 cell line. In vitro evaluation of the HER2 expression after NVP-AUY922 treatment was assessed by flow cytometry and in a cell binding assay with ^{89}Zr-trastuzumab. The in vivo experiments were performed in SKOV-3 xenograft-bearing nude mice. NVP-AUY922 was administered intraperitoneally every other day in a dose of 50mg/kg. For ^{89}Zr-trastuzumab immunoPET imaging, animals were injected intravenously with 5 MBq ^{89}Zr-trastuzumab (100 μg) 6 days before NVP-AUY922 treatment and after 3 doses of NVP-AUY922. MicroPET and microCT imaging was performed at 1, 3 and 6 days after injection of the tracer. Ex-vivo biodistribution was performed at day 6.

The SKOV-3 HER2 expression, assessed in vitro by flow cytometry, showed a 76±1.3% reduction after 24hr NVP-AUY922 treatment. The SKOV-3 ^{89}Zr-trastuzumab cellular binding was reduced by 75±9.3% after 24hr NVP-AUY922 treatment. Quantification of the PET images showed a reduction of 37% ($p = 0.0143$) in ^{89}Zr-trastuzumab tumor uptake after NVP-AUY922 treatment. PET results were confirmed by comparing the ex-vivo biodistribution tumor uptake in NVP-AUY922 treated mice and control mice.

HER2 immunoPET provides a tool to image and quantify the reduction in HER2 expression in the tumor following HSP90 inhibition non-invasively. Since the ^{89}Zr-trastuzumab PET tracer is already used clinically, this technique can easily be translated to determine the early molecular effects of HSP90 inhibitors in patients.

3.1.15 Melanoma therapy by co-treatment with scFvMCSP:sTRAIL and rimcazole

In cooperation with Surgical Research Laboratory / Tumor Immunology Group

Sigma receptor (σR) ligands can enhance the anti-tumor actions of cytostatics. Previously, we have shown that sub-toxic amounts of σR ligands, haloperidol

or rimcazole, and sTRAIL (a tumor-selective pro-apoptotic protein) synergistically kill cultured A375M (melanoma), OVCAR-3, SKOV-3 (ovarian), HCT116 and HT29 (colon) cancer cells. In addition, we used ^{18}F-FDG to monitor the *in vitro* responses of A375M melanoma to mono- and combination treatment. The treatment with sub-toxic doses of sTRAIL did not significantly affect glucose metabolism, however higher sTRAIL concentrations dose-dependently decreased ^{18}F-FDG uptake per viable cell. In contrast, treatment with σR ligands resulted in a dose-dependent increase of cellular ^{18}F-FDG uptake. Importantly, the ^{18}F-FDG uptake was further increased after co-treatment and it reflected drug synergy.

In this study, we aimed to verify the *in vivo* effect of combination therapy with rimcazole and scFvMCSP:sTRAIL in a s.c. A375M melanoma model in Athymic Nude-Foxn1^{nu} mice. In addition, we wanted to trace the therapeutic outcome by performing ^{18}F-FDG microPET. For this purpose, 20 animals were injected with 2.1 x 10^6 of A375M cells suspended in 100 µl matrigel. Four groups of five animals were included: 1) control; 2) rimcazole-treated (~26 mg/kg); 3) scFvMCSP:sTRAIL-treated (~0.14 mg/kg) and 4) rimcazole- and scFvMCSP:sTRAIL-treated (with a 30 min interval between drug administrations). After two weeks of tumor growth (0.041 ± 0.006 cm^3), we started a 14 day-treatment schedule with a regimen of daily doses. Three microPET scans were scheduled on day 1, day 7 and day 14 of treatment. In addition, a biodistribution study was performed after the last scan.

Treatment did not affect glucose levels, animal weight, behavior or appearance. Rimcazole treatment resulted in a fourfold reduction of tumor weight in comparison to control (Table). At the same time, scFvMCSP:sTRAIL did not have any effect on tumor weight. The ^{18}F-FDG biodistribution data were corrected for the level of nonradioactive glucose in plasma, which was measured before injection of ^{18}F-FDG. Whereas rimcazole treatment did not significantly alter SUVs, tumor/plasma and tumor/muscle ratios of FDG, scFvMCSP:sTRAIL significantly reduced the tumor-to-plasma uptake ratio from 5.6±0.4 to 3.1±0.5 (Table 7).

In conclusion, rimcazole inhibited A375M melanoma growth *in vivo* and, therefore, it is of great interest to explore this compound in further pre-clinical studies. The reduction of tumor growth was not associated with reduced FDG uptake.

Table 7. Tumor growth and uptake data in the various treatment groups

		Control (n=5)	Rim (n=5)	sTRAIL (n=5)	Rim + sTRAIL (n=1)
Tumor wt [g]		0.40±0.10	0.10±0.03*	0.67±0.16	0.12
SUV	**Tumor**	0.97±0.17	1.14±0.17	0.89±0.15	2.01
	Plasma	0.17±0.02	0.24±0.03	0.28±0.03	0.31
	Muscle	0.31±0.07	0.21±0.02	0.32±0.06	0.42
Tumor/Plasma		5.6±0.4	4.8±0.7	3.1±0.5*	6.4
Tumor/Muscle		3.5±0.6	5.5±0.8	2.9±0.5	4.8

3.1.16 ^{18}F-Interleukin-2, a novel radioactive probe for insulitis imaging by PET

In cooperation with Nuclear Medicine Unit, 2nd Faculty of Medicine, University "Sapienza", Rome, Italy, Regina Apostolorum Hospital, Albano, Rome, Italy, Depts. Endocrinology and Medical Biology, Section Transplantation and Immunoendocrinology, University Medical Center Groningen, and Dept. Endocrinology, University Campus Bio-Medico, Rome, Italy

Insulitis is an autoimmune disease that occurs in the first phase of diabetes type 1, characterized by a chronic lymphomononuclear cell infiltration of the pancreas. Activated T lymphocytes migrate to the pancreatic beta-cells causing tissue damage and the progression of diabetes. Interleukin-2 (IL2) is a small cytokine of 15.5 KDa that binds with high affinity to IL2 receptors (CD25) which are over-expressed on activated T-lymphocytes. In order to synthesize a new probe that can detect infiltrating lymphocytes in vivo, a PET isotope, ^{18}F, was conjugated to IL2 using N-succinimidyl 4-[^{18}F]fluorobenzoate ([^{18}F]SFB). Here we describe a novel radiopharmaceutical for in vivo detection of insulitis by PET.

The synthesis of ^{18}F-SFB was fully automated using a Zymark Robotic system. ^{18}F-SFB was incubated with 100 µl IL2 (Proleukin®) in borate buffer (pH 8.5)/ethanol at 50ºC for 10 minutes. The purified product,^{18}F-FB-IL2, was used to make several in vitro quality controls including stability test in PBS and in human plasma, (TCA precipitation assay) biological binding assay in activated PBMc isolated from peripheral human blood (MTS) and SDS-PAGE. Preliminary PET experiments were performed in diabetic prone BB/W rats. After intravenous injection of ^{18}F-FB-IL2, a dynamic PET scan of the abdomen was made for 90 minutes. After imaging, rats were dissected and individual organs were weighed and counted. In addition ex-vivo biodistribution studies were performed in Normal Wistar rats used as a control group.

The labelling procedure gave ^{18}F-FB-Il2 as a major product. Labelled-IL2 is stable in PBS and plasma; more than 95% of the protein remains intact after 2 hrs of incubation. The MTS assay shows that the biological activity of IL2 is retained during the labelling, SDS-Page demostrates that there is no degradation of the protein during the labeling procedure. The dynamic PET scans showed highest tracer uptake in kidneys and bladder, due to renal clearance of the tracer. Uptake in the pancreas/spleen region was variable, but the pancreas/spleen could be clearly distinguished in several animals. This variability may reflect the variance in the extent of insulitis between animals. However, the correlation between insulitis and tracer uptake should still be examined. The time-activity curves demonstrate retention of the tracer in the pancreas in contrast to liver, ileum and heart which show only non-specific binding.

In conclusion, ^{18}F-FB-IL2 is a promising PET tracer to visualize infiltrating lymphocytes in the pancreas and could be a suitable new probe for PET imaging of activated T-lymphocytes. Additional animal studies to further evaluate this tracer are in progress.

3.1.17 Radiolabeled Humanized Anti-CD3 Monoclonal Antibody Visilizumab for Imaging Human T-Lymphocytes

In cooperation with Nuclear Medicine Unit, II Faculty of Medicine and Surgery, Sapienza University of Rome, Rome, Italy; Department of Biopathology and Diagnostic Imaging, University Tor Vergata, Rome, Italy; PDL BioPharma, Inc., Redwood City, California and Institute of Biomedical Engineering (IsIB)—National Council of Research, Rome, Italy

Visilizumab is an IgG2 humanized monoclonal antibody (mAb) characterized by non-FcgR binding and specific to the CD3 antigen, expressed on more than 95% of circulating resting T-lymphocytes and on activated T-lymphocytes homing in inflamed tissues. We hypothesized that the use of a radiolabeled anti-CD3 antibody might serve as a diagnostic tool for imaging T-cell traffic and lymphocytic infiltration of tissues and organs affected by autoimmune diseases. Here we describe the results of in vitro and animal experiments with ^{99m}Tc-succinimidyl-6-hydrazinonicotinate hydrochloride (SHNH)–visilizumab.

For mAb labeling, we used a 2-step method with a heterobifunctional linker SHNH. Several titrations were performed to obtain the best labeling efficiency. In vitro quality controls included stability assay, cysteine challenge, sodium

dodecyl sulfate polyacrylamide gel electrophoresis, binding assay, and immunoreactivity assay. High-resolution U-SPECT images of mice were made 6 and 24 h after the injection of ^{99m}Tc-SHNH–visilizumab. These included cell-targeting experiments in BALB/c mice xenografted subcutaneously with an increasing number of HuT78 cells in the leg and displaced with an excess of cold antibody.We also studied irradiated severe combined immunodeficient (SCID) mice reconstituted with human peripheral blood mononuclear cells (hPBMCs) and injected with ^{99m}Tclabeled visilizumab or control mAb. After dynamic imaging for 3 h, major organs were removed, counted, and processed for immunohistologic examination.

Visilizumab was labeled with HYNIC with high labeling efficiency (90%) and high specific activity (SA; 10.4–11.1 GBq/mg), with retained biochemical integrity and in vitro binding activity to CD3-positive cells. The in vivo targeting experiment showed a proportional increase of specific uptake with the number of injected cells, both at 6 and at 24 h, and the in vivo competition study demonstrated a greater than 60% decrease of uptake after administration of an excess of unlabeled antibody. In SCID mice, hPBMCs in different tissues were detected by ^{99m}Tc-labeled visilizumab and confirmed by histology.

In conclusion, visilizumab can be efficiently labeled with ^{99m}Tc with high efficiency and specific radioactivity and could be a valuable tool for the study of human T-lymphocyte trafficking and lymphocytic infiltration of tissues and organs.

3.1.18 Biodistribution of ^{89}Zr-alemtuzumab compared to ^{111}In-IgG in human non-Hodgkin's B-cell lymphoma bearing mice

In cooperation with Depts. Hospital and Clinical Pharmacy, and Haematology, UMCG

Alemtuzumab is a monoclonal antibody targeting the CD52 antigen expressed on (malignant) B and T cells, and is indicated for haematological malignancies. Not all patients benefit equally from therapy with alemtuzumab, underlining the need for a better selection of patients before start of therapy. Radiolabeled alemtuzumab may prove useful as a non invasive technique for patient selection. Therefore, alemtuzumab labeled with the PET isotope 89-Zirconium was developed and tested in mice bearing a human non-Hodgkin's B cell lymphoma xenograft.

Irradiated male NOD/SCID mice were injected subcutaneously with 107 DoHH2 (CD52 positive) cells. ^{89}Zr-alemtuzumab was developed for PET-imaging and tested in vitro and in vivo. Biodistribution and tissue/organ including tumour uptake was compared to 111-Indium labeled non specific human immunoglobulin G (^{111}In-IgG). Small-animal PET imaging and ex vivo

biodistribution was performed at 144h after co-injection of ^{89}Zr-alemtuzumab and ^{111}In-IgG. Furthermore, uptake of both tracers was compared in both tumour and non-tumour bearing mice.

Subcutanous injection of DoHH2 cells in resulted in a palpable tumour 5 weeks after inoculation in 50% of the mice. ^{89}Zr-alemtuzumab was stable in saline at 4°C and in serum at 37°C for seven days. Radiochemical purity was 97.6 ± 1.8%. PET showed intense uptake of ^{89}Zr-alemtuzumab in tumour and spleen at 144h. Uptake in tumour of ^{89}Zr-alemtuzumab was 14.9 ± 16.6 % injected dose per g tissue (%ID/g) vs 4.5 ± 7.7 %ID/g for ^{111}In-IgG (n=6, p=0.06). The tumour to blood ratio of ^{89}Zr-alemtuzumab was 63 ± 51 vs 2 ± 3 for ^{111}In-IgG ($p< 0.05$). Furthermore, significant uptake of ^{89}Zr-alemtuzumab was seen in spleen, liver, and bone ($p< 0.05$). Spleen uptake of ^{89}Zr-alemtuzumab in tumour positive mice was 101.3 ± 67.2 %ID/g (n=6) vs 25.0 ± 9.9 %ID/g in tumour negative mice (n=10, $p< 0.05$). ^{111}In-IgG uptake did not differ substantially in both groups.

Radiochemical purity, stability and binding properties of ^{89}Zr-alemtuzumab were good. PET imaging correlated well with ex vivo biodistribution data of ^{89}Zr-alemtuzumab. However, quantification of images was difficult. Specific uptake of ^{89}Zr-alemtuzumab in tumour xenograft and spleen was observed. Therefore, radiolabeled alemtuzumab is a new tracer suitable for noninvasive in vivo imaging of CD52 expressing tumours.

3.1.19 Synthesis of ^{99m}Tc-anti-DR monoclonal antibody for molecular imaging of HLA-DR positive cells: *in vitro* and *in vivo* studies

In cooperation with Nuclear Medicine Unit, Second Faculty of Medicine and Surgery, "Sapienza" University of Rome, Rome, Italy

It is known that HLA-DR is highly expressed on B-cell lymphomas and in a variety of autoimmune and inflammatory diseases. Therefore, a radiolabelled fully humanised IgG4 monoclonal antibody (mAb), can provide a useful tool for molecular imaging and therapy decision making. The aims of the present study were (1) to radiolabel an anti-HLA-DR mAb with technetium-99m and (2) to validate the binding activity of this radiolabelled antibody in athymic nude mice engrafted with DR+ tumor cells.

To radiolabel the anti-DR mAb with 99m-technetium we compared a direct labelling method via 2-ME reduction of disulphide bonds with a two-step method using a hetero-bifunctional linker SHNH/S-HYNIC (succinimidyl-6-hydrazinonicotinate hydrochloride). Several titrations were performed to obtain best labelling efficiency. *In vitro* quality controls (QC) included SDS-PAGE

and autoradiography of labelled antibody, Cysteine challenge, Immunoreactive fraction assay, binding assay on DAUDI cell line (DR+).

In-vivo studies included a tumour targeting experiment in athymic nude Balb/c mice xenografted subcutaneously with increasing number of DAUDI cells in the leg ($10x10^6$, $20x10^6$ and $30x10^6$). On the contralateral thigh, animals were implanted with $10x10^6$ DR negative tumor cells as control. Two hours after implant mice were injected in a tail vein with about 300 µCi (about 2µg) of radiolabelled anti-DR mAb. Mice groups were sacrificed at different time points (1h, 6h and 24h p.i.), and single organ counting assay was performed. An *in-vivo* displacement assay was also performed for the *in*-vivo QC of the antibody.

Anti-DR mAb was best labelled with a direct method via 2-ME reduction with a high labelling efficiency (>95%) and high specific activity (SA = 150 mCi/mg) with retained biochemical integrity and binding activity. SDS-PAGE and autoradiography analysis demonstrated its structural integrity, moreover, Cysteine challenge and immunorective fraction assay also confirms its *in-vitro* stability and binding property. In tumor targeting experiment, we observed an increase of uptake of radiolabelled mAb to DR+ cells compared to DR- cells and the binding activity was proportional to the number of injected cells, at 1h, 6h and 24h. *In vivo* displacement assay confirmed the high *in vivo* specificity of the radiolabelled mAb to the HLA-DR positive cells.

Thus, we efficiently labelled a humanized anti-DR mAb with ^{99m}Tc with high labeling efficiency and specific activity, using a direct labelling method with 2-ME reduction. Radiolabelled mAb binds to human HLA-DR antigens, therefore, could be used as a prognostic/diagnostic tool in lymphoma patients or in patients with autoimmune diseases.

3.2 Cell and in vitro studies

3.2.1 [^{18}F]FB-IL2: a novel PET tracer for detection of activated T-lymphocytes

In cooperation with Nuclear Medicine Unit, 2nd Faculty of Medicine, University "Sapienza", Rome, Italy, and Regina Apostolorum Hospital, Albano, Italy.

Interleukin 2 (IL2) is a small single-chain glycoprotein (15.5 kDa) of 133 amino acids that is synthesized and secreted in vivo by activated T lymphocytes. IL2 binds with high affinity and specificity to the cell membrane IL2 receptor (CD25), which is overexpressed on activated T lymphocytes in various pathological conditions (Signore A et al., J Endocrinol Invest. 1999; 22:151-8). Radiolabelled IL2 could therefore be a promising radiopharmaceutical with high diagnostic potential to detect activated T lymphocytes during the early stage of inflammatory and autoimmune diseases. Here, we report the synthesis of the new PET tracer [^{18}F]FB-IL2 by conjugation of N-succinimidyl 4-[^{18}F]fluorobenzoate ([^{18}F]SFB) to a lysine residue in the IL2 protein.

[^{18}F]SFB was synthesized in three steps by slight modification of the procedure described by Wester et al (Nucl. Med. Biol. 1996; 23:365-372). The synthesis was fully remote-controlled using a Zymark robotic system. Conjugation of [^{18}F]SFB to IL2 was performed in borate pH 8.3 buffer/ethanol (1/1). Reaction temperature (37–60 ^{o}C) and time of conjugation (5–30 min) were optimized. [^{18}F]FB-IL2 was purified by semi-preparative HPLC. The stability of [^{18}F]FB-IL2 in PBS and human plasma was tested in vitro by TCA precipitation. The integrity of [^{18}F]FB-IL2 was investigated by SDS-PAGE electrophoresis and the biological activity of the tracer was determined with an MTT proliferation assay using activated human lymphocytes.

[^{18}F]SFB was reliably produced in 34–38% radiochemical yield. After SPE purification, the radiochemical purity of [^{18}F]SFB was 93–96%. The optimal reaction temperature for the conjugation of [^{18}F]SFB to IL2 was 50 ^{o}C. Higher temperatures caused degradation of the protein and hydrolysis of [^{18}F]SFB, whereas the reaction was substantially slower at lower temperatures. At 50 ^{o}C, the reaction was complete within 10 min. Under the optimized conditions, radiochemical yield of HPLC-purified [^{18}F]FB-IL2 was 25-35%. SDS-PAGE showed a single band for [^{18}F]FB-IL2 at the same height as that of native IL2, which indicates that no covalent aggregates of [^{18}F]FB-IL2 or degradation products were formed during labelling. The TCA precipitation assay showed that [^{18}F]FB-IL2 is stable in PBS and human plasma, as >80 % remained intact after 2 hrs of incubation. The MTT assay demonstrated that [^{18}F]FB-IL2

stimulated lymphocyte proliferation to a similar extent as IL2, which indicates that the biological activity of [^{18}F]FB-IL2 is retained during labelling.

In conclusion, IL2 was successfully labelled with fluorine-18. [^{18}F]FB-IL2 is stable and its biological activity is retained during labelling and therefore could be a suitable new probe for PET imaging of activated T- lymphocytes. Animal PET imaging studies to further evaluate the tracer in-vivo are currently in progress.

TECHNOLOGY

4.1 Cyclotron

Statistics regarding radionuclide production of the cyclotron (Scanditronix MC-17) are presented in Figure 11. The figure gives an overview of cyclotron use in 2009. Average values for the whole period of use since 1992 are presented in Table 8. In 2009 all repairs could be performed within the scheduled time for maintenance. Maintenance work was done every Monday morning before 9:00 a.m.

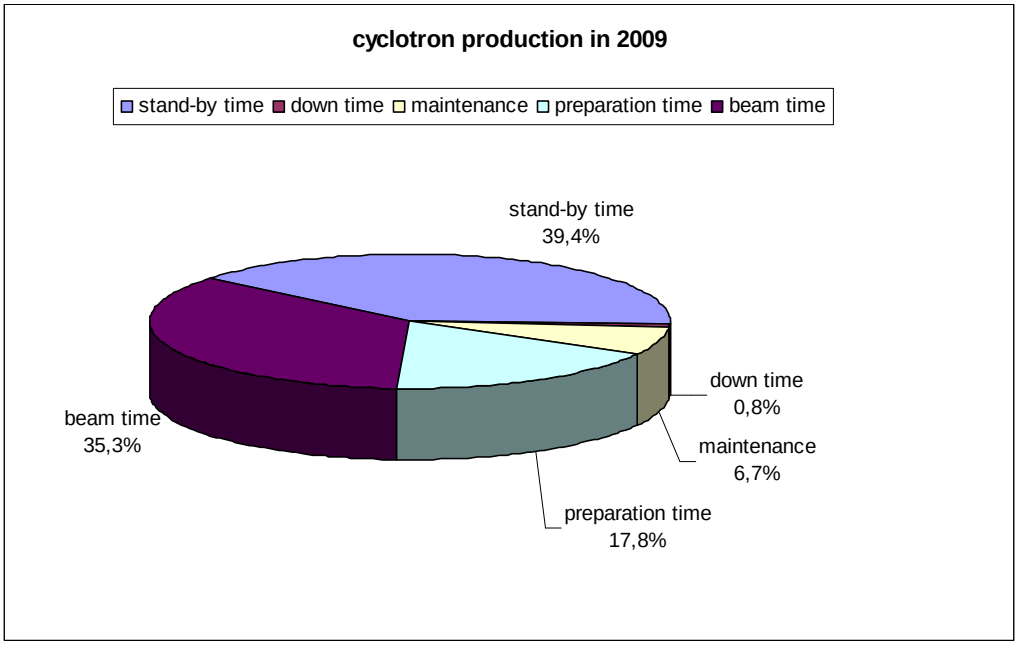

Figure 11: Cyclotron use in 2009.

Table 8: Average values for cyclotron use (2009 and previous period)

	average value (1992-2008)	**2009**
Number of beams	1854	1886
Beam time (hours)	590	787
Preparation time (hours)	248	398
Maintenance (hours)	198	149
Unscheduled down time (hours)	84	18
Stand-by time (%)	50	39

Tables 9 to 12 present values for individual years in the 2002-2009 period.

Table 9: Irradiations

Radionuclide	2002	2003	2004	2005	2006	2007	2008	2009
^{15}O	313	578	413	718	169	102	30	**367**
^{13}N	244	343	261	120	89	179	158	**165**
^{11}C	454	336	253	648	543	553	412	**455**
$^{18}F^-$	571	430	377	654	331	336	465	**509**
$^{18}F_2$	129	176	232	474	414	382	442	**390**

Table 10: Irradiation time (hours)

radionuclide	2002	2003	2004	2005	2006	2007	2008	2009
^{15}O	14.4	28.7	28.8	25.1	11.1	2.3	1.5	11.1
^{13}N	21.7	40.1	41.9	11.9	10.4	34.6	18.2	16.0
^{11}C	194.8	101.6	94.7	211.6	212.2	240.1	270.1	311.3
$^{18}F^-$	355.2	283.7	217.4	324.6	418.5	130.9	201.0	215.4
$^{18}F_2$	81.2	136.0	148.2	307.5	242.1	264.3	356.5	233.5

Table 11: Mean irradiation time (min)

radionuclide	2002	2003	2004	2005	2006	2007	2008	2009
^{15}O	2.7	3.0	4.2	2.1	3.9	1.3	3.0	1.8
^{13}N	5.3	7.0	9.6	6.0	7.0	11.6	6.9	5.8
^{11}C	25.7	18.1	22.5	19.6	23.4	26.0	39.3	41.1
$^{18}F^-$	37.3	39.6	34.6	29.8	75.9	23.4	25.9	25.3
$^{18}F_2$	37.8	46.4	38.3	38.9	39.4	41.5	48.4	35.9

Table 12: Total activity (GBq)

radionuclide	2002	2003	2004	2005	2006	2007	2008	2009
^{15}O	960	1700	3055	2090	920	336	239	885
^{13}N	1466	2300	2499	679	573	1234	1056	1110
^{11}C	22766	11900	9033	20519	27380	31317	33671	46349
$^{18}F^-$	6701	5300	4044	5987	7683	9008	12868	13678
$^{18}F_2$	599	800	926	2874	2837	2724	3784	2580

Down time of the cyclotron in 2009 was 0.8%, slightly higher but comparable to the value of 2008 (0.7 %). It is significantly lower than the average value since 1992 (3.6 ± 2.2 %, or 80 ± 51 h, see Figure 12), due to the substantial cleaning of the Dee's which was performed in 2007. Causes underlying the 0.8% (= 18 hours) down time in 2009 are listed in Table 13.

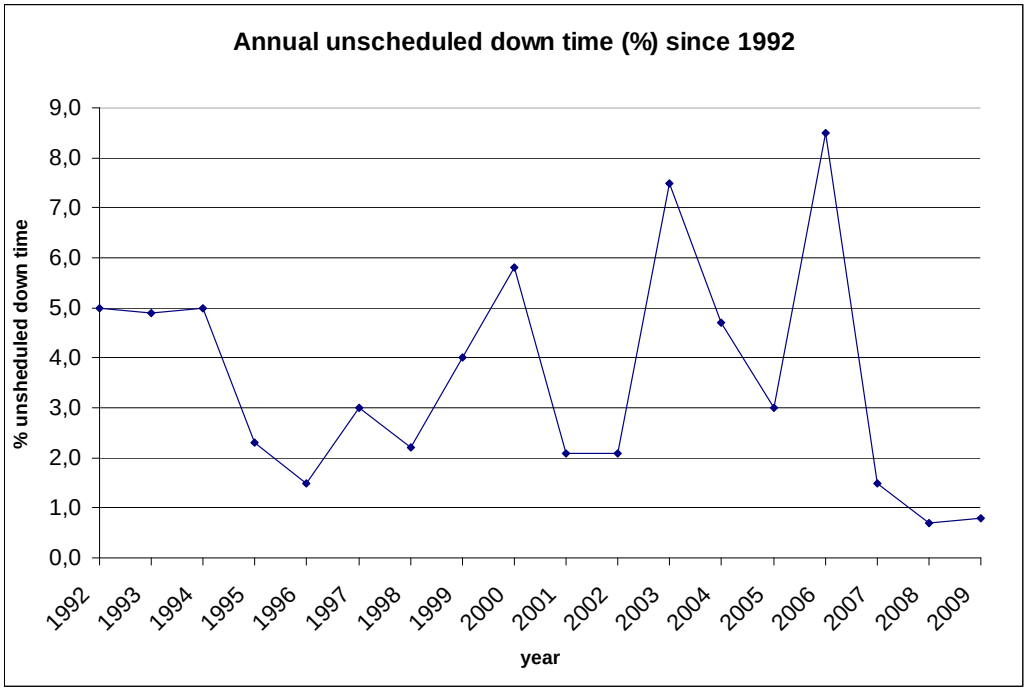

Figure 12. Yearly unscheduled down time (%) since the installation of the cyclotron

Table 13: Cyclotron failures in 2009.

Subsystem cyclotron	**Hours**
General (general supply hospital)	2.5
Magnet (gradient coils)	2.5
RF-system (APS)	-
Ion-source	-
Extraction	4
Diagnostic	-
Vacuum	1
Control	-
Target	5
Process system	-
Water cooling of cyclotron	3

One hundred and forty-nine hours were required for maintenance, which included replacement or modification of the following parts:

- Upgrade of PLC software (step-5 program)
- Festo air pressure valves were replaced
- The type of valves in the filling system for the fluorine targets was changed (Figure 13)
- The cooling liquid for the $^{18}F_2$-tagets was changed from water to glycol
- A new power supply for the gradient coils was installed
- A new pump was installed for water cooling of the cyclotron (Figure 14)
- All Teflon/PEEK tubing from target to valve box was replaced.
- Foils of the $^{18}F_2$ target were replaced (2x)
- A new niobium insert for the $^{18}F^-$ target was installed (1x)
- The O-ring of the target-chamber was replaced (5x)
- The O-ring on the high vacuum valve was replaced
- The 24 VAC coil on the yoke lifting jack was replaced
- The bellow of the Faraday cup was replaced (4x)
- The cathodes of the ion source were replaced (1x)

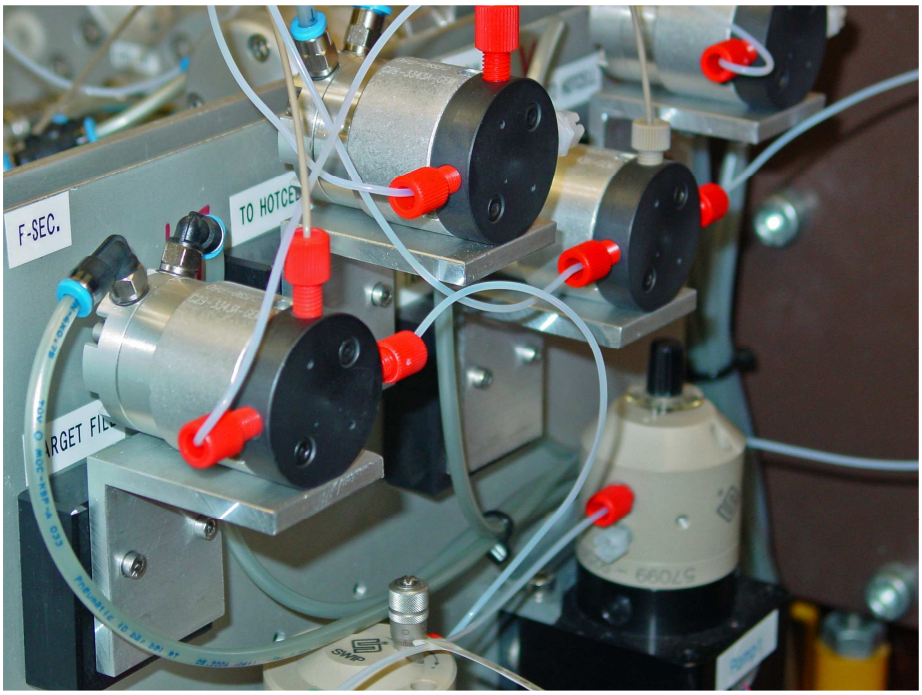

Figure 13. The new valves of the filling system for the fluorine targets.

Figure 14. The new pump for water cooling of the cyclotron .

4.2 Gamma cameras and clinical PET scanners

In 2009, we started to replace our old gamma cameras and one of the PET cameras. First, a Siemens HR+ was replaced by a Siemens mCT PET/CT system. With the introduction of a CT in our department, the shielding for ionizing radiation was re-evaluated. Until now, shielding was only about 2.5 meters high. Current standards for CT installation however require shielding from floor to ceiling. We calculated that 2 mm lead shielding or equivalent was required. After dismantling and removal of the old system the first step was to prepare the room for the new system including proper shielding. Unfortunately, a quality check revealed several areas were shielding was not adequate. Once the shielding was fixed and approved, installation of the camera could commence. The mCT is a water cooled system and it turned out that it was quite difficult to provide cooling according to specifications. Once this problem was solved, the camera could be tested and prepared for clinical use. The system quality tests did not reveal any deviations except that time of flight (ToF) was not directly available for clinical use.

Once the room for the mCT was finished, two of the old gamma cameras were removed and their rooms prepared for the new Siemens Symbia S systems. The first room required minimal changes whereas the second was extended to fit the Symbia camera. Lead shielding was adapted and checked. Note that for these rooms, a shielding from floor to ceiling is not required. System installation and acceptance testing went according to schedule.

After both systems had been accepted and clinical studies were started, we could start to install a Symbia T2 and T16. For this purpose, the rooms housing our last two gamma cameras were rebuilt since the Symbia T systems require more space than their predecessors. Also we decided to create a room for the operating technicians (the so called cockpit) with both Symbia systems on either side of the cockpit. This required that both systems were removed simultaneously and during that period, only the newly installed Symbia S systems were available for clinical use. In addition, the wall of the neighboring room housing the DEXA bone-density scanner had to be moved to create enough space for the Symbia T16. Installation of the T systems should be completed in the first months of 2010 and clinical studies on these cameras will then be initiated.

Once the installation is finished, our department will have four state-of-the-art gamma cameras, two of them combined with a CT. One of the nice aspects of these systems is that their gamma camera part is identical, and so are the quality control, data acquisition and data processing software. To further facilitate the data processing, a new computer platform is installed. Installation should be finished in 2010. We decided to purchase a local archive to facilitate

data analysis of both our clinical and preclinical research. A tentative overview of cameras and computer platform is given in Figure 15.

Because of the necessary renovation procedures, there are several periods of time in which camera capacity is limited. First, only one PET camera is available and until all SPECT and SPECT/CT cameras are operational, only 2 SPECT cameras will be active. So for a certain amount of time only 50% of the PET or SPECT capacity is available. To prevent formation of a large back log of patients, we have planned to work in extended time shifts during this period, in order to maximize the use of the available camera systems.

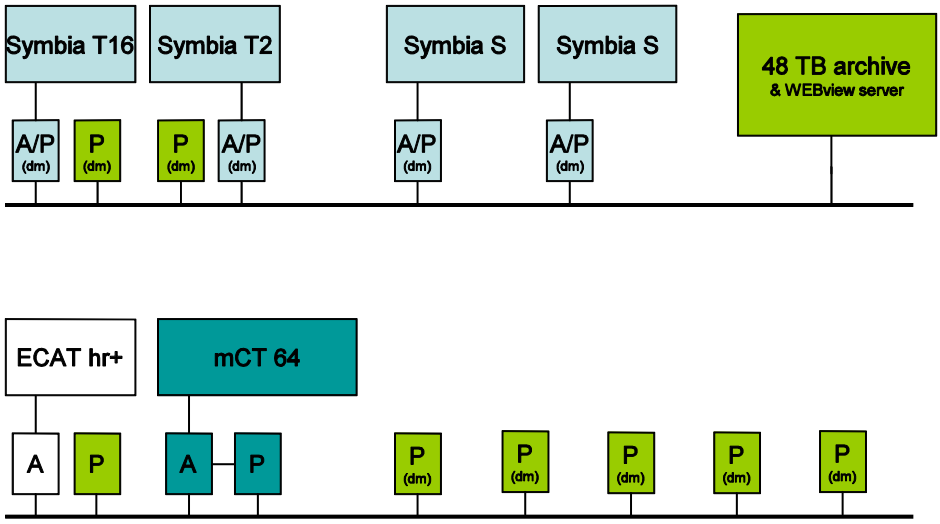

Figure 15: Overview of the PET, PET/CT, SPECT and SPECT/CT cameras with the future computer platform. A: Acquisition workstations; A/P: Acquisition/Processing workstations; P: Processing workstations. The location of the workstations shown in green is to be determined.

4.3 Facilities for small animal imaging

The µPET camera (Focus 220) was used very frequently in 2009. Total use amounted to 1400 hours/yr (average occupancy during working hours 85% - which approaches the maximum, since time is also required for maintenance of the hard- and software). In the spring of 2009, the scanning of animals was not possible for about 3 weeks because the Central Animal Laboratory was moved from its old address (Antonius Deusinglaan 50) to a new location (Antonius Deusinglaan 1, next to the UMCG complex). For an additional 2 weeks in

2009, we could not make any µPET scan because the radiochemistry laboratory was renovated and maintenance had to be done on our cyclotron.

The µCT system (microCAT) was used less frequently than the uPET camera: for about 300 hours in 2009 (average occupancy during working hours 20%). The µSPECT (U-SPECT II) was still in its start-up and testing phase. Average occupancy during working hours was about 15%. Other imaging institutions (e.g., University of Tübingen, dr.B.Pichler) have reported that their microPET cameras are also used very frequently, in contrast to their microCTs. The microCT camera is mainly used for the study of bone growth and regeneration (e.g., by investigators of the Department of Oral and Maxillofacial Surgery, UMCG and Ocean Ecosystems, Haren). Investigators from the Department of Medical Oncology fuse PET and CT images to combine anatomic and metabolic information.

Statistics for scanner use in the past 4 years are presented in Table 14:

Table 14

Year	**2006**	**2007**	**2008**	**2009**
µPET scans*	358	306	651	659
µCT scans	232	223	226	160
µSPECT scans	None	None	64	130
Total	**590**	**529**	**941**	**949**

**Transmission scans are not included in the figures for µPET scans. If transmission scans were included, the number of µPET scans would become twice as large. Many scans involved the simultaneous scanning of two experimental animals. Thus, the number of animals scanned was greater than the figures which are provided here. Also note that scanning protocols have become increasingly complex: from static whole-body scans in the Spring of 2006 to protocols with complex pharmacological treatments, rapid arterial sampling, tracer-kinetic modelling, and difficult surgery (e.g. myocardial infarction in rats and mice). Thus, the yearly figures are not directly comparable.*

4.4 Analysis of the risks of administration of radiopharmaceuticals

A large number of nuclear medicine examinations are performed daily in our Department. During these examinations, some employees are exposed to potentially harmful ionizing radiation. It is necessary to estimate the risks of this exposure by means of an appropriate scientific analysis.

We have limited ourselves to the risks of exposure for employees who are involved in administration of radiopharmaceuticals (to patients, human volunteers or experimental animals). Using the method prepared by the task group “Risk Assessment and Evaluation” of the Dutch Society for Medical Physics, we have categorized all administration procedures into a low- and a high risk group, and have distinguished four different types of calamities: (undesired) inhalation, ingestion, injection and contamination of the skin. Administration procedures belonging to the low risk category will be considered sufficiently safe. However, administration procedures belonging to the high risk category can not be assumed to be safe. We have performed an additional analysis in these particular cases.

Two different techniques for risk assessment have been employed: i) the Fine-Kinney analysis and ii) the SAFER analysis. In contrast to the Fine-Kinney analysis, SAFER is not dependent on quantification of risk “severity”. This means that the SAFER method can not only include consequences that can be translated into a radiation burden or a financial loss, but also other consequences such as damage to someone’s reputation.

In the Fine-Kinney analysis, the effect parameter has been categorized based on the radiation dose received in case of a calamity. A comparable link between dose and severity does not yet exist in the SAFER method. Therefore, the Fine-Kinney method is more objectively applicable to the risks of ionizing radiation than the SAFER method.

The question which immediately arises is whether the Fine-Kinney method has more to offer than the SAFER/HFMEA if risk severity can be quantified. The reported analyses show that when conclusions are drawn regarding the safety of processes, both methods lead to the same verdict. When both methods are applicable, they produce a mutually consistent outcome. In our particular situation, both methods finally predicted that the risk of all established procedures in our Department are acceptable and that no further action or critical analysis is required.

.

It should be noted that the report was limited to internal contamination of employees (by accidental inhalation, ingestion, injection or exposure of the skin). The preliminary analysis which has been performed thus far should

therefore become part of a more extended analysis in which exposure of employees to external irradiation is also concerned. When entire processes are being studied, the risks of production of the radiopharmaceuticals should also be included.

Performing an analysis of the risks proved to provide useful insights regarding the critical/risky steps in administration procedures. Existing opinions regarding these risks based on intuition may not be correct.

Employees should also be aware of the importance (and the limitations) of the wearing of gloves. The main spin-off of a risk analysis is an improved awareness of critical steps and how accidents can be best avoided. In many cases, “common sense” will be sufficient to differentiate between acceptable risks and dangerous actions. In a hospital setting, a risk analysis should result in more than just a printed report on a book shelf indicating that the standard operational procedures are safe. The conclusions should be shared with the employees involved, so that they lead to greater awareness of everyone.

Within the framework of our analysis and with reference to the procedures mentioned in our report, employees in our hospital are safe. This is indicated by all employed methods of risk assessment: the technique of the Dutch Society for Medical Physics (task group RI&E), the SAFER analysis and the Fine-Kinney method. The last two techniques of risk assessment have shown to lead to mutually consistent conclusions. The Fine-Kinney technique is the method of choice since its discriminating power is better, particularly in the case of low risks, because it is quantitative. The SAFER method can be more widely used and it has a decision tree structure. The 'best of both worlds' can be combined by replacing the risk assessment matrix of the SAFER by a quantitative evaluation similar to the Fine-Kinney method, whenever possible.

4.5 OK detector

In cooperation with Veenstra Instruments (Joure, the Netherlands) our Department has developed new equipment for TNF perfusion procedures in operation theatres.

The system disposes of two models to measure leakage of blood: the single and the dual nuclide method. The last model has the advantage that the measured value is independent of changes in geometrical efficiency during the measuring procedure.

In order to guarantee the safety and quality of the new equipment, and in order to facilitate the transition of the old to the new equipment, the following actions have been taken:

i) Extensive quality and acceptation tests have been performed. The operation of both the hardware and the software has been examined. A comparison with the previous version of the equipment showed that the characteristics of both systems are virtually identical.

ii) The electrical safety of the system has been examined by the "Dienst Instrumentele Zaken" of the University Medical Center Groningen. The equipment was found to meet the criteria for a class B instrument in a class 3 room. The system is now included in the maintenance contract system of the "Dienst Instrumentele Zaken".

iii) A user's meeting (single afternoon) was organized to instruct future users of the system. The operation and correct use of the equipment has been discussed.

From a physics perspective, the new equipment for TNF perfusions is ready to be used and has been transferred to the medical staff for clinical use in operation theatres.

4.6 Click for PET: One Pot 'Click' Reactions: Tandem Enantioselective Biocatalytic Epoxide Ring Opening and [3+2] Azide Alkyne Cycloaddition

In cooperation with Stratingh Institute for Chemistry, University of Groningen

The discovery that copper catalyzes the 1,3-dipolar cycloaddition of azides and alkynes to form 1,4-disubstituted triazoles has significantly contributed to the popularization of 'click' chemistry and its subsequent application to the areas of drug discovery, polymer chemistry, medicinal and biological sciences, amongst others. Recently, efforts have been pursued to involve the copper

catalyzed azide alkyne cycloaddition (CuAAC) in one-pot multicomponent reactions, and interest in broadening the scope of these reactions has emerged. The bioorthogonality of the azide-alkyne cycloaddition makes it uniquely suited to one-pot procedures and as such should be exploited in tandem processes.

An attractive possibility to execute a tandem reaction is the combination of azide induced ring opening of epoxides with the copper catalyzed 1,3-dipolar cycloaddition of azides and alkynes.

We have previously reported on the biocatalytic azidolysis of aromatic epoxides using HheC, the halohydrin dehalogenase from *Agrobacterium radiobacter*. This enzyme catalyzes azidolysis of substituted styrene oxides to their corresponding chiral 1,2-azido alcohols in a highly enantioselective (E>200) and *β*-regioselective manner (Scheme 1).

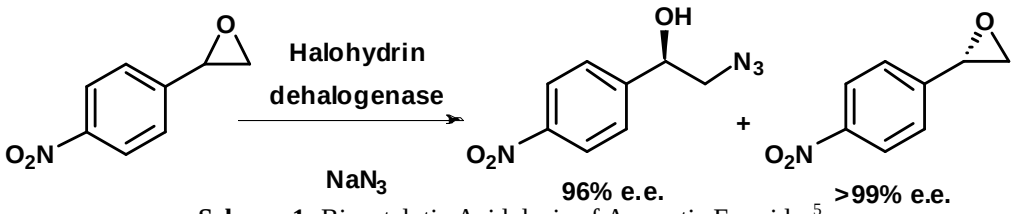

Scheme 1- Biocatalytic Azidolysis of Aromatic Epoxides[5]

We envisioned that this exquisite selectivity could be combined with the copper catalyzed [3+2] cycloaddition of azides and alkynes to produce optically pure triazoles. These products are particularly interesting, not only due to the presence of the 1,2,3-triazole moiety which has proven to be a promising pharmacophore but also due to their role as *β*-adrenergic receptor blocker analogues illustrating their potential as imaging agents for positron emission tomography.

We demonstrate herein the first example of a one-pot tandem biocatalytic enantioselective epoxide ring opening and click reaction to produce optically pure hydroxy triazoles. This method uses inexpensive and readily available racemic epoxides and allows for the subsequent click reaction to occur in one pot, thus limiting the experimental steps and proceeding in a more environmentally friendly fashion. Both traditional copper(I) catalyzed and copper free click reactions give excellent results.

The investigation was initiated by exploration of the reactivity and selectivity of the enzyme in the presence of the click additives, namely, $CuSO_4 \cdot 5H_2O$, the reducing agent sodium ascorbate and the MonoPhos ligand used to enhance the rate of the azide-alkyne cycloaddition as recently demonstrated. In anticipation of the one-pot reaction, the buffer used to store the enzyme, 10 mM Tris-HCl

(pH 7.5, 1.0 mM EDTA, 10 % glycerol), had to be changed due to the presence of EDTA which has the ability to chelate copper thereby inhibiting catalysis. Potassium phosphate buffer was chosen as a substitute (pH 7.5, 50 mM). Styrene oxide **1** was used as the initial substrate.

Table 15 Enzymatic Activity in the Presence of Click Additives

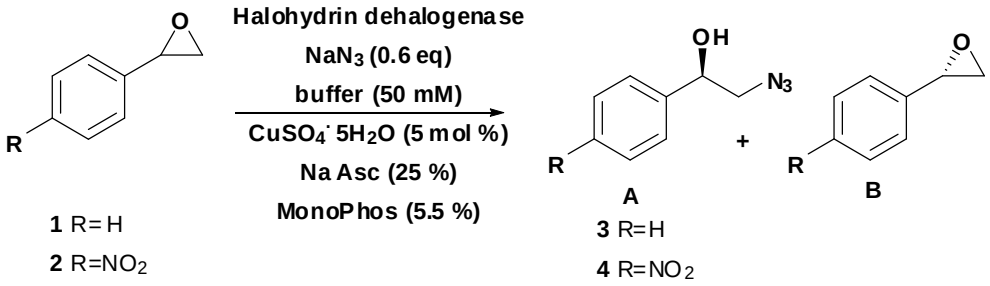

	R	Concentration[a]	Solvent[b]	Additives[c]	Conv.[d]	ee A (%)	ee B (%)	E
1	H	2.0	Buffer	No	47 %	>99	89	>200
2	H	2.0	Buffer	Yes	26%	>99	35	>200
3	NO_2	2.0	Buffer	No	46%	>99	83	>200
4	NO_2	2.0	Buffer	Yes	50 %[e]	97	98	>200
5	NO_2	4.0	Buffer	No	17%	>99	20	>200
6	NO_2	25.0	Water	Yes	< 1%	n.d.	n.d.	n.d.
7	NO_2	25.0	Water	No	< 1 %	n.d.	n.d.	n.d.
8	NO_2	50.0	Buffer	No	< 1 %	n.d.	n.d.	n.d.

[a] Epoxide concentration (mM). [b]Reactions were conducted either in 50.0 mM potassium phosphate buffer (pH=7.5) or in distilled water. [c] Includes copper(II) sulfate pentahydrate, sodium ascorbate and MonoPhos. [d]Conversion at 16 h. Max. conv. 50 %. [e]Conversion after 24 h.

We were pleased to find that the alteration of buffer had no apparent impact on the enantioselectivity of the conversion of epoxide to azido alcohol **3** giving the product with 99% ee (Table 15, entry 1) albeit with slightly lower conversion overnight (47 % of the available 50 % conversion for a kinetic resolution). The same reaction was performed in the presence of $CuSO_4 \cdot 5H_2O$ (5 mol %), sodium ascorbate (25 mol %) and MonoPhos (5.5 mol %).[1] Fortunately, the presence of these additives proved to have no effect on the optical purity of **3**, but we found that the rate decreased considerably in their presence (Table 15, entry 2).

The conversion of 2-(4-nitrophenyl)oxirane **2** to its corresponding azido alcohol **4** in potassium phosphate buffer was also investigated (Table 15, entry 3). Nearly full conversion was achieved overnight with > 99 % and 83 % ee in

[1] Under these conditions, after 72 h, no evidence of copper catalyzed azide ring opening of the epoxides could be detected.

the azide and the epoxide, respectively. The same reaction in the presence of the additives (Table 15, entry 4) showed full conversion to **4** after 24 h with 97% ee and 98 % ee for the azide and the epoxide, respectively. A higher substrate concentration (4.0 mM) proved to have a detrimental effect upon the conversion while retaining the perfect enantioselectivity of the transformation (Table 15, entry 5).

Previous work has shown us that the click step of the cascade proceeds faster in distilled water than in potassium phosphate buffer. However, when the enzymatic conversion to azido alcohol was attempted in water, no conversion was detected (Table 15, entry 6). In the absence of click additives, the same result was observed (Table 15, entry 7). The poor result is thus attributed to the inability of the enzyme to perform under these buffer-free conditions. High substrate concentration (50 mM) also proved too challenging for the enzyme, and no trace of **4** was detected (Table 15, entry 8).

Having established the ability of the reaction to proceed in potassium phosphate buffer in the presence of the necessary additives with essentially unaltered selectivity, it was possible to attempt the one-pot ring opening and subsequent click reaction. In the first attempt, with 5 mol % of catalyst, after 24 h, the triazole product **5** could be detected with 99 % ee, and the remaining epoxide with 75 % ee (Table 16, entry 1). Thus, the first step of the cascade maintains its high level of selectivity, and the click reaction proceeds at such a rate that with 5 mol % of copper, no azido alcohol remained in the reaction mixture.

Table 16. Optimization of One Pot Enzymatic and Click Reactions

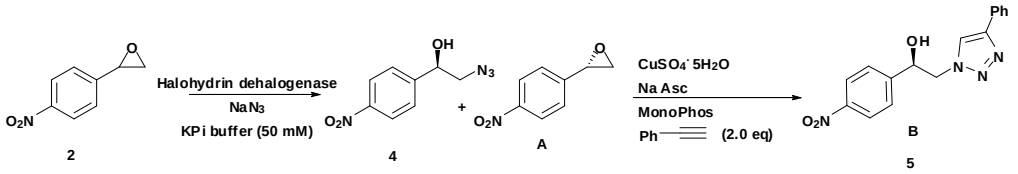

	Concentration	Cu (mol %)	Time (h)	Conv.[b]	ee A (%)	ee B (%)	E
1	2.0 mM	5	24	43 %	75	>99	>200
2	4.0 mM	5	24	34 %	51	97	109
3	4.0 mM	5	67	39 %	62	97	124
4	4.0 mM	1	24	n.d.[a]	85	99	>200
5	50.0 mM	5	67	24 %	23	42	2.8

[a]Azido alcohol remaining.[b] Max. conversion 50 %.

There appears to be a slight effect on the efficiency of the overall process, either on the part of the phenylacetylene, or due to a process within the

catalysis of the click reaction, on the rate of the ring opening, as only 43 % conversion occurs after 24 h. The same experiment at a higher concentration showed a slight drop in the ee of **4** (97 %) and lower conversion (Table 16, entry 2). Repetition of the experiment with a longer reaction time gave a slight increase in conversion (Table16, entry 3). Reducing the amount of catalyst to 1 mol % also gave excellent results, 99 % ee for **5** and 85 % ee for the remaining epoxide (Table 16, entry 4). Comparing entries 2 and 4 it can be ascertained that the concentration of the catalytic additives affects the ee. With 1 mol % of copper the effective copper complex concentration is lowered (from 0.20 mM to 0.04 mM) and the ee rises while the starting substrate concentration is kept constant at 4.0 mM. However, detection of azido alcohol in the reaction mixture indicates that with 1 mol % of catalyst the cycloaddition slows to the extent that it becomes the rate limiting step in the cascade. Of particular interest is a reaction performed at 50 mM concentration (Table 16, entry 5). As aforementioned, no trace of **4** had been detected when the enzymatic transformation was attempted at such high substrate concentration (Table 15, entry 8). However, in the presence of click additives and phenylacetylene, after 24 h, 24 % conversion to triazole **5** was detected. Although the enantioselectivity was lower (42 %) in the product than usual, it is significant that the occurrence of the second reaction appears to promote formation of azido alcohol in the first.[2]

Thus with optimized one-pot conditions, it is possible to get 43 % conversion (max 50 %) to the triazole with >99 % ee.

Curious as to the effect of the epoxide and the alkyne upon the outcome of the reaction, a selection of substrates was made for further investigation. In the instance of styrene oxide as a substrate, the results were even more satisfying. At 4.0 mM substrate concentration triazole was detected with > 99% ee, and conversion from epoxide to product was 44 % (max 50 %), with 78 % ee for the epoxide (Table 17, entry 1). Reducing the catalyst loading from 5 to 3 % again proved insufficient, as azido alcohol **3** remained in the reaction mixture (Table17, entry 2).

We also tested propiolic acid as an alkyne substrate (Table17, entry 4). Interestingly, the triazole product was detected with nearly racemic distribution. We hypothesized that the presence of the acid could impact the functionality of the enzyme. Thus the corresponding ester, ethyl propiolate, was tested as well (Table17, entry 5). Indeed, the resulting triazole showed a dramatic improvement in ee to 80 % but the conversion of epoxide remained low after 24 h. We can conclude from these observations that not only is the epoxide important as the substrate undergoing enzymatic conversion, but the choice of accompanying acetylene is equally relevant with regards to both rate and selectivity.

[2] The possibility of enzyme inhibition by the azidoalcohol product at higher concentrations cannot be excluded.

Table 17 Substrate Scope

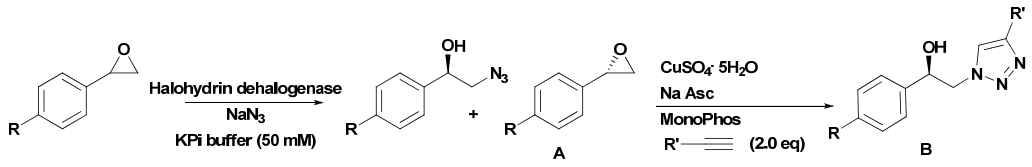

	R[a]	R'	Cu (mol%)	Conv. (%)[b]	ee A (%)	ee B (%)	E
1	H	Ph	5	44	78	99	>200
2	H	Ph	3	n.d.[c]	78	98	>200
3	NO_2	Ph	5	34	51	97	109
4	NO_2	COOH	5	n.d.	n.d.	2	n.d.
5	NO_2	COOMe	5	20[d]	20	80	10

[a] 4.0 mM substrate concentration. [b] After 24 h. Max. conversion 50 %. [c] Azido alcohol remaining in the reaction mixture. [d] Enzyme added in two portions (at 0 h and 12 h).

Given the success of the one-pot cascade with the traditional copper catalyzed [3+2] azide alkyne cycloaddition, we attempted the more biologically interesting copper free click reaction. Cyclooctyne was chosen as a model substrate and the reaction was allowed to proceed for 24 h. Analysis by HPLC revealed the triazole with 96 % ee, and the epoxide with 24 % ee, indicating 20 % conversion (Table18, entry 1). We repeated the reaction over 48 h, adding the enzyme in two portions (half at the start of the reaction, and the other half after 24 h) to ensure constant enzymatic activity. This resulted in a significant increase in the ee of the epoxide to 47 % along with an improvement in conversion. The scope of the one-pot ring opening click reaction can therefore be extended to include the variety of strained cyclic cyclooctyne derivatives that have been developed recently.

Table 18 Copper Free Cycloaddition of Cyclooctyne to *in situ* Generated Azido Alcohol

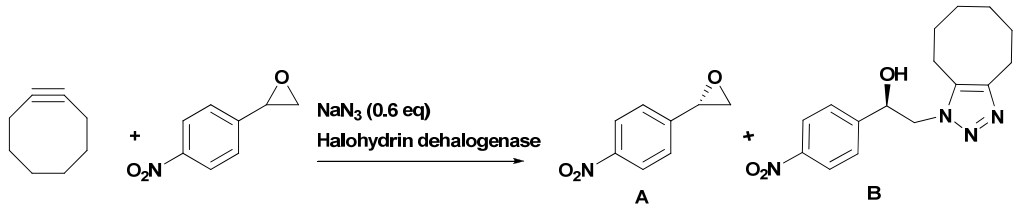

	Time (h)	Conversion (%)[b]	ee A (%)	ee B (%)	E
1	24	20	24	96	83
2	48[a]	32	47	96	78

[a] Enzyme added in two portions (half at t=0 h, half at t=24 h).[b] Max. conversion 50 %.

In conclusion, we have developed a methodology to enzymatically catalyze azidolysis of aromatic epoxides in an enantioselective fashion to the corresponding azido alcohols, and in the same pot, click the resulting azides to alkynes. The reaction conditions are very mild, proceeding in aqueous solution with neutral pH at room temperature. The one-pot nature of the process allows for a simpler, faster and more environmentally friendly reaction, work-up and purification. We have demonstrated that biocatalysis is compatible with one-pot multicomponent reactions. This transformation can be promoted either through copper catalysis or by ring strain, opening the possibility for a wide variety of applications. This methodology was then applied to synthesize a molecule that bears resemblance to a known beta adrenergic receptor blocker in an attempt to develop a new tracer that may serve for cerebral imaging (Scheme 2). Biological investigations of this compound are on-going.

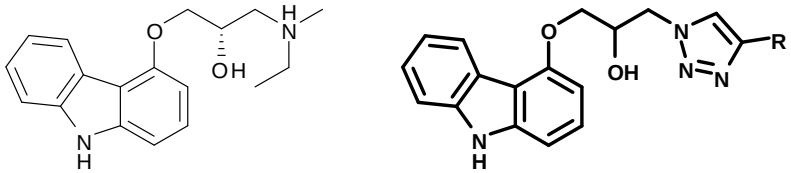

Scheme 2 (S)-[^{18}F]-fluorocarazolol (left) and general structure of analogues prepared by "click"chemistry

4.7 Exploration of reaction parameters in F-18 click chemistry

In cooperation with Stratingh Institute for Chemistry, University of Groningen

The Huisgen 1,3-dipolar cycloaddition of azides and alkynes using copper-I as catalyst, has now been recognized as the most commonly applied 'click reaction'. This reaction has been widely applied to many bioorganic and medicinal research fields, because it proceeds under mild and tolerable conditions, in aqueous media, at neutral PH, and at room temperature, all within a reasonable reaction time. We report herein the first example of dramatic rate acceleration of the 1,3-dipolar cycloaddition using phosporamidite ligands and the application of the developed methodology to positron emission tomography imaging precursors. Phosphoramidites prove to be excellent, high yielding, easily recovered ligands.

Preliminary studies to find an optimal condition of 1,3-dipolar cycloaddition for the two-step F-18 labeling procedure were performed in which 1,3-dipolar cycloaddition of 4-methoxybenzyl azide and phenyl acetylene was employed as a model reaction. In a CuSO4/ Na-ascorbate system, aqueous DMSO was the best reaction media regardless of the water content.

In addition, monodentate phosphoramidite ligands are used to accelerate the Huisgen 1,3-dipolar cycloaddition rapidly yielding a wide variety of functionalized 1,4-disubstituted-1,2,3-triazoles. Phosphoramidites are used as monodentate ligands for copper in a number of stereoselective transformations and have demonstrated strong ligand accelerating effects. Cu(I) and Cu(II) salts both function as the copper source in aqueous solution to provide excellent yields.

To test our methodology on the required time scale of radiolabelling, we designed a small azido prosthetic group, [^{18}F]-fluorinated 1-azido-4-fluorobutane (Scheme 1) and [^{18}F]-fluorinated 1-ethynyl-4-(fluoromethyl)benzene (Scheme 2).

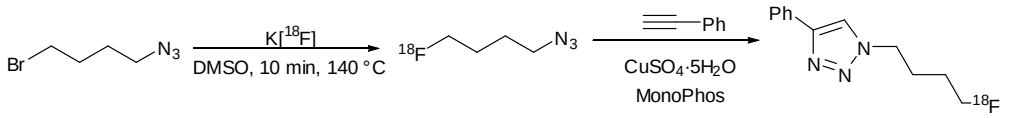

Scheme 1 Synthesis of [18F]-labelled triazole using [18F]alkyl azide

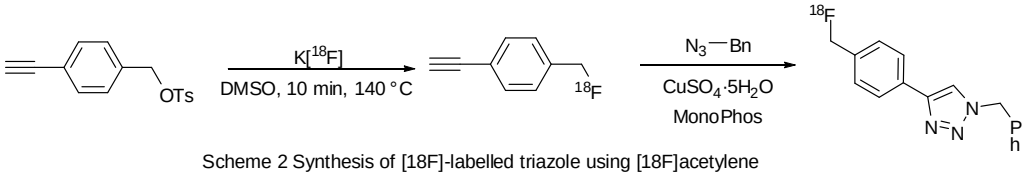

Scheme 2 Synthesis of [18F]-labelled triazole using [18F]acetylene

After fluorination, the tag was attached to its complementary cold acetylene or azide in the presence of $CuSO_4 \cdot 5H_2O$ and MonoPhos. Further optimization reaction was performed by varying the amount of acetylene from 0.01 mg to 0.5 mg (Fig. 2) or azide from 0.05 mg to 0.1 mg, to find the optimal yield of reaction in DMSO/H2O (1/3).

Full conversion to the labelled triazole was detected after 10 min (as determined by HPLC and radio-TLC). In the absence of MonoPhos under identical conditions, only minor conversion to the triazole product was detected (<20 %). (Figure 16)

With regard to F-18, 1mol % of CuSO4 showed a sufficient catalysis effect within a short time.(Figure 17)

In conclusion, the Cu(I)-catalyzed, 1,3-dipolar cycloaddition 'click chemistry' reaction was applied successfully to the synthesis of small, F-18-labeled molecules, and an optimal condition was developed for one-pot, two-step reaction after purification by semipreparative HPLC. The [18F]fluoroalkyne and azide were prepared in yields ranging from 36% to 81%. Conjugation of [18F]fluoroalkynes and azides to various amount (> 0.01 mg) of acetylenes or

azide with via CuI mediated 1,3-dipolar cycloaddition yielded the desired 18F-labeled products in 10 min with yields of 54–99% and excellent radiochemical purity 99%. The total synthesis time was 30 min from the end of bombardment.

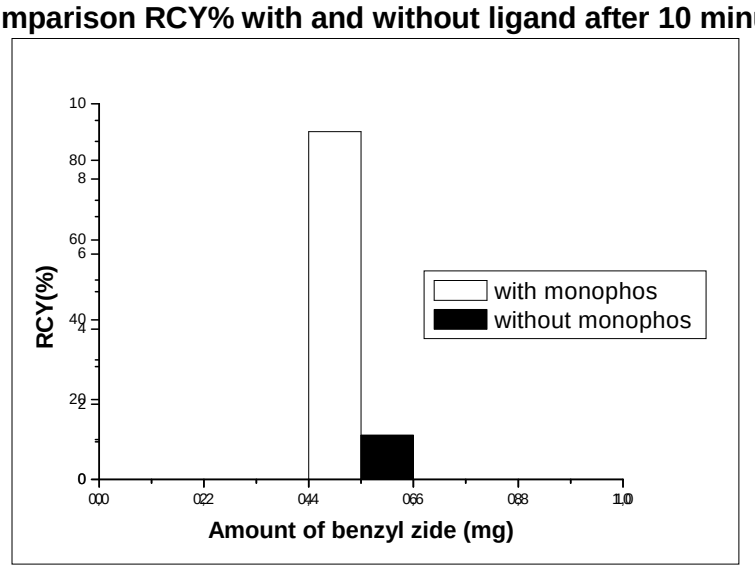

Figure 16

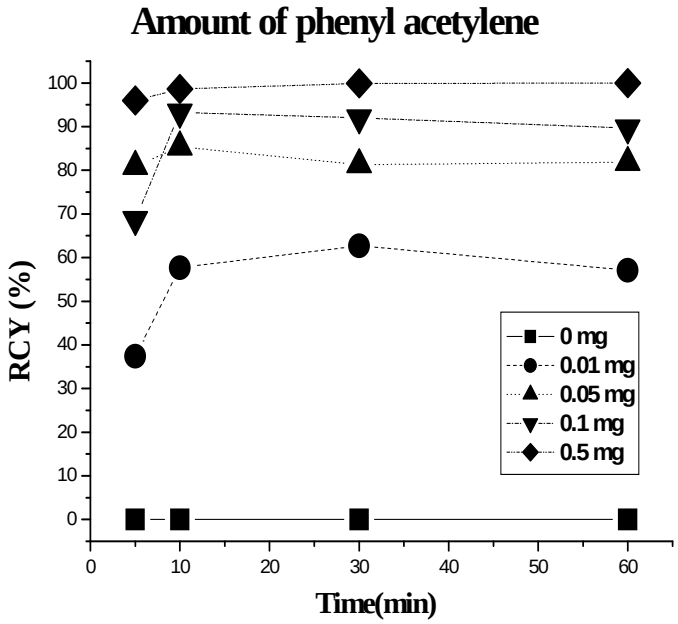

Figure 17

4.8 A Chemical Proteomics Approach towards Profiling and Imaging of Metalloprotease Activity

Proteases are essential in tumor formation and metastatic spread. Numerous clinical studies have shown a correlation between matrix metalloproteinase (MMP) expression and poor outcome of disease. Various MMP inhibitors have been developed for therapeutic purposes in oncology. The ability to image MMP expression non-invasively *in vivo* would allow the characterization of tumours, assessment of the binding of therapeutic drugs to individual subclasses of MMPs in target tissue and monitoring of the effect of treatment on MMP expression or activity as a function of time.

Besides, MMPs are upregulated in a variety of other diseases, such as asthma and neurodegenerative disorders. Molecular imaging of MMP expression would thus potentially allow evaluation of proteinase involvement in tissue remodelling at an early stage of the disease and monitoring of changes in MMP expression after the onset of therapy.

A few MMP inhibitors (selected for high affinity, selectivity for their target and low or moderate lipophilicity) will be labelled with ^{18}F, ^{123}I and ^{99m}Tc. These strategies will be tested first on ML5 whose structure is described in Figure 18 because of its high affinity. Each labelling will take place on the amino group of the lysine moiety of ML5.

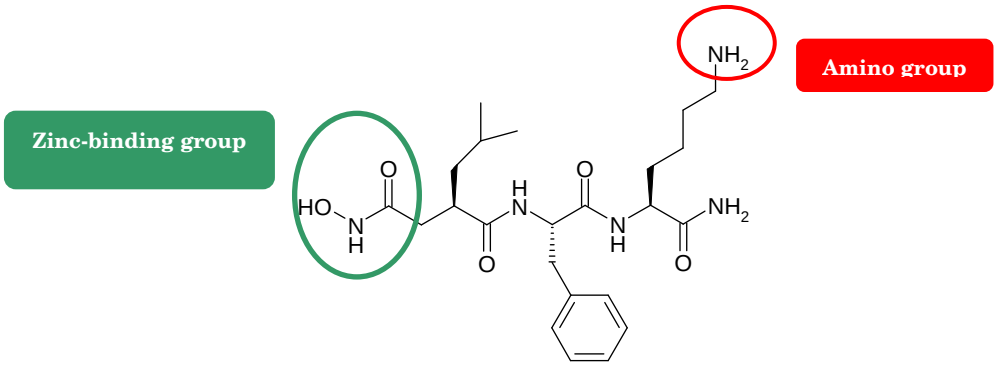

Figure 18: Structure of ML5

	IC_{50} MMP-12	IC_{50} ADAM-17
ML5	5.27 nM	10.7 nM

Two labelling procedures were tested on ML5:
- Direct acylation with N-succinimidyl-4-[^{18}F] fluorobenzoate (^{18}F-SFB) (**Scheme 1**),
- Conjugation of HYNIC followed by hydrazone formation by ^{99m}Tc labelling (**Scheme 2**).

The binding of radiolabeled MMP inhibitors to carefully selected epithelial (16HBE) or tumor cell lines (MCF-7 and MDA-MB-231) will first be quantified *in vitro*. The imaging potential of the most promising candidates will subsequently be assessed in an appropriate *in vivo* tumor model. Successful radiotracers can finally be evaluated in an *in vivo* model of chemotherapy. Treatment of animals with combination chemotherapy is expected to result in a down-regulation of MMP expression within the tumors, which will be assessed by PET or SPECT imaging.

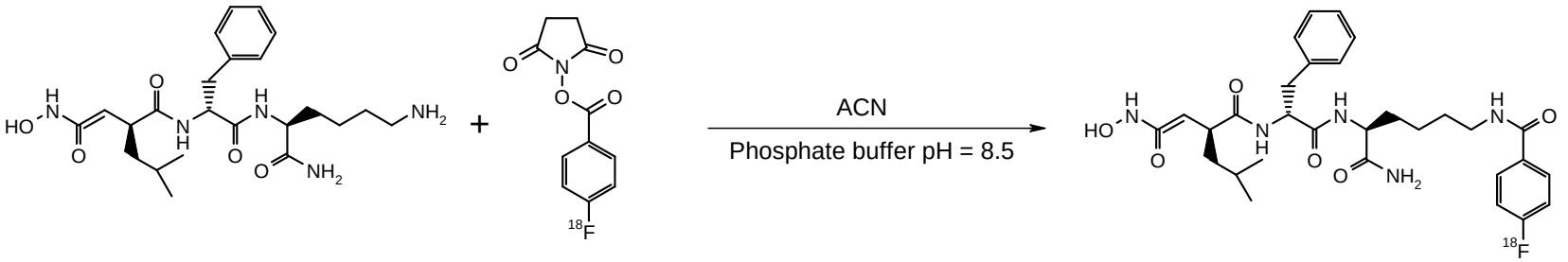

ML5 ^{18}F-SFB ^{18}F-FB-ML5

Scheme 1: Acylation of ML5 with ^{18}F-SFB

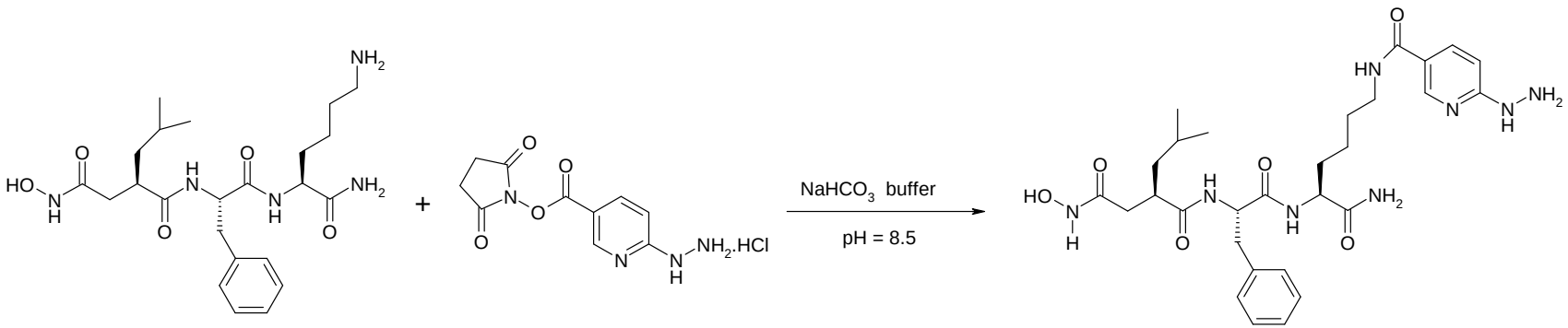

ML5 SHNH HYNIC-ML5

SHNH : Succinimidyl 6-**h**ydrazinium**n**icotinate **h**ydrochloride
HYNIC : 6-**H**ydrazinopyridine-3-carboxylic acid

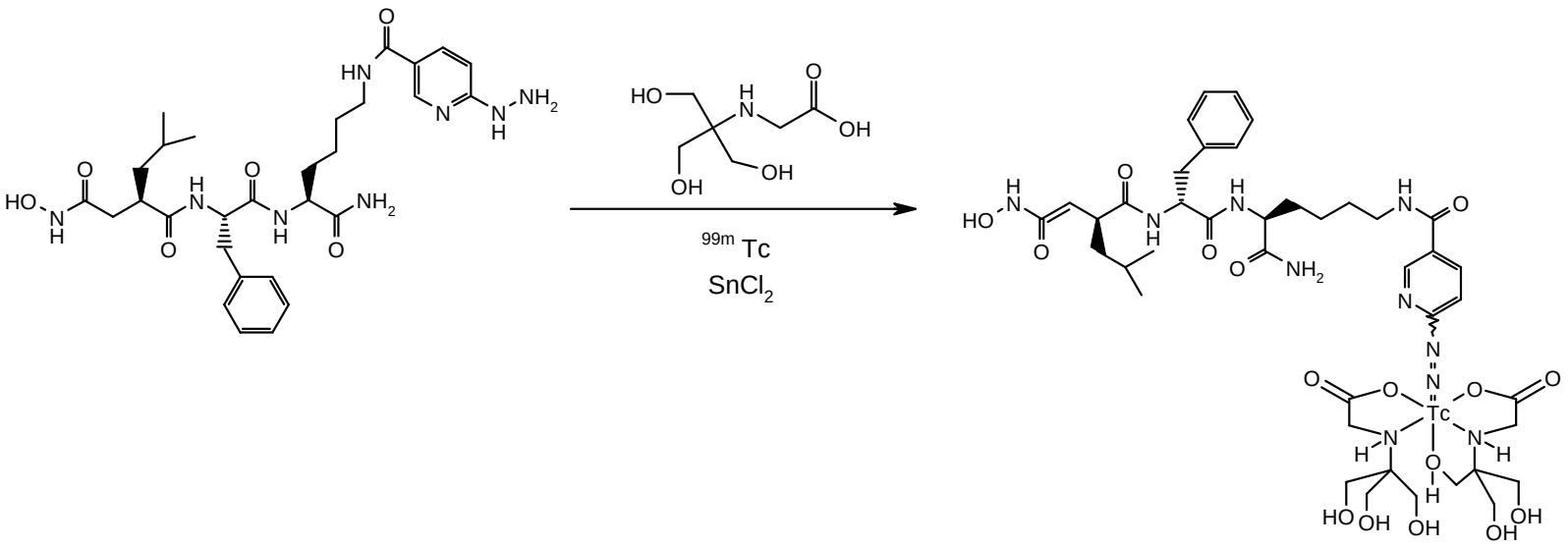

ML5 99mTc(HYNIC-ML5)(tricine$_2$)

Scheme 2: Conjugation of ML5 with SHNH following by labelling with ^{99m}Tc

PUBLICATIONS 2009

5.1 Ph.D. theses and books

1. Bodei, L. Peptide Receptor Radionuclide Therapy with Radiolabelled Somatostatin Analogues. Ph.D.thesis, University of Groningen, May 6, 2009. [Promotores: **R.A.J.O.Dierckx, A.Signore**, co-promotor: G.Paganelli] 143 pages.

2. Breeuwsma,A.J. Molecular Medicine in Staging and Restaging of Prostate Cancer. Ph.D.thesis, University of Groningen, September 2, 2009. [Promotores: J.M.Nijmans, **R.A.J.O.Dierckx**, co-promotores I.J.de Jong, **J.Pruim**] 127 pages.

3. **Eshuis,S.A.** Radiotracer Imaging in PD. Value of In Vivo Presynaptic Dopaminergic Measures in Animal Models and Human Disease. Ph.D.thesis, University of Groningen, October 5, 2009 [Promotores: K.L.Leenders, **R.A.J.O.Dierckx**; co-promotor: **P.L.Jager**] 169 pages.

4. Lazzeri,E. Nuclear Medicine Imaging of Vertebral Infections: Role of Radiolabeled Biotin. Ph.D.thesis, University of Groningen, May 6, 2009. [Promotores: **R.A.J.O.Dierckx**, **A.Signore**, G.Mariani] 166 pages.

5. Nagengast,W.B. New Molecular Imaging in Oncology: a Focus on Angiogenesis. Ph.D.thesis, University of Groningen, December 16, 2009 [Promotor: E.G.E.de Vries, co-promotores: **A.H.Brouwers, M.N.Lub-de Hooge,** G.A.P.Hospers] 165 pages. *[In this thesis, uPET and uSPECT were used as imaging modalities]*

5.2 Papers in international journals

1. Al-Ansari S, Zeebregts CJ, **Slart RH,** Peppelenbosch M, Tio RA, 2009. Galectins in atherosclerotic disease. Trends Cardiovasc Med. 19, 164-169.

2. Bartels,A.L., Zeebregts,C.J., Enting,R.H., **Slart,R.H.** Fluorodeoxyglucose and 11C-Choline positron emission tomography for distinction of metastatic plexopathy and neuritis: a case report. Cases J Dec 15;2:9323.

3. Bartels,A.L., Kortekaas,R., Bart,J., **Willemsen,A.T.,** de Klerk,O.L., de Vries,J.J., van Oostrom,J.C., and Leenders,K.L., 2009. Blood-brain barrier P-glycoprotein function decreases in specific brain regions with aging: a possible role in progressive neurodegeneration. Neurobiol. Aging 30, 1818-1824.

4. Bartels,A.L., Zeebregts,C.J., Bijl,M., Tio,R.A., and **Slart,R.H.,** 2009. Fused FDG-PET and MRI imaging of Takayasu arteritis in vertebral arteries. Ann. Nucl. Med. 23, 753-756.

5. Bastiaannet,E., Hoekstra-Weebers,J.E., Francken,A.B., **Jager,P.L.,** van der Jagt,E.J., and Hoekstra,H.J., 2009. Perception of burden experienced during diagnostic tests by melanoma patients with lymph node metastases. Melanoma Res. 19, 36-41.

6. Bastiaannet,E., Wobbes,T., Hoekstra,O.S., van der Jagt,E.J., **Brouwers,A.H.**, Koelemij,R., de Klerk,J.M., Oyen,W.J., Meijer,S., and Hoekstra,H.J., 2009. Prospective comparison of [18F]fluorodeoxyglucose positron emission tomography and computed tomography in patients with melanoma with palpable lymph node metastases: diagnostic accuracy and impact on treatment. J. Clin. Oncol. 27, 4774-4780.

7. Been,L.B., Hoekstra,H.J., Suurmeijer,A.J., **Jager,P.L.,** van der Laan,B.F., and **Elsinga,P.H.,** 2009. [(18)F]FLT-PET and [(18)F]FDG-PET in the evaluation of radiotherapy for laryngeal cancer. Oral Oncol. 45, e211-e215.

8. Bodei,L., Ferone,D., Grana,C.M., Cremonesi,M., **Signore,A., Dierckx,R.A.,** and Paganelli,G., 2009. Peptide receptor therapies in neuroendocrine tumors. J. Endocrinol. Invest 32, 360-369.

9. Campbell-Verduyn,L.S., **Mirfeizi,L., Dierckx,R.A., Elsinga,P.H.,** and Feringa,B.L., 2009. Phosphoramidite accelerated copper(i)-catalyzed [3 + 2] cycloadditions of azides and alkynes. Chem. Commun. (Camb.) 2139-2141.

10. Chianelli,M., Todino,V., Graziano,F.M., Panunzi,C., Pace,D., Guglielmi,R., **Signore,A.,** and Papini,E., 2009. Low-activity (2.0 GBq; 54 mCi) radioiodine post-surgical remnant ablation in thyroid cancer: comparison between hormone withdrawal and use of rhTSH in low-risk patients. Eur. J. Endocrinol. 160, 431-436.

11. Coert,J.H., Stenekes,M.W., **Paans,A.M.,** Nicolai,J.P., and de Jong,B.M., 2009. Clinical implications of cerebral reorganization after primary digital flexor tendon repair. J. Hand Surg. Eur. Vol. 34, 444-448.

12. Dasselaar,J.J., **Slart,R.H.,** Knip,M., **Pruim,J.,** Tio,R.A., McIntyre,C.W., de Jong,P.E., and Franssen,C.F., 2009. Haemodialysis is associated with a pronounced fall in myocardial perfusion. Nephrol. Dial. Transplant. 24, 604-610.

13. de Jong,R.M., Tio,R.A., van der Harst,P., Voors,A.A., Koning,P.M., Zeebregts,C.J., van Veldhuisen,D.J., **Dierckx,R.A.,** and **Slart,R.H.,** 2009. Ischemic patterns assessed by positron emission tomography predict adverse outcome in patients with idiopathic dilated cardiomyopathy. J. Nucl. Cardiol. 16, 769-774.

14. de Klerk,O.L., **Willemsen,A.T.,** Roosink,M., **Bartels,A.L.,** Hendrikse,N.H., Bosker,F.J., and den Boer,J.A., 2009. Locally increased P-glycoprotein function in major depression: a PET study with [11C]verapamil as a probe for P-glycoprotein function in the blood-brain barrier. Int. J. Neuropsychopharmacol. 19, 1-10.

15. **Dierckx,R.,** Maes,A., Peeters,M., and **Van de Wiele,C.,** 2009. FDG PET for monitoring response to local and locoregional therapy in HCC and liver metastases. Q. J. Nucl. Med. Mol. Imaging 53, 336-342.

16. Dijkers,E.C., Kosterink,J.G., Rademaker,A.P., Perk,L.R., van Dongen,G.A., Bart,J., **de Jong,J.R.,** de Vries,E.G., and **Lub-de Hooge,M.N.,** 2009. Development and characterization of clinical-grade 89Zr-trastuzumab for HER2/neu immunoPET imaging. J. Nucl. Med. 50, 974-981.

17. **Doorduin,J., de Vries,E.F., Willemsen,A.T.,** de Groot,J.C., **Dierckx,R.A.,** and Klein,H.C., 2009. Neuroinflammation in schizophrenia-related psychosis: a PET study. J. Nucl. Med. 50, 1801-1807.

18. **Doorduin,J.,** Klein,H.C., **Dierckx,R.A.,** James,M., Kassiou,M., and **de Vries,E.F.,** 2009. [11C]-DPA-713 and [18F]-DPA-714 as new PET tracers for TSPO: a comparison with [11C]-®-PK11195 in a rat model of herpes encephalitis. Mol. Imaging Biol. 11, 386-398.

19. Duiker,E.W., de Vries,E.G., Mahalingam,D., Meersma,G.J., Boersma-van Ek,W., Hollema,H., **Lub-de Hooge,M.N.,** van Dam,G.M., Cool,R.H., Quax,W.J., Samali,A., van der Zee,A.G., and de Jong,S., 2009. Enhanced antitumor efficacy of a DR5-specific TRAIL variant over recombinant human TRAIL in a bioluminescent ovarian cancer xenograft model. Clin. Cancer Res. 15, 2048-2057.

20 **Elsinga P.H.,** 2009. Obituary: Professor Willem Vaalburg. Nucl. Med. Biol. 36, 233-234.

21. **Eshuis,S.A., Jager,P.L.,** Maguire,R.P., **Jonkman,S., Dierckx,R.A.,** and Leenders,K.L., 2009. Direct comparison of FP-CIT SPECT and F-DOPA PET in patients with Parkinson's disease and healthy controls. Eur. J. Nucl. Med. Mol. Imaging 36, 454-462.

22. Fiebrich,H.B., **Brouwers,A.H., Koopmans,K.P.,** and de Vries,E.G., 2009. Combining 6-fluoro-[18F]l-dihydroxyphenylalanine and [18F]fluoro-2-deoxy-d-glucose positron emission tomography for distinction of non-carcinoid malignancies in carcinoid patients. Eur. J. Cancer 45, 2312-2315.

23. Fiebrich,H.B., **Brouwers,A.H.,** van Bergeijk,L., and van den Berg,G., 2009. Image in endocrinology. Localization of an adrenocorticotropin-producing pheochromocytoma using 18F-dihydroxyphenylalanine positron emission tomography. J. Clin. Endocrinol. Metab 94, 748-749.

24. Fiebrich,H.B., **Brouwers,A.H.,** Kerstens,M.N., Pijl,M.E., Kema,I.P., **de Jong,J.R., Jager,P.L., Elsinga,P.H., Dierckx,R.A.,** van der Wal,J.E., Sluiter,W.J., de Vries,E.G., and Links,T.P., 2009. 6-[F-18]Fluoro-L-dihydroxyphenylalanine positron emission tomography is superior to conventional imaging with (123)I-metaiodobenzylguanidine scintigraphy, computer tomography, and magnetic resonance imaging in localizing tumors causing catecholamine excess. J. Clin. Endocrinol. Metab 94, 3922-3930.

25 Fonteyne,P., Casneuf,V., Pauwels,P., Van Damme,N., Peeters,M., **Dierckx,R.,** and **Van de Wiele,C.,** 2009. Expression of hexokinases and glucose transporters in treated and untreated oesophageal adenocarcinoma. Histol. Histopathol. 24, 971-977.

26. Georgiadis,J.R., Reinders,A.A., **Paans,A.M.,** Renken,R., and Kortekaas,R., 2009. Men versus women on sexual brain function: Prominent differences during tactile genital stimulation, but not during orgasm. Hum. Brain Mapp. 30, 3089-3101.

27 **Glaudemans,A.W., Slart,R.H.,** Zeebregts,C.J., **Veltman,N.C.,** Tio,R.A., Hazenberg,B.P., and **Dierckx,R.A.,** 2009. Nuclear imaging in cardiac amyloidosis. Eur. J. Nucl. Med. Mol. Imaging 36, 702-714.

28 Hoeksma,M., Reijngoud,D.J., **Pruim,J.,** de Valk,H.W., **Paans,A.M.,** and van Spronsen,F.J., 2009. Phenylketonuria: High plasma phenylalanine decreases cerebral protein synthesis. Mol. Genet. Metab 96, 177-182.

29 Hollevoet,K., Bernard,D., De Geeter,F., Walgraeve,N., Van den Eeckhaut,A., Vanholder,R., **Van de Wiele,C.,** Stove,V., van Meerbeeck,J.P., and Delanghe,J.R., 2009. Glomerular filtration rate is a confounder for the measurement of soluble mesothelin in serum. Clin. Chem. 55, 1431-1433.

30 Holm,P.W., **Slart,R.H.,** Zeebregts,C.J., Hillebrands,J.L., and Tio,R.A., 2009. Atherosclerotic plaque development and instability: a dual role for VEGF. Ann. Med. 41, 257-264.

31 Hospers,I.C., van der Laan,J.G., Zeebregts,C.J., Nieboer,P., Wolffenbuttel,B.H., **Dierckx,R.A.,** Kreeftenberg,H.G., **Jager,P.L.,** and **Slart,R.H.,** 2009. Vertebral fracture assessment in supine position: comparison by using conventional semiquantitative radiography and visual radiography. Radiology 251, 822-828.

32. Jorna,F.H., Hollema,H., Hendrikse,H.N., Bart,J., **Brouwers,A.H.,** and Plukker,J.T., 2009. P-gp and MRP1 expression in parathyroid tumors related to histology, weight and (99m)Tc-sestamibi imaging results. Exp. Clin. Endocrinol. Diabetes 117, 406-412.

33. **Koopmans,K.P., Neels,O.,** Kema,I.P., **Elsinga,P.H.,** Links,T.P., de Vries,E.G., and **Jager,P.L.,** 2009. Molecular imaging in neuroendocrine tumors: molecular uptake mechanisms and clinical results. Crit Rev. Oncol. Hematol. 71, 199-213.

34. Krabbe,C.A., **Pruim,J.,** van der Laan,B.F., Rodiger,L.A., and Roodenburg,J.L., 2009. FDG-PET and detection of distant metastases and simultaneous tumors in head and neck squamous cell carcinoma: a comparison with chest radiography and chest CT. Oral Oncol. 45, 234-240.

35. Krabbe,C.A., **Pruim,J.,** Dijkstra,P.U., Balink,H., van der Laan,B.F., de Visscher,J.G., and Roodenburg,J.L., 2009. 18F-FDG PET as a routine posttreatment surveillance tool in oral and oropharyngeal squamous cell carcinoma: a prospective study. J. Nucl. Med. 50, 1940-1947.

36. Krug,B., **Van Zanten,A.,** Pirson,A.S., Crott,R., and van den Borght,T., 2009. Activity-based costing evaluation of a [(18)F]-fludeoxyglucose positron emission tomography study. Health Policy 92, 234-243.

37. Lambert,B. and **Van de Wiele,C.,** 2009. Selective internal radiation therapy of HCC and liver metastases: a locoregional or worldwide therapy? Q. J. Nucl. Med. Mol. Imaging 53, 302-304.

38. Lazarenko,S.V., van der Vleuten,P.A., Tio,R.A., **Willemsen,A.T., Paans,A.M.,** Douma,J.E., Zeebregts,C.J., **Dierckx,R.A.,** Zijlstra,F., and **Slart,R.H.,** 2009. Left ventricular volume assessment by planar radionuclide ventriculography evaluated by MRI. Nucl. Med. Commun. 30, 727-735.

39. Liuti,T., de Vos,J., Bosman,T., **Van de Wiele,C.,** Grinwis,G.C., van Bree,H., and Peremans,K., 2009. 67Gallium citrate scintigraphy to assess metastatic spread in a dog with an oral melanoma. J. Small Anim Pract. 50, 31-34.

40. Loose,D. and **Van de Wiele,C.,** 2009. The immune system and cancer. Cancer Biother. Radiopharm. 24, 369-376.

41. **Luurtsema,G.,** Schuit,R.C., Klok,R.P., Verbeek,J., Leysen,J.E., Lammertsma,A.A., and Windhorst,A.D., 2009. Evaluation of [11C]laniquidar as a tracer of P-glycoprotein: radiosynthesis and biodistribution in rats. Nucl. Med. Biol. 36, 643-649.

42. Malviya,G., D'Alessandria,C., Bonanno,E., Vexler,V., Massari,R., Trotta,C., Scopinaro,F., **Dierckx,R.,** and **Signore,A.,** 2009. Radiolabeled humanized anti-CD3 monoclonal antibody visilizumab for imaging human T-lymphocytes. J. Nucl. Med. 50, 1683-1691.

43. Mees,G., Fonteyne,P., Ceelen,W., Boterberg,T., Pauwels,P., Vangestel,C., Van Damme,N., Peeters,M., **Dierckx,R.,** and **Van de Wiele,C.,** 2009. Combined effect of EPO and radiotherapy on the expression of endogenous molecular markers of tumor metabolism and metastasis. Cancer Biother. Radiopharm. 24, 565-572.

44. Mees,G., **Dierckx,R.,** Vangestel,C., and **Van de Wiele,C.,** 2009. Molecular imaging of hypoxia with radiolabelled agents. Eur. J. Nucl. Med. Mol. Imaging 36, 1674-1686.

45. Muijs,C.T., Schreurs,L.M., Busz,D.M., Beukema,J.C., van der Borden,A.J., **Pruim,J.,** van der Jagt,E.J., Plukker,J.T., and Langendijk,J.A., 2009. Consequences of additional use of PET information for target volume delineation and radiotherapy dose distribution for esophageal cancer. Radiother. Oncol. 93, 447-453.

46. Otte,A., **Van de Wiele,C.,** and **Dierckx,R.A.,** 2009. Radiolabeled immunotherapy in non-Hodgkin's lymphoma treatment: the next step. Nucl. Med. Commun. 30, 5-15.

47. Oude Munnink TH, **Nagengast WB**, **Brouwers AH,** Schröder CP, Hospers GA, **Lub-de Hooge MN**, van der Wall E, van Diest PJ, de Vries EGE. 2009. Molecular imaging of breast cancer. The Breast 18(S3), S66-S73

48. Prakash,J., Bansal,R., Post,E., Jager-Krikken,A., **Lub-de Hooge,M.N.,** and Poelstra,K., 2009. Albumin-binding and tumor vasculature determine the antitumor effect of 15-deoxy-Delta-(12,14)-prostaglandin-J(2) in vivo. Neoplasia. 11, 1348-1358.

49. Rikhof,B., van Doorn,J., Suurmeijer,A.J., Rautenberg,M.W., Groenen,P.J., Verdijk,M.A., **Jager,P.L.,** de Jong,S., Gietema,J.A., and van der Graaf,W.T., 2009. Insulin-like growth factors and insulin-like growth factor-binding proteins in relation to disease status and incidence of hypoglycaemia in patients with a gastrointestinal stromal tumour. Ann. Oncol. 20, 1582-1588.

50. Rottey,S., Van den Bossche,B., Slegers,G., Van Belle,S., and **Van de Wiele,C.,** 2009. Influence of chemotherapy on the biodistribution of [99mTc]hydrazinonicotinamide annexin V in cancer patients. Q. J. Nucl. Med. Mol. Imaging 53, 127-132.

51. Ruers,T.J., Wiering,B., van der Sijp,J.R., Roumen,R.M., de Jong,K.P., Comans,E.F., **Pruim,J.,** Dekker,H.M., Krabbe,P.F., and Oyen,W.J., 2009. Improved selection of patients for hepatic surgery of colorectal liver metastases with (18)F-FDG PET: a randomized study. J. Nucl. Med. 50, 1036-1041.

52. **Rybczynska,A.A., Elsinga,P.H., Sijbesma,J.W.,** Ishiwata,K., **de Jong,J.R., de Vries,E.F., Dierckx,R.A., and van Waarde,A.,** 2009. Steroid hormones affect binding of the sigma ligand 11C-SA4503 in tumour cells and tumour-bearing rats. Eur. J. Nucl. Med. Mol. Imaging 36, 1167-1175.

53. Sathekge,M., Goethals,I., Maes,A., and **Van de Wiele,C.,** 2009. Positron emission tomography in patients suffering from HIV-1 infection. Eur. J. Nucl. Med. Mol. Imaging 36, 1176-1184.

54. **Signore,A.,** Soroa,V.A., and **de Vries,E.F.,** 2009. Radiobelled white blood cells or FDG for imaging on inflammation and infection? Q. J. Nucl. Med. Mol. Imaging 53, 23-25.

55. **Slart,R.H., Tio,R.A.,** Zijlstra,F., and **Dierckx,R.A.,** 2009. Diagnostic pathway of integrated SPECT/CT for coronary artery disease. Eur. J. Nucl. Med. Mol. Imaging 36, 1829-1834.

56. **Sturkenboom MG,** Hoekstra OS, Postema EJ, Zijlstra JM, Berkhof J, Franssen EJ, 2009. A randomised controlled trial assessing the effect of oral diazepam on ^{18}F-FDG uptake in the neck and upper chest region. Mol Imaging Biol. 11, 364-368.

57. Tan,E.S., Jessurun,G.A., Anthonio,R.L., **Slart,R.H.,** Zijlstra,F., and Tio,R.A., 2009. Electromechanical mapping of the left ventricle: possible tool for online decision making in the catheterization laboratory. J. Cardiovasc. Med. (Hagerstown.) 10, 415-419.

58. Tio,R.A., Dabeshlim,A., Siebelink,H.M., de Sutter,J., Hillege,H.L., Zeebregts,C.J., **Dierckx,R.A.,** van Veldhuisen,D.J., Zijlstra,F., and **Slart,R.H.,** 2009. Comparison between the prognostic value of left ventricular function and myocardial perfusion reserve in patients with ischemic heart disease. J. Nucl. Med. 50, 214-219.

59. Tio, R.A., **Slart, R.H.J.A.,** de Boer, R.A., van der Vleuten P.A., de Jong, R.M., van Wijk, L.M., Willems,T., Lubbers, D.D., Voors A.A., van Veldhuisen, D.J., 2009. Reduced regional myocardial perfusion reserve is associated with impaired contractile performance in idiopathic dilated cardiomyopathy Netherlands Heart Journal, 17(12), 470-474.

60. Tolboom,N., Yaqub,M., Boellaard,R., **Luurtsema,G.,** Windhorst,A.D., Scheltens,P., Lammertsma,A.A., and van Berckel,B.N., 2009. Test-retest variability of quantitative [(11)C]PIB studies in Alzheimer's disease. Eur. J. Nucl. Med. Mol. Imaging 36, 1629-1638.

61. Tolboom,N., Yaqub,M., van der Flier,W.M., Boellaard,R., **Luurtsema,G.,** Windhorst,A.D., Barkhof,F., Scheltens,P., Lammertsma,A.A., and van Berckel,B.N., 2009. Detection of Alzheimer pathology in vivo using both 11C-PIB and 18F-FDDNP PET. J. Nucl. Med. 50, 191-197.

62. van Bockel,E.A., Lind,J.S., Zijlstra,J.G., Wijkstra,P.J., Meijer,P.M., van den Berg,M.P., **Slart,R.H.,** Aarts,L.P., and Tulleken,J.E., 2009. Cardiac assessment of patients with late stage Duchenne muscular dystrophy. Neth. Heart J. 17, 232-237.

63. **Van de Wiele,C.,** Defreyne,L., Peeters,M., and Lambert,B., 2009. Yttrium-90 labelled resin microspheres for treatment of primary and secondary malignant liver tumors. Q. J. Nucl. Med. Mol. Imaging 53, 317-324.

64. van Oostrom,J.C., Dekker,M., **Willemsen,A.T.,** de Jong,B.M., Roos,R.A., and Leenders,K.L., 2009. Changes in striatal dopamine D2 receptor binding in pre-clinical Huntington's disease. Eur. J. Neurol. 16, 226-231.

65. van Velden,F.H., Kloet,R.W., van Berckel,B.N., Buijs,F.L., **Luurtsema,G.,** Lammertsma,A.A., and Boellaard,R., 2009. HRRT versus HR+ human brain PET studies: an interscanner test-retest study. J. Nucl. Med. 50, 693-702.

66. **van Waarde,A., Ramakrishnan,N.K., Rybczynska,A.A., Elsinga,P.H.,** Berardi,F., **de Jong,J.R., Kwizera,C.,** Perrone,R., Cantore,M., **Sijbesma,J.W., Dierckx,R.A.,** and Colabufo,N.A., 2009. Synthesis and preclinical evaluation of novel PET probes for P-glycoprotein function and expression. J. Med. Chem. 52, 4524-4532.

67. Vangestel,C., **Van de Wiele,C.,** Mees,G., and Peeters,M., 2009. Forcing cancer cells to commit suicide. Cancer Biother. Radiopharm. 24, 395-407.

68. Vergote,V., Burvenich,C., **Van de Wiele,C.,** and De Spiegeleer,B., 2009. Quality specifications for peptide drugs: a regulatory-pharmaceutical approach. J. Pept. Sci. 15. 697-710.

69. Vergote,V., Van Dorpe,S., Verbeken,M., Burvenich,C., **Van de Wiele,C**., Banks,W.A., and De Spiegeleer,B., 2009. Development of peptide receptor binding assays: Methods to avoid false negatives. Regul. Pept. 158, 97-102.

70. Visser,F.W., Krikken,J.A., Muntinga,J.H., **Dierckx,R.A.,** and Navis,G.J., 2009. Rise in extracellular fluid volume during high sodium depends on BMI in healthy men. Obesity. (Silver. Spring) 17, 1684-1688.

71. Wallis de Vries,B.M., Hillebrands,J.L., van Dam,G.M., Tio,R.A., de Jong,J.S., **Slart,R.H.,** and Zeebregts,C.J., 2009. Images in cardiovascular medicine. Multispectral near-infrared fluorescence molecular imaging of matrix metalloproteinases in a human carotid plaque using a matrix-degrading metalloproteinase-sensitive activatable fluorescent probe. Circulation 119, e534-e536.

72. Wedman,J., **Pruim,J.,** Langendijk,J.A., and van der Laan,B.F., 2009. Visualization of small glottic laryngeal cancer using methyl-labeled 11C-methionine positron emission tomography. Oral Oncol. 45, 703-705.

73. Willemsen, H.M., van der Horst, I.C., Nieuwland, W., **Slart, RH,** Zeebregts, C.J., de Boef, E., Schuitemaker, J.H., Zijlstra, F., Tio, R.A., 2009. The diagnostic value of soluble CD163 in patients presenting with chest pain. Clin Biochem 42, 1662-1666.

74. Yaqub,M., Boellaard,R., van Berckel,B.N., Tolboom,N., **Luurtsema,G.,** Dijkstra,A.A., Lubberink,M., Windhorst,A.D., Scheltens,P., and Lammertsma,A.A., 2009. Evaluation of tracer kinetic models for analysis of [18F]FDDNP studies. Mol. Imaging Biol. 11, 322-333.

5.3 Publications in Dutch journals

1. **Slart RHJA.** SPECT-CT bij patiënten met verdenking op kransslagaderlijden. Nederlands Tijdschrift voor Nucleaire Geneeskunde 2009.

5.4 Abstracts in international journals

1. Agool,A., Vellenga,E., **Dierckx,R.A,** de Wolff,J., and **Slart,R.,** 2009. ^{18}F-FLT is an excellent tool to visualize the bone marrow compartment in patients with aplastic anemia. Eur.J.Nucl.Med.Mol.Imaging 36(Suppl.2):S215.

2. **Antunes, I., de Vries, E.F., Elsinga, P.H.,** Haisma, H., and **Dierckx,R.A.,** 2009. [^{18}F]FEANGA: A PET tracer for extracellular beta-glucuronidase. J.Label.Comp.Radiopharm. 52(Suppl.1):S138.

3. Campbell-Verduyn,L.S., **Mirfeizi, L., Dierckx, R.A., Elsinga, P.H.,** and Feringa,B.L., 2009 Click for PET: Development and application of accelerated 1,3-dipolar cycloadditions of azides and alkynes to [^{18}F]-positron emission tomography. J.Label.Comp.Radiopharm. 52(Suppl.1):S24.

4. Cicone, F., del Mastro, C., di Santo, G., Tofani, A., **Signore, A.,** and Scopinaro, F. ^{111}In and ^{89}Y-Bremsstrahlung scan in the assessment of Zevalin biodistribution. Eur.J.Nucl.Med.Mol.Imaging 36(Suppl.2):S363.

5. De Vries EGE, Oude Munnink TH, Nagengast WB, Brouwers AH, Schroder CP, Hospers GAP, **Lub-de Hooge MN**. Growth Factor Receptors Targeting. Imaging. Impakt Breast Cancer Conference 2009 Brussels, Belgium, May 7-9, 2009. Ann Oncol 20:21,2009

6. **Doorduin, J., Klein, H.C., Dierckx, R.A.,** and **de Vries, E.F.,** 2009. Evaluation of [^{11}C]DAA1106 for imaging and quantification of neuroinflammation in a rat model of herpes encephalitis. J.Label.Comp.Radiopharm. 52(Suppl.1):S92

7. Fiebrich HB, **Brouwers AH,** Kerstens MN, Pijl MEJ, Kema IP, **de Jong JR,** van der Wal JE, Sluiter WJ, de Vries EGE, Links TP. Sensitivity of 6-[F-18]fluoro-L-dihydroxyphenlylalanine positron emission tomography for localizing tumors causing catecholamine excess. J Clin Oncol 27:15s, 2009

8. **Gialleonardo,V.di, de Vries, E.F., Chianelli,M., Dierckx, R.A.,** and **Signore, A.,** 2009. [^{18}F]FB-IL2: A novel PET tracer for detection of activated T-lymphocytes. J.Label.Comp. Radiopharm. 52(Suppl.1):S118.

9. **Gialleonardo,V.di, de Vries,E.F., Chianelli,M.,** Wolffenbüttel,B.H.R., de Vos,P., Pozzilli,P., **Dierckx,R.A.,** and **Signore,A.,** 2009. ^{18}F-Interleukin-2, a novel radioactive probe for insulitis imaging by PET. Eur.J.Nucl.Med.Mol.Imaging 36(Suppl.2):S211.

10. **Golestani R, Slart RH,** Zeebregts CJ, **Dierckx RA, Boersma HH,** Hillege HL, Tio RA, 2009. Abdominal aortic calcification detected with routine vertebral fracture assessment: A strong predictor of cardiovascular events. Circulation 120:S359-S360

11. Groot DMG de, Cappaert N, De Esch C, De Groot M, Heerschap A, Jetten N, Kuper F, Muijser H, Stierum R, Veltien A, Voet B, **De Vries EFJ, van Waarde A,** Wadman W, Wolterbeek A, Radonjic M. Comparison of conventional and innovative technologies for (regulatory) developmental neurotoxicity testing: A model study in rats with MeHg. Toxicologist 108:37,2009.

12. Kruizinga,S., **Slart,R.H.J.A.,** Stegger,L., Tio,R.A., Szymanski,M.K., Schoemaker,R.G., van Veldhuisen,D., **Dierckx,R.A.,** Schäfers,M., and Hillege,H.L. ^{13}N-Ammonia enables quantification of left ventricular volume and left ventricular ejection fraction in rats using ECG-gated micro-PET. Eur.J.Nucl.Med.Mol.Imaging 36(Suppl.2):S323.

13. **Maas B.,** Westera, G., **Medema, J.,** van der Vliet, L., and **Elsinga, P.H,** 2009. Simplified and automated preparation method for ^{18}F-fluoromethylcholine using a new synthesis module. J.Label.Comp.Radiopharm. 52(Suppl.1):S140.

14. Malviya, G., **Dierckx, R.A.,** and **Signore,A.,** 2009. Radiolabelling of a fully human anti-DR monoclonal antibody with 99m-technetium: a potential new imaging agent for lymphoma and autoimmunity. Eur.J.Nucl.Med.Mol.Imaging 36(Suppl.2):S404.

15. **Mirfeizi, L.,** Campbell-Verduyn, L.S., Feringa, B.L., **Dierckx, R.A.,** and **Elsinga, P.H.,** 2009. Ligand acceleration and exploration of reaction parameters of F-18 click chemistry. J.Label.Comp.Radiopharm. 52(Suppl.1):S27

16. **Negenman-Wiegersma, B.J., Eshuis, S.A., Glaudemans, A.W.J.M., Koopmans, K.P.,** and **Pruim, J.,** 2009. Optimalisation of the interval between injection and F-DOPA PET scan in patients with Parkinson's disease. Eur.J.Nucl.Med.Mol.Imaging 36(Suppl.2):S161.

17. Oude Munnink T, Dijkers E, **Lub-de Hooge M**, Kosterink JGW, **Brouwers, AH, de Jong, JR,** van Dongen GA, de Vries EGE. HER2-PET imaging with ^{89}Zr-trastuzumab in metastatic breast cancer patients. J Clin Oncol 27;15s, 2009 (suppl; abstr 1045)

18. **Rybczynska,A.,** De Bruyn,M., **Elsinga,P., Dierckx,R.,** Helfrich,W., and **van Waarde,A**., 2009. Cancer cell killing by {sigma}-ligands and sTRAIL: Monitoring synergy with PET. J Nucl Med 50, 1551.

19. **van Waarde,A., Ramakrishnan,N., Elsinga,P.,** Berardi,F., **Willemsen,A.,** Perrone,R., Cantore,M., **Dierckx,R.,** and Colabufo,N., 2009. Synthesis and evaluation of novel PET probes for P-gp expression and function. J.Nucl Med. 50, 619.

5.5 Conference proceedings, invited lectures, etc

1. **Boersma HH**. Good Radiopharmacy Practice and Good Manufacturing Practice. [2 lectures]. IAEA meeting, Shanghai, China, 4-10 July, 2009

2. **Boersma HH.** The Role of the QP in an R&D Environment. Lecture on PET in clinical research within the frame of a workshop. QP-Forum, Barcelona, 3-4 December 2009

3. **Brouwers AH**. Nieuwe imaging technieken in de nucleaire geneeskunde. Invited lecture, Patiëntenvereniging Multipele Endocriene Neoplasie (MEN), Breukelen, april 2009

4. **Brouwers AH.** Bijschildklierscintigrafie bij hyperparathyreoidie. Invited lecture, Nederlandse AIOs Nucleaire Geneeskunde, Rotterdam, april 2009

5. **Brouwers AH.** De ins en outs van poliklinische ^{131}I therapie. Invited lecture, Nederlandse Vereniging Medische Beeldvorming en Radiotherapie (NVMBR), mei en september 2009 (onderwijs voor medisch nucleair werkers)

6. **Brouwers AH.** SPECT en PET imaging van hersentumoren. Invited lecture, Nederlandse AIOs Nucleaire Geneeskunde, Nieuwegein, september 2009

7. Bruggink JLM, Saleem B, Meerwaldt R, van Dam G, Prins T, **Glaudemans A, Slart RHJA,** Zeebregts CJ. Consensus in FDG-PET en CT beoordeling bij de diagnostiek van vaatprothese infecties. Jaarlijkse Bijeenkomst Nederlandse Vereniging voor Heelkunde, 2009.

8. Groot DMG de, Cappaert N, De Esch C, De Groot M, Heerschap A, Jetten N, Kuper F, Muijser H, Stierum R, Veltien A, Voet B, **De Vries EFJ, van Waarde A,** Wadman W, Wolterbeek A, Radonjic M. Comparison of conventional and innovative Technologies for (regulatory) developmental neurotoxicity testing: a model study in rats with MeHg. 48th Annual Meeting of the Society of Toxicology, Baltimore MD, March 15-19, 2009 (poster presentation)

9. Groot DMG de, **de Vries EFJ,** Heerschap A. Testing developmental neurotoxicity: Saving animals by in vivo imaging with PET and MRI. Jubileum Conference, Dutch Society of Toxicology, Veldhoven, The Netherlands, June 18-19, 2009 (oral presentation)

10. Groot DMG de, Cappaert N, De Esch C, De Groot M, Heerschap A, Jetten N, Kuper F, Muijser H, Stierum R, Veltien A, Voet B, **De Vries EFJ, van Waarde A,** Wadman W, Wolterbeek A, Radonjic M. Comparison of conventional and innovative Technologies for (regulatory) developmental neurotoxicity testing: a model study in rats with MeHg. World Congress on Alternatives and Animal Use in Life Sciences, Rome, Italy, August 29 – September 4, 2009 (poster presentation)

11. Groot DMG de, Jetten N, Voet B, Wolterbeek A, Veltien A, Heerschap A, **Dierckx RA, van Waarde A, Willemsen ATM, de Vries EFJ.** Saving animals by in vivo imaging with PET and MRI: Proposed innovations in developmental neurotoxicity testing. World Congress on Alternatives and Animal Use in Life Sciences, Rome, Italy, August 29 – September 4, 2009 (oral presentation)

12. Groot DMG de, Berk M, Bogaard M, Cappaert N, de Groot VJ, Heerschap A, Kuper F, Jetten N, Nederlof R, Stierum R, Uitvlugt E, Veltien A, Voet B, **de Vries EFJ, van Waarde A,** Wadman W, Wolterbeek A, Radonjic M. MRI and PET scan of the brain. 7th European Congress of Toxicologic Pathology, The Hague, The Netherlands, September 15-18, 2009 (oral presentation)

13. **De Vries EFJ**, PET imaging of hormone receptors. New trends in Molecular Imaging and Nuclear Medicine. Bologna, Italy, September 14, 2009.

14. **De Vries EFJ**. Tracer development and production. Two lectures, 2nd year biotechnology students, La Sapienza University, Rome, Italy, May 2009.

15. **De Vries EFJ**. PET radiochemie. Lecture, 4^{e}-jaars MBRT studenten, Hanzehogeschool, Groningen, September 2009

16. Klerk OL de, Bosker FJ, **Willemsen ATM, van Waarde A, Visser AKD,** de Jager T, Dagyte G, den Boer JA, Meerlo P. Opposite effects of chronic stress and antidepressant treatment on the efflux pump P-glycoprotein at the blood-brain barrier: an experimental PET study in rats. 22d Congress of the European College of Neuropsychopharmacology, Istanbul, Turkey *[this contribution won a prize for the best poster at this meeting]*.

17. Klerk OL de, **Willemsen ATM,** Bosker FJ, **Dierckx RA,** den Boer JA. Increased P-glycoprotein function in schizophrenia. A PET study with [^{11}C]verapamil as a probe for P-glycoprotein function in the blood-brain barrier. 22d Congress of the European College of Neuropsychopharmacology, Istanbul, Turkey

18. **Lub-de Hooge MN.** 99mTc-radiofarmaca: bereiding en kwaliteitscontrole. PUOZ Radiofarmacie, Eindhoven, June 2009.

19. **Lub-de Hooge MN**. Bloedcellabelingen. PUOZ Radiofarmacie,Eindhoven, June 2009.

20. **Lub-de Hooge MN**. Development of new radiopharmaceuticals. Bezoek Bordet. 25 May 2009

21. Nagengast WB, **Lub-de Hooge MN**, Gietema JA, Oosting SF, Warnders F, de Korte MA, Timmer-Bosscha H, **de Jong JR**, Hospers GA, den Dunnen WF, Hollema H, de Vries EGE. ^{89}Zr-ranibizumab VEGF microPET imaging during sunitinib treatment visualizes changes with low tracer uptake in the center of the tumor and high uptake at the rim with a rebound tumor uptake after end of treatment. Abstract, Annual Meeting of the American Association for Cancer Research (AACR) 2009.

22. Oude Munnink TH, de Korte MA, Nagengast WB, Timmer-Bosscha H, Schröder CP, **Brouwers AH, de Jong JR, de Hooge M.N.,** Jensen MR, de Vries, EGE. ^{89}Zr-trastuzumab immunoPET visualizes HER2 downregulation induced by the HSP90 inhibitor NVP-AUY922 in human tumor xenograft. AACR meeting abstracts 2009;abstract # 3998.

23. Tio RA, Dabeshim A, Siebelink HMJ, de Sutter J, Hillege JL, Zeebregts CJ, **Dierckx RAJO**, van Veldhuisen DJ, Zijlstra F, **Slart RHJA**. Comparison between the prognostic value of left ventricular function and myocardial perfusion reserve in patients with ischemic heart disease. ICNC, Barcelona, 2009

24. **van Waarde A.** Small animal PET for quantification of neuroreceptor density, neurotransporter activity and neurotransporter expression. Course on Membranes, Signal Transduction and Transport, Graduate School GUIDE, March 13, 2009 [lecture]

25. **van Waarde A.** Guided tour of the facilities for PET imaging in Groningen. Master students of the Graduate School GUIDE. March 12, March 16 and March 19, 2009 [3 groups of 10 students, guided tour of 2 hours]

26. **van Waarde A.** PET imaging: Assessment of in vivo biochemistry. Course on Functional Neuroscience. BCN Research Masters, Graduate School BCN, Groningen, September 14, 2009 [2 invited lectures]

27. **van Waarde A.** Small Animal PET: Principles, Background, Applications. Topmaster II MPD 2009 Course on Research Methods, Groningen, November 26, 2009 [2 invited lectures]

28. **Wu C**, van der Have F, Vastenhouw B, **Dierckx R**, **Paans A**, Beekman F. Absolute quantitative focusing pinhole SPECT. 10th International Meeting on Fully Three-Dimensional Image Reconstruction in Radiology and Nuclear Medicine, Beijing, China, September 5-10, 2009

29. Zeebregts CJ, Bruggink JLM, Meerwaldt R, Prins TR, **Glaudemans AWJM, Slart RHJA**. Concordance in FDG PET and CT reading in diagnosing vascular prosthetic graft infection: a single center experience. SITE 2009.

30. **Zeilstra A, Golestani R,** Zeebregts CJ, Tio RA, **Boersma HH,** Hillege JL, **Dierckx RA, Slart RHJA.** Abdominale aorta calcificatie detectie met de Instant Vertebral Assessment. Een vergelijkende studie met conventionele laterale X-LWK. NVMBR Jaarcongres, 15 mei 2009

5.6 Book chapters

1. **Boersma HH, Signore A** Contributors to: “Clinical translation of radiolabeleled monoclonal antibodies and peptides”. IAEA Human Health Series No. 8, International Atomic Energy Agency Vienna, 2009.

2. **Brouwers AH, Jager PL.** Radionuclide Imaging in Renal Cell Carcinoma. In: Imaging in urologic oncology. Editors: De la Rosette JJMCH, Manyak MJ, Harisingani MG, Wijkstra H. Springer-Verlag, London, 2009; pp.85-104.

3. **Glaudemans AWJM, Klein HC, de Vries EFJ, Doorduin J, Dierckx RAJO.** De rol van nucleaire geneeskunde bij het chronische-vermoeidheidssyndroom. In: Moe of Vermoeid? CVS gewikt en gewogen. Antwerpen: Standaard Uitgeverij, pp.205-219, 2009.

4. **Glaudemans AWJM,** Lam MGEH, **Veltman NC, Dierckx RAJO, Signore A.** The Contribution of Nuclear Medicine in the Diagonosis of Bone Metastases. Chapter 7 in: Bone Metastases, Cancer Metastasis – Biology and Treatment 12, Berlin: Springer Science, pp.137-161, 2009.

PERSONNEL

Listed by function in alphabetic order

6.1 Medical Staff

Adrienne H Brouwers MD PhD
Prof. Rudi A.Dierckx MD PhD (Head of the Department)
Andor Glaudemans MD
Jan Pruim MD PhD
Riemer HJA Slart MD PhD
Ali Agool MD (independent collaborator)
TTH Phan MD PhD (independent collaborator)

6.2 Residents-in-Training

Sylvia Eshuis MD
Klaas Pieter Koopmans MD
Olga V.Mirankova MD
Niels Veltman MD
Leo Weijs MD
Ronald van Rheenen MD
Walter Noordzij MD

6.3 Medical Physics

Johan R de Jong PhD (medical physicist-in-training)
Sergiy Lazarenko MSc (medical physicist-in-training)
Prof Anne MJ Paans PhD (medical physicist)
Marcel Segbers MSc (medical physicist-in-training)
Klaas Willem Sietsma (system administrator)
Roel Wierts MSc (medical physicist-in-training)
Antoon TM Willemsen PhD (medical physicist)

6.4 Radiochemistry

H.H. Boersma, PhD, Pharmacist
Joost Bruns (lab technician)
Hilde Dekens (lab technician)
Prof Philip H.Elsinga PhD (radiochemist)
Marissa Heijnen (assistant)
Chantal Kwizera (lab technician)
Vanathee Logendran (assistant)
Marjolijn Lub-de Hooge PhD (pharmacist)
Gert Luurtsema, PhD, lab coördinator

Bram Maas (lab technician)
Hugo Nijnuis (lab technician)
Esther Olthoff (assistant)
Hans Pol (lab technician)
Bertha Tamming (lab technician)
Erik FJ de Vries PhD (radiochemist)
Michel de Vries (lab technician)
Aren van Waarde PhD (biologist)

6.5 Nuclear Medicine Technologists

Marijke Broersma
José Douma
Karin Groeneveld
Yvonne van der Knaap
Remko Koning
Clara Lemstra
Bregtsje Negenman
Yvonne Reitsma
Leonie Segenhout
Eelco Severs
Jurgen Sijbesma
Paul van Snick
Hans ter Veen
Hedy C Vrakking
Johan Wiegers
Aafke Zeilstra

6.6 Medical & Financial Administration

Annelies Boer (until March 1)
Ineke (GA) ten Have (after June 1)
Arja RJ Hoekman
Jitze Medema, TQM senor advisor
Peggy A. Radjiman (after July 1)
Ilse Sewnandan
Hanna van der Sloot (until June 1)
Rika C van der Werff
Erna R van der Wijk
Annie K van Zanten ML

6.7 PhD Students

Mershima Abdoli
Janine Doorduin MSc
Inês Farinha Antunes MSc
Valentina di Gialleonardo MSc
Reza Golestani MD

Onno L de Klerk MD
Silvana Kruizinga MSc
Willem Jan Kuik, MSc
Nisha Kuzhuppilly Ramakrishnan MSc
Gaurav Malvyia MSc
Nathalie Matusiak MSc
Gilles Mees, MSc
Leila Mirfeizi MSc
Ania Rybczynska MSc
Anniek Visser, MSc
Chao Wu MSc
Zilin Yu MSc

6.8 Visiting Scientists

Marco Chianelli MD PhD
Andre Dobbeleir PhD
A. Piepsz Ph.D.
Alberto Signore MD PhD
Christophe van de Wiele MD PhD
Habib Zaidi PhD

6.9 Trainees

Sali Al Ansari
Ruben Buijs
Hans de Haas
Vincent Haver
Ming Kai Lam
Marleen Masteling
Aline van der Schaaf

OTHER RESPONSIBILITIES

7.1 Teaching activities

On April 23 and 24, 2009, the Department organized an international symposium (2 days, about 150 participants) entitled: “Molecular Imaging in Drug Discovery”. Sponsors were (in alphabetic order) Advion, Astellas, Bayer Health Care, Comecer, Covidien, Ecce Dutoit, GE, IBA, IC Medical, MILabs, PRA International, Siemens, Veenstra Instruments, and Von Gahlen. The local organizing committee consisted of R.A.J.O. Dierckx, P.H. Elsinga A.M.J. Paans, J. Pruim, E.F.J. de Vries and A. van Waarde, with external support from J.Zomer.

An overview of our other teaching activities is provided in Tables 19, 20 and 21. The total number of teaching hours was 360.

7.2 Appointments, diploms, (inter) national cooperation

Onno de Klerk has won the 2009 ECNP Poster Award for his contribution entitled “Opposite effects of chronic stress and antidepressant treatment on the efflux pump P-glycoprotein at the blood-brain barrier: an experimental PET study in rats” (22^{nd} Congress of the European College of Neuropsychopharmacology, Istanbul, Turkey).

During the 11th Netherlands Catalysis and Chemistry Conference (Noordwijkerhout, The Netherlands), Lachlan Campbell-Verduyn has won one of the three lecture prizes awarded to PhD students. The title of Lachlan’s talk was: "Development of Ligand Accelerated Copper Catalyzed 1,3-dipolar Cycloadditions of Azides and Alkynes and Application to [^{18}F]- PET". During the Bi-annual meeting of the International Society for Radiopharmaceutical Sciences (Edmonton, Canada, July 2009), Lachlan also won the Wiley award for her contribution about click chemistry.

P.H.Elsinga was invited to edit a book on PET Imaging in Drug Development. Co-editors will be R.A.J.O.Dierckx, A.M.J.Paans and A.van Waarde. The book will be published in 2010.

A.van Waarde was invited to edit a special issue of the international journal *Current Topics in Medicinal Chemistry* on molecular imaging of ABC transporter function and expression. Prof.N.A.Colabufo (Department of Pharmacochemistry, Bari, Italy) will be co-editor. The issue will appear in 2010.

7.3 Social responsibilities

Algemeen Stralings Deskundige, Universitair Medisch Centrum Groningen (A.M.J.Paans, until February 1,2009; A.T.M.Willemsen, since February 1)

Beoogd voorzitter, Visitatiecommissie, Nederlandse Vereniging voor Nucleaire Geneeskunde (J.Pruim)

Chairman, Dutch Society of Radiopharmaceutical Chemistry (P.H.Elsinga)
Dagvoorzitter, Nascholing Longen voor Medisch Nucleair Werkers, NVMBR (C.Lemstra)
Editor, PET in Drug Development (textbook, P.H.Elsinga, R.A.Dierckx, A.M.J.Paans, A.van Waarde)
European Editor, Nuclear Medicine Communications (R.A.Dierckx)
Executive Guest Editor, Current Topics in Medicinal Chemistry (A.van Waarde)
Lid, Beoordelingscommissie (20 proefschriften, R.A.Dierckx)
Lid, Beoordelingscommissie (3 proefschriften, A.M.J.Paans)
Lid. Beoordelingscommissie (1 proefschrift, A.T.M.Willemsen)
Lid, Beroepscommissie van de Medische Specialisten Registratie Commissie namens de Nederlande Vereniging voor Nucleaire Geneeskunde (J.Pruim)
Lid, CBO richtlijn ontwikkeling Hypopharynxcarcinoom (namens de Nederlandse Vereniging voor Nucleaire Geneeskunde (J.Pruim)
Lid, CIM, Universitair Medisch Centrum Groningen (M.N.Lub-De Hooge)
Lid, Commissie Kwaliteit Bevordering, Nederlandse Vereniging voor Nucleaire Geneeskunde (A.H.Brouwers)
Lid, Concilium, Nederlandse Vereniging voor Nucleaire Geneeskunde (R.A.Dierckx)
Lid, Disciplinegroep Medische Beeldvorming, Stichting Kinderoncologie Nederland (A.H.Brouwers)
Lid, Examencommissie Biomedische Technologie (A.M.J.Paans)
Lid, Hemato-Oncologie voor Volwassenen Nederland (HOVON) Imaging Group (J.Pruim, A.T.M.Willemsen).
Lid, Landelijke Nascholingscommissie Medisch Nucleair Werkers, NVMBR (C.Lemstra)
Lid, Medisch-Ethische Toetsings Commissie, Universitair Medisch Centrum Groningen (A.M.J.Paans)
Lid, Netwerk Nederlands Kenniscentrum voor Farmacotherapie bij Kinderen (M.N.Lub-De Hooge)
Lid, Onderwijscommissie, Nederlandse Vereniging voor Nucleaire Geneeskunde (J.Pruim)
Lid, Onderwijscommissie, Nederlandse Vereniging voor Nucleaire Geneeskunde (R.H.J.A.Slart)
Lid, Redactie Leerboek Nucleaire Geneeskunde (C.Lemstra)
Lid, Redactie Tijdschrift voor Nucleaire Geneeskunde (R.H.J.A.Slart)
Lid, SIG Kindergeneeskunde, Nederlandse Vereniging van Ziekenhuis Apothekers (M.N.Lub-de Hooge)
Lid, Visitatiecommissie Nederlandse Vereniging voor Nucleaire Geneeskunde (R.A.Dierckx)
Lid, Werkgroep Atriumfibrilleren, Proeftuin Groningen t.b.v. Groninger Transmuraal Formularium (M.N.Lub-De Hooge)
Lid, Werkgroep Nederlandse Federatie van Universitaire Ziekenhuizen (R.A.Dierckx)
Lid, Werkgroep Nucleaire Cardiologie, cardiale MSCT en MRI voor de Nederlandse Vereniging voor Cardiologie (R.H.J.A.Slart)
Member, Board of Directors, International Society of Radiopharmaceutical Sciences (P.H.Elsinga)
Member, Board International Research Group in Immuno-Scintigraphy and Therapy (IRIST) (M.N.Lub-De Hooge)
Member, Committee on Radiopharmacy, European Association of Nuclear Medicine (P.H.Elsinga)

Member, Dutch Medicines for Children Research Network (MCRN) (M.N. Lub-de Hooge).

Member, Editorial Board, European Journal of Nuclear Medicine and Molecular Imaging (R.A.Dierckx)

Member, European Organisation for Research and Treatment of Cancer (EORTC) Imaging Group (J.Pruim)

Opleider Klinische Fysica (A.M.J.Paans, A.T.M.Willemsen)

Opleider Nucleaire Geneeskunde (R.A.J.O.Dierckx)

Teacher, Annual Course on PET/CT, European Association of Nuclear Medicine, Vienna (J.Pruim)

Vervangend Opleider Nucleaire Geneeskunde (J.Pruim)

Voorzitter, SIG Nucleaire Geneeskunde en Radiofarmacie, Nederlandse Vereniging van Ziekenhuis Apothekers (M.N.Lub-De Hooge)

Table 19. Trainingships/Internships

Recipient(s)	Duration	Frequency	Location	Teacher(s)	Subject(s)	h
NMP resid. Radiol. Departm.	3-6 mths	Approx 1/yr	RAD	Dierckx, Pruim, vd Jagt	General radiology	0
Radiol. resid. NM&MI departm.	Ad hoc	Sept/Oct 2009	NM&MI	vd Jagt, Dierckx, Pruim	General nuclear medicine	0
Endocr. resid.	2 d	1/yr	NM&MI	Brouwers	Endocr. diagn & therapy	10
Cardiol. resid.	Tu Th morning	Every week	NM&MI	Slart, Tio	Nuclear cardiology	0
Hospital Pharmacist i.t. yr 1	2 wks	1/yr	NM&MI	de Hooge, Sturkenboom	Radiopharmacy	0
Hospital Pharmacist i.t. yr 3-4	4-8 wks	1/yr	NM&MI	de Hooge, Sturkenboom	Radiopharmacy	0
Technologist i.t. yr 1	3 d	1/yr	NM&MI	Lesterhuis, ter Veen	Nuclear medicine technique	0
Technologist i.t. yr 3	20 wks	1/yr	NM&MI	Lesterhuis, ter Veen	Nuclear medicine technique	0
Technologist i.t. yr 4	12 wks dual	1/yr	NM&MI	Lesterhuis, ter Veen	Nuclear medicine technique	0
Medical physicist i.t.	Ad hoc	Frequently	NM&MI	Willemsen, NM physician	Nuclear medicine technique	0
Pharm. Student yr 4-5	6 mths	1/yr	NM&MI	de Hooge, Sturkenboom	Radiopharmacy subsidiary subject	0
Pharm. Student yr 3	3 wks	1/yr	NM&MI	de Hooge, Sturkenboom	Radiopharmacy scientific internship	0
M3 medical student yr 6	3-6 mths	On request	NM&MI	Slart, Haayer, Bloem	On request	3
Medical student PPP yr 3	10 d	1/yr	NM&MI	Slart	Blok 2.3 PPP Syllabus	8
Mentorship medical yr 1	17 d	1/yr	NM&MI	Glaudemans	Gen medical training and teaching	100
Foreign student cardiol.	1/2 d	1/yr	NM&MI	Slart, vd Broek	Nuclear cardiology	2
Semi-medical resid. Yr 6	3 mths	On request	NM&MI	Slart, Dierckx	General nuclear medicine	0
Radiochemists (foreign) i.t.	3 mths	On request	NM&MI	de Vries	Radiochemistry	0
NNCO	1/2 d	1/yr	NM&MI	Dierckx	Master oncology imaging	2

NB Zero hours in the last column indicates that no regular teaching was performed by our Department but an internship (stage period) was provided

Table 20. Continuous Education

Recipient(s)	Duration	Frequency	Location	Teacher(s)	Subject(s)	h
Medical student yr 2	1/2 d	1/yr	NM&MI	Slart, vd Broek	Angina pectoris	2
Medical student yr 2	1/2 d	1/yr	NM&MI	Brouwers	Thyroid	2
Medical internship M1	1 hr	8/yr	NM&MI	Slart	General nuclear medicine	3
Medical internship M1	2 hr	8/wk	NM&MI	Brouwers, Pruim	Interactive lecture neck swellings	16
NMP resid. & Hospital Pharm. i.t.	3 d	1/yr	PUOZ Eindhoven	de Hooge, Slart	Radiopharmacy, nuclear cardiology	0
Orthopedic Resident	1 hr	1/yr	Dept. Orthopedics	Nuclear medicine physicians	Bone and joint scintigraphy	0
Pharmacy Student yr 4-5	1/2 d	1/yr	NM&MI	de Hooge, Sturkenboom	Introduction radiopharmacy etc	2
Pharmacy Student yr 6	1/2 d	1/yr	NM&MI	de Hooge, Sturkenboom	Introduction radiopharmacy etc	2
Radiopharmacistis in training	1 hr	1/yr	Teaching Center	Brouwers	Introduction to nuclear medicine	1
Morning session cardiology	30 min	3/yr	NM&MI	Slart	Nuclear cardiology	0
Morning session internal medicine	30 min	1-2/yr	Internal Medicine	Glaudemans	PET	2
Oncology nurses	1.5 h	1/yr	Teaching Center	Pruim, Brouwers	PET	1.5
Lecture evenings NM&MI	2 hr	5/yr	Teaching center	Dierckx	Various nuclear medicine subjects	10
Chemistry students	1 mo	1/yr	Groningen Univ.	Elsinga	Organic chemistry	40
Morning meetings (Mondays)	1 hr	35/yr	Teaching center	Elsinga	Various PhD subjects	0
Afternoon meetings	30 min	200/yr	NM&MI	Supervisor SPECT&PET	Various clinical cases	0
Interactive lectures	1.5 hr	40/yr	NM&MI	Piers	Various clinical cases	50
Morning presentations (Wednesdays)	1 hr	30/yr	NM&MI	Pruim	Various subjects	30
BMT & FWN	2 hr	20/yr	NM&MI	Willemsen	Nuclear medicine and techniques	40
Researchers GUIDE (course)	1/2 d	1/yr	OWC, NMMI	van Waarde	PET transporter systems	4
Junior Scientific Masterclass	Continuous	yr	NM&MI	Dierckx, Slart, de Vries	Various subjects	0
Researchers BCN (course)	2 hr	1/yr	NIC	van Waarde	PET-brain	2
Topmaster II MPDI 2009	2 hr	1/yr	ADL1	van Waarde	Research methods: animal PET	2
MBRT	2 hr	1/yr	MBRT	Pruim	General nuclear medicine	1.5
MBRT	2 hr	1/yr	MBRT	de Vries	Radiochemistry	1.5
MBRT	2 hr	1/yr	MBRT	Paans	PET & gamma camera	1.5
University Hospital Ghent	3 d	1/yr	Ghent	Dierckx	NM instrumentation	0
University Hospital Ghent	5 d	1/yr	Ghent	Dierckx	Radiation biology / pathology	0
University Hospital Ghent	1 d	1/yr	Ghent	Dierckx	General introduction nucl.medicine	0

University Hospital Ghent	1 d	1/yr	Ghent	Dierckx	Models in Dutch healthcare	0
Life Sciences	1 hr	1/yr	Haren	Slart	Oncology symposium	0

Table 21. Ad hoc Teaching and Training

Recipients	Duration	Frequency	Location	Teacher(s)	Subject(s)	h
Biotechnology students	2 hr	2009 (2x)	Rome, Italy	de Vries	PET oncology lecture	4
Biotechnology students	2 hr + 4 hr	2009	Rome, Italy	de Vries	Antibody labeling lab & workshop	6
Faculty tutor (student J.de Boer)	3 mths	2009	NM&MI	de Vries	Inflammation imaging	0
Patient Federation	1 hr	2009	MEN Pat.Federation	Brouwers	NM techniques for MEN rel.disease	1
Oral surgery	1 hr	2009 (2x)	NVMBR Utrecht	Brouwers	Iodine treatment outpatient setting	2
Eur Assoc Nuclear Medicine	1 hr	2009	EANM Barcelona	Elsinga	CME Microfluidics	2
Eur Assoc Nuclear Medicine	2 d	2009	EANM	Pruim	PET	0
First year students of medicine	1/2 d	2009	Carroussel	Slart		3
Ph.D. students nuclear medicine	1 hr	2009 (3x)	NMP resid. NVNG	Brouwers, Pruim	Parathyroid/brain tumor imaging	3

NB Zero hours in the last column indicates that no regular teaching was performed by our Department but an internship (stage period) was provided

Total number of teaching hours in 2008 (Tables 18, 19 and 20 summed): 360